Insights into alpha-defensin modulation of non-enveloped viral infection

Ciara Tipping Hu

A dissertation

submitted in partial fulfillment of the

requirements for the degree of

Doctor of Philosophy

University of Washington

2023

Reading Committee:

Jason G. Smith, Chair

Alexander L. Greninger

Jennifer L. Hyde

Program Authorized to Offer Degree:

Microbiology

University of Washington

Abstract

Insights into alpha-defensin modulation of non-enveloped viruses

Ciara Tipping Hu

Chair of the Supervisory Committee;
Jason G. Smith
Department of Microbiology

Alpha-defensins are small antimicrobial peptides that play a crucial role in innate immunity across various mammalian species. Possessing broad antimicrobial properties, they have neutralizing activity against bacteria and both enveloped and non-enveloped viruses. These peptides are either constitutively secreted into the intestinal lumen (enteric) or stored inside granules in neutrophils which subsequently fuse to pathogen-carrying vesicles (myeloid). Despite the presence of defensins, some pathogens can resist their antimicrobial effects or even exploit these antimicrobial peptides to enhance their infection. Given the observed trend of many enteric pathogens being resistant to or enhanced by enteric alpha-defensins, we hypothesized that alpha-defensins can assert selective pressure on pathogens. To investigate this hypothesis, I focused on two non-enveloped viruses: adenovirus and rotavirus.

Prior studies on adenoviruses identified the vertex proteins, fiber and penton base, as being important determinants of defensin antiviral activity. Using a directed evolution approach, a different major capsid protein, hexon, was identified as being an additional determinant of defensin activity and a driver of defensin-mediated

enhancement. My infection and biochemical assays suggest that a balance between increased cell binding and a downstream block in intracellular trafficking mediated by defensin interactions with all the major capsid proteins dictates the outcome of infection.

Investigation into defensins' effects and mechanisms of action on rotavirus are in their infancy. We examined how defensins impact the infection of various rotavirus strains, and we observed that rotaviruses were resistant to or enhanced by their host's enteric defensins. We also interrogated the potential role of myeloid and non-host alpha-defensins as cross-species barriers and found that the outcome varied depending on the specific rotavirus strain tested. To elucidate the proteins involved, we used reassortant viruses, and identified the rotaviral spike protein, VP4, as a determinant for defensin-mediated modulation of rotavirus infection. Subsequently, I investigated if using a directed evolution approach, similar to that employed with adenovirus, would provide greater insight into defensins' ability to drive viral evolution. Moreover, I sought to identify specific regions of the rotavirus virion that are targeted by defensin. I found that rotavirus was able to evolve resistance to a previously neutralizing myeloid defensin and that most of those mutations were in the spike protein. This reinforces the significance of VP4 in determining defensins' effect on rotavirus. Interestingly, despite the emergence of defensin resistance mutations in the receptor binding pocket, I found that defensin does not inhibit rotavirus binding to cells. Future investigations into entry and trafficking may reveal that rotavirus neutralization by defensins follows a similar overarching mechanism observed for other non-enveloped viruses. This mechanism involves α-defensins disrupting proper trafficking of the virus by altering capsid dynamics.

Table of contents

List of Figures

Acknowledgements

I would like to thank many people for their technical assistance that contributed to this work. Karina Diaz for generating the data in Fig. 2-1 and for optimizing the refolding protocols for the rhesus defensins used in chapters 3 and 4. Phillip C. Burke for generating the AF488-labeled HAdV-64 used in Fig. 2-2. Jason G. Smith for operating the flow cytometer used in Fig. 2-2. Youngmee Sul and Beth Bromme for technical assistance with HPV experiments in Fig. 3-2. Neel Salukhe for sharing a quikchange protocol that was used for generating the mutants used in chapter 4. Liliana Sánchez-Tacuba for insight and assistance on optimizing the rotavirus reverse genetics system used in chapter 4. Tobias Herrmann for generously sharing an unpublished and optimized version of recombinant VP4 purification that is discussed in chapter 5 and 6. I especially want to thank Daniel Pfalmer and Alexander L. Greninger for their help with the whole-genome sequencing of the mutant rotaviruses in chapter 4, as well as their help in verifying the purity of our rotaviral stocks.

I also want to acknowledge the help of core facilities that made this project feasible. Defensin purification and analysis was supported in part by the Proteomics & Metabolomics Core Shared Resource of the Fred Hutch/University of Washington Cancer Consortium. Additional mass spectrometry analysis was performed by the Mass Spectrometry center of the Department of Medicinal Chemistry of the University of Washington School of Pharmacy. Flow cytometry data was acquired with the assistance of the Cell Analysis Facility Flow Cytometry Shared Resource Lab in the Department of Immunology of the University of Washington. Whole genome sequencing for chapter 4 was done at the NGS core lab at the University of Washington's Clinical Virology Lab.

This work was supported financially by R01 AI104920 (to Jason G. Smith), F30 AI140620 (to Karina Diaz), and R01 AI125249 (to Harry B. Greenberg) from the National Institute of Allergy and Infectious Disease and by the Office of the Director, National Institutes of Health under Award Number S10 OD026741 (to Jason G. Smith). Karina Diaz and I were also supported by Public Health Service, National Research Service Award T32 AI083203 from the National Institute for Allergy and Infectious Diseases. Harry B. Greenberg was also supported by Merit Grant GRH0022 from the U.S. Department of Veterans Affairs. Additional support to Jason G. Smith in the form of pilot awards and subsidized core service was provided by NIH grants P51 OD010425 from the Office of Research Infrastructure Programs, UL1 TR000423 from the National Center for Advancing Translational Sciences, and P30 CA015704 from the National Cancer Institute.

I would also like to thank my thesis committee: Jennifer L. Hyde, Alexander L. Greninger, Adam P. Geballe, and Ning Zheng for their excellent scientific questions and help throughout my project. A special thank you to Jennifer, Alexander, and Jason for being on my reading committee.

As for more personal acknowledgements, I need to first extend a special thank you to everyone in the Smith lab who overlapped with me for their insights into my project as well as camaraderie. To Karina Diaz, thank you for enticing me to rotate in the Smith lab as well as spearheading a lot of social activities and board game adventures. To the lab managers, Mackenzi Oswald, Anjali Sharma, and Jess Porter, thank you for being my friends and confidants throughout my grad school experience. To the postdocs, Cheng Zhao and Kaitlin Hulce, thank you for being amazing scientists. I can only hope that after I get my PhD, I will magically be able to work as hard and present as well as you all. I must give a special shout out to Yiyu Sun for being an amazing undergrad. Additionally, she worked hard on optimizing the rotavirus reverse genetics system for our lab by doing countless midi preps, making master mixes of plasmids, tracking if the volume of plasmids added in addition to their concentration matters, etc. all to improve our chances of viral recovery. Finally, you can't have the Smith lab without Jason G. Smith. I have learned a lot scientifically, professionally, and personally from you. Thank you for your mentorship and commitment to making me a better scientist even during the challenging times.

I also want to thank all my previous scientific mentors, Navneet Bhasin, Nico Cecchini, Jean Greenberg, Hyun Min Jung, and Brant Weinstein for helping me reach this milestone. Your guidance and advice, with a special emphasis on embracing my achievements, have played a vital role in shaping my success. Additionally, I want to thank my former swim coach, Neil Romney, and my music teacher, George Konopik, for instilling in me the values of self-accountability, persistence, and fostering pride in my work. Your mentorships have left an enduring impact on my personal and academic journey.

To all the microbiology graduate students, thank you for your support and for being the heart of the micro community. To those who started their journey before me, thank you for welcoming me into the program, for your help in preparing me for my exams, and for helping me navigate the more challenging parts of graduate school. To those who've started their journey after me, thank you for bringing fresh excitement to the program and for making me feel old. To my cohort: Elliot Lee, Lauren Gonsalves, Lincoln Lewerke, and Lyndsey Moore, I couldn't have asked for better people to be my 'Lil Bug-Buddies. Your eagerness to celebrate any achievement brought sunshine to the gray Seattle days.

I especially want to thank the Lagunoff lab graduate students Lyndsey, JC Alexander, Ricky Lira, and Blake Dodson for letting me mooch some fun off your lab. Graduate school was hard, and I'm glad I had some friends close by to check in on me when I was having a rough day.

I also want to extend my sincere thanks to the anime night folks: Blake, Lucy Kwiatkowski, Marshall Godsil, and Sarina Kao. Your willingness to participate in our group viewings of anime, starting with Attack on Titan, and your ongoing interest in exploring more shows collectively, have meant a lot to me. While the nights are dedicated to anime watching, we all know that the pre-show conversations are the best part, and I will truly cherish them. Your genuine enthusiasm for both science and life in general helped rekindle those feelings in me.

Last and certainly not least are all my non-grad school friends and family. I could not have made it through this journey without your love and support. While there are so many people that I need to thank, this acknowledgment section is already long, so I will only list a few groups of people.

I am grateful to my former college roommates, Joyce Lu, Jen Law, and Gabby Wimer (The Treehouse), for always inspiring me to be a better person. I am honored to be your friend and I am excited to see you all become real doctors.

Pam and Jonny Burge, our shared seafood adventures and board game nights have provided consistent sources of anticipation and joy in both Chicago and Seattle– even if my winning rate hovers around a mere 3%. Your authenticity, competitive spirits, and overall “seeming to have your lives together” really make me treasure our friendship.

My Dungeons and Dragons group which included Kevin You, Dave Giltner, Mike Smith, Kevin Wise, Emily Courcy, Ross Bernard, Emerald Mojica, Christine Huynh, Lincoln, JC, Ale Valdez, Dietrich Geisler, Michael Norcia, and led by none other than Elliot. I have been blessed to have such funny, creative, and kind people to hang out with every Thursday evening. During the height of the pandemic, our video call DnD sessions were one of the only things keeping me on the mortal plane. I cannot thank you all enough for how much you’ve impacted my life. I am really going to miss you all.

Tom (Xinyuan) Zhang, thank you for your patience throughout our long-distance relationship and not getting *too* upset when I chose a graduate school far from Chicago. Your help with editing my applications, important emails, scientific proposals, etc. have been instrumental to my success. I know I can always count on you to have my back and support me through tough times. I love having you as my partner, and I am excited to be starting a new chapter of our lives together.

Finally, I want to thank my family for always supporting me and believing in my capabilities. John and Price, thank you for all the laughs, for being empathetic ears to complain to, and for being positive influences in my life. My parents, Ben and Janet, thank you for your unconditional love and always striving to make my life easier. I love you all.

Dedication

This thesis is dedicated to everyone who had to work in person during the SARS-CoV-2 pandemic. You sacrificed your physical and mental health to keep the world functioning in the “new normal”.

This dedication also extends to all those who showed exceptional empathy and kindness in response to the pandemic. In a time where it felt like the world was collapsing, your acts of compassion were a thread that kept at least one person alive.

Chapter 1: Introduction

Adenovirus

Pathogenesis: In humans, adenoviruses cause many diseases, ranging from fever, respiratory illness, acute gastroenteritis, urinary tract infection, to conjunctivitis (pink eye). Human adenoviruses (HAdVs) can be divided into seven species (A-G) and encompass over 100 different genotypes[1]. The HAdVs used in this dissertation, HAdV-5 and HAdV-64, are of species C and D, respectively. HAdV-B, -C and -E are usually associated with respiratory disease, and HAdV-A, -F and -G are associated with gastroenteritis[2]. Of note, HAdVs, like species F types 40/41, are the third leading cause of fatal diarrhea in infants and children <5 years of age [3]. HAdV-B, -D, and -E can cause conjunctivitis, with the HAdV-D species containing members (including HAdV-64) causing highly contagious epidemic keratoconjunctivitis[4]. While most HAdV infections are self-limiting, chronic ocular adenoviral infections can occur in immunocompromised individuals[5]. Additionally, latent adenoviral infections can reactivate and be lethal in immunocompromised individuals, with stem cell and organ transplant recipients at particularly high risk[6].

Adenovirus can be transmitted by the fecal-oral route, by aerosols, and by fomites. Due to adenovirus being a non-enveloped virus, it can remain viable outside of the host for many days and can withstand common disinfection agents such as ethanol. People who live in close quarters, such as in military barracks, hospitals, and at schools are at higher risk of infection. There are currently no FDA approved drugs specific to adenovirus available, although cidofovir, which is a nucleotide analog that inhibits viral DNA polymerases and is used to treat cytomegalovirus, has been used to treat

adenoviral infections as a last resort[7,8]. Additionally, while recombinant adenovirus vectors have been used for vaccines, the most notable examples being the Janssen and the Oxford-AstraZeneca SARS-CoV-2 vaccines, there are no adenovirus specific vaccines available to the public. The vaccines against HAdV-4 and -7 are replication competent and only available for the United States military. The prevalence of HAdV disease burden in combination with the lack of preventative and curative measures highlights the importance of continued research into HAdV pathogenesis and interactions with the host's immune system.

Structure: Adenovirus is a non-enveloped virus with a linear double-stranded DNA genome of approximately 35 kilobase pairs in HAdVs[9]. HAdVs encode for over 40 different proteins of which 13 are incorporated into the virion[9,10]. The icosahedral AdV capsid consists of three major proteins: hexon, penton base (PB), and fiber. Hexon makes up the facets on the virion. Hexon trimers have a pseudo-hexagonal base and the outer-facing "towers" contain long loops that are regions of hyper variation (hyper variable regions; HVR)[10]. A pentamer of PB is at each of the twelve vertices. Fiber is one of HAdVs' viral attachment protein and is composed of three domains: the head (or knob), shaft, and N-terminal tail. Trimeric fiber is non-covalently attached to the PB pentamer, and the head and shaft protrude away from the rest of the virion. The AdV capsid also has other minor capsid proteins - IIIa, VI, VIII, and IX - which are involved in capsid assembly, stabilization, maturation and entry[10,11].

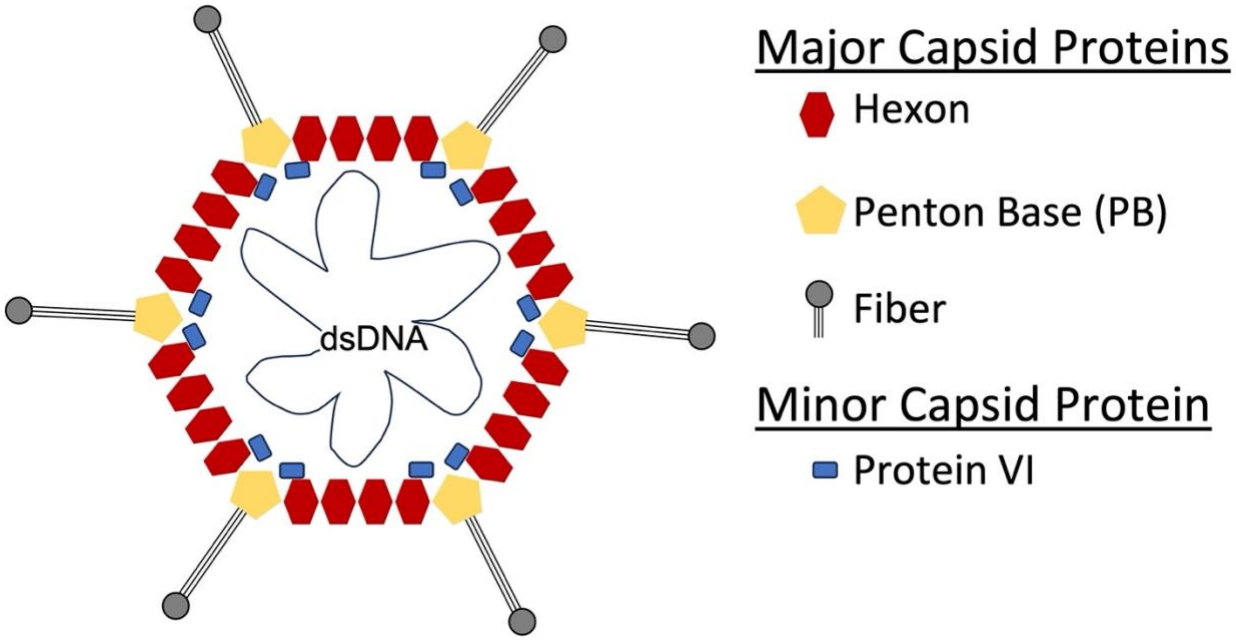

Figure 1-1: Adenovirus structure.
A simplified diagram of a cross-section of an adenovirus. The facets are composed of hexon, while the vertex contains penton base and fiber. Most of the minor and all the core proteins are not displayed for simplicity's sake. Note that the proteins are not depicted to scale.

Cell binding, entry, and trafficking: Fiber mediates attachment to HAdVs' primary receptors. The different cellular tropism of the HAdV species, which is in part determined by primary receptor expression, plays a role in determining their clinical manifestation. Many HAdV species (A, C, most D, E, and F) use the Coxsackie and Adenovirus Receptor (CAR) for attachment[12–14]. HAdV-B serotypes use either CD46 or DSG2 for attachment, and some HAdV-D use sialylated glycoproteins for attachment[15–20]. Hexon from HAdV-C has also been identified to be able to interact with a scavenger receptor (SR-A6) on macrophage cells[21–25]. Hexon can also bind to receptors via an intermediary, for example coagulation factors IX and X can help HAdV-5 bind to heparan sulfate proteoglycans on hepatocytes, and lactoferrin interaction with HAdV-5

hexon can increase cell binding and infection[26–31]. Finally, the PB in all but HAdV-F contains an RGD sequence, which is an integrin binding motif, in a variable loop that allows the HAdVs to bind to α_v integrin coreceptors[32–34]. The attachment to integrin facilitates entry and internalization into a clathrin-coated endosomal compartment[35].

In the endosomes the vertex proteins, PB and fiber, disassociate from the capsid[36]. Whether the disassociation is caused by the acidification of the endosome or tension caused by the fiber being bound to its primary receptor while PB is bound to integrin during membrane rearrangement is still an area of debate[37,38]. The disassociation of the vertex proteins allows the internalized protein VI to disrupt the endosome and the rest of the virion to escape the endosome[39]. Adenovirus then uses the cell's microtubule transport system to traffic the hexon-protected genome to the nucleus[2]. The capsid docks at the nuclear pore complex through direct interactions with hexon[40]. Ubiquitination by Mib1 of protein V, which secures the AdV genome to the capsid, as well as proteasome mediated disassembly of the capsid allows the genome to then be imported into the nucleus for replication[41,42].

Rotavirus

Pathogenesis: Rotavirus is a fecal-oral pathogen and, despite the availability of vaccines, remains one of the leading causes of severe gastroenteritis in young children[3,43,44]. In 2016, it was estimated that rotaviruses were responsible for over 200,000 deaths globally, and over half of those deaths were in children less than 5 years of age[3,44]. Rotaviruses primarily infect mature enterocytes and enteroendocrine cells in the small intestine. The death of the enterocytes due to rotaviral infection leads to villi blunting, accelerated migration of immature enterocyte cells from the crypts, and an overall loss of the absorptive capacity of the intestine[45]. Additionally, rotavirus has an enterotoxin, non-structural protein 4 (NSP4), that causes calcium ion dysregulation leading to increased fluid secretion[46–48]. Currently, there is no specific curative treatment for rotavirus. Moreover, the mortality of rotavirus is disproportionally higher in low-income countries, in part due to malnutrition and reduced access to hydration therapy, but also due to the circulation of rarer serotypes and possible co-morbidities caused by other gastrointestinal pathogens. In addition to humans, rotaviruses can infect a large range of animals and cross-species reassortants are increasingly being recovered[49–51], but the barriers that prevent cross-species transmission are not completely known.

There are nine species or groups of rotavirus (A-D, F-J) that infect a broad range of animals and pose a concern for both human health and agriculture[52]. These groups are assigned based on the antigenic properties of the viral protein 6 (VP6), which is part of the rotaviral capsid. In humans, group A rotaviruses (RVA) are, by far, the most epidemiologically relevant, however groups B, C, and H also infect humans. RVA have been further divided based on the constellation of the 11 segments of double-stranded

RNA genome the virus contains[53]. Each gene segment is assigned a letter and then given a number based on sequence identity. Most viruses are referred to by their G and P type, which correspond to the glycoprotein that covers the majority of the outer layer of the virion surface (VP7), and the protease sensitive spike protein (VP4), respectively. The most common G genotypes in humans are: G1, G2, G3, G4, G9, G12; and the most common P genotypes are: P[4], P[6] and P[8][51,54]. Two major genogroups, Wa-like (usually G1P[8]) and DS-1-like (usually G2P[4]), together account for ~90% of circulating strains[55,56]. Changes in the distribution of circulating RVA as well as limitations to reassortment are not fully understood.

Structure: The rotavirus capsid consists of three concentric layers of protein[57,58]. VP2 forms the innermost layer, and it encapsulates the 11 segments of double-stranded RNA which are bound to the viral RNA-dependent RNA-polymerase (VP1) and the capping enzyme (VP3). The middle-layer is formed by trimers of VP6 that interact with VP2. This VP6 coated particle is also known as the double layered particle (DLP). The outer most layer, which makes rotavirus a triple layered particle (TLP), is composed of the protease sensitive spike protein (VP4) and calcium ion-stabilized trimers of the glycoprotein (VP7)[59] (Fig. 1-2). The N-terminal arms of the VP7 trimer grip the VP6 trimer below, and this grip is the main interaction between VP7 and VP6[60]. VP7 association with VP6 also helps lock the spike protein (VP4) into place[61]. The maturation of the TLP into an infectious particle relies on tryptic cleavage of VP4 into VP5* and VP8*[62,63]. An asymmetric trimer of VP5* makes up the foot and the stalk of the spike while a dimer of VP8* forms the head. VP8*

has lectin properties and is involved in viral attachment to its receptor, which is often a glycan[164].

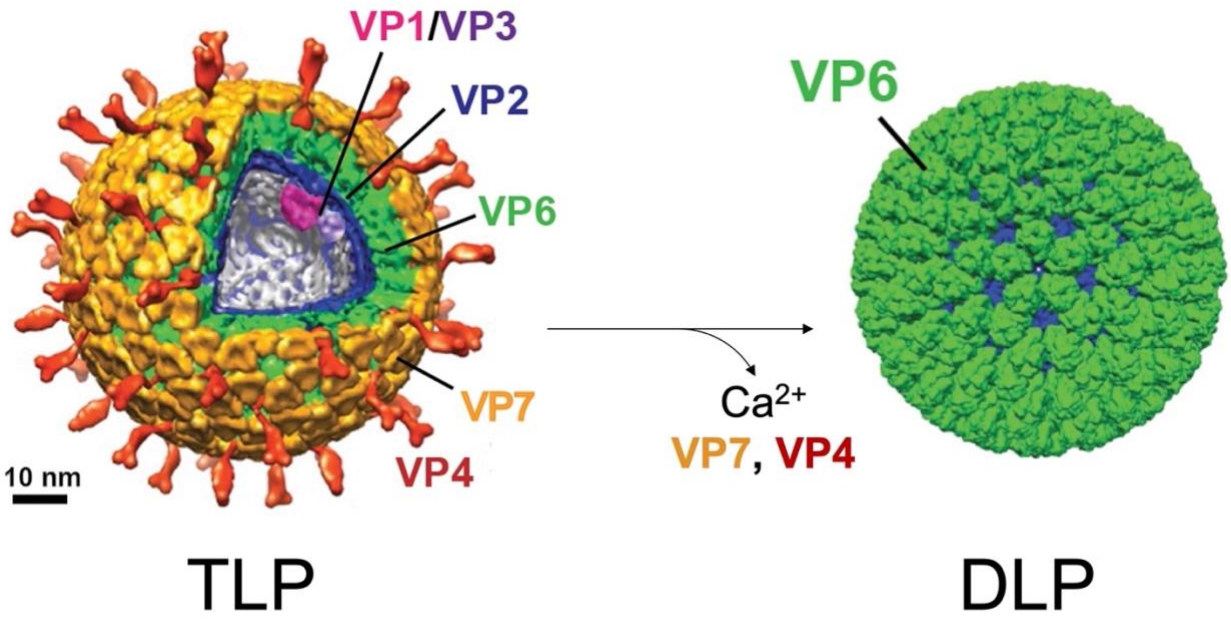

Figure 1-2 Rotavirus structure. A triple-layered rotavirus particle (TLP) and double-layered rotavirus particle (DLP) rendering from cryo-electron microscopy (PDB: 4V7Q and 3KZ4)[61,65]. Viral protein locations are indicated on the cross section of the TLP, with VP1 and VP3 modeled into the structure. Upon calcium loss, the rotavirus uncoats and loses VP7 and VP4 (VP5*+VP8*), revealing the DLP. Figure modified from Courtney P. Long and Sarah M. McDonald with permission[66].

Cell binding, entry, and trafficking: Rotavirus entry is complex and still an active area of research. VP4 determines both the receptor the virus attaches to as well as the entry pathway[67]. Many animal rotaviruses, like rhesus rotavirus (RRV) and simian rotavirus SA11, use VP8* to bind to terminal sialic acids[68]. However other rotaviruses can use sub-terminal sialic acids for attachment and others still, like the human strains, can use histo-blood group antigens (HBGA) as their primary receptor. Additionally, some RV strains can interact with hsc70 and/or integrin as post-attachment receptors using VP5*[69–73].

VP8*'s attachment to the receptor exposes VP5*'s hydrophobic loops located just below VP8*. This exposure helps drive the transition of VP5* into its membrane penetrating reverse conformation[74].

With the only known exception being RRV, most rotaviral strains, including SA11 and the human strains DS-1 and Wa, enter through clathrin-dependent endocytosis[75,76]. RRV instead is internalized in a caveolin- and clathrin-independent manner[77,78]. The endocytosis of all rotaviral strains studied thus far depend on dynamin and the presence of cholesterol on the membrane. In the early endosomes, the loss of Ca^{2+} can lead to the disassociation of the VP7 trimers and viral uncoating to the transcriptionally active DLP, although transcription does not occur until the virus has escaped the endosome and reached the cytoplasm[79–82]. The timing of the virion's escape from the endosomal pathway varies by strain.

Rotaviruses go through the early endosomes in MA104 cells, but then the subsequent escape from maturing endosomes or late endosomes is strain dependent. As endosomes mature, the vesicle undergoes changes in pH and Ca^{2+} concentration as well as the addition and removal of various proteins including the Rab GTPases; Rab5, Rab7, and Rab9. RRV and SA11 exit the endosomal network from maturing endosomes, while the human strains Wa and DS-1 exit from late endosomes[81]. Interestingly, one mutation in RRV VP4-K187R, which allows RRV to infect in the absence of terminal sialic acid, changes the viral escape from early endosomes to late endosomes[83,84]. The dependence on and interaction of certain endosomal markers and endosomal conditions for triggering different rotaviral strains' escape is still not fully understood.

Most entry studies have used MA104 cells, however a different entry pathway was observed for RRV in BSC-1 cells[85]. Upon receptor interaction, RRV was wrapped in a tight-fitting membrane, the invagination of which was independent of dynamin and clathrin. The engulfed RRV was able to uncoat, and the DLP was able to be released into the cytosol. This whole entry process was much faster than what has been observed in MA104 cells[86]. Whether this method of entry is applicable to other rotaviral strains and used in other cell lines has yet to be investigated.

Replication and assembly occur in a viroplasm that is formed by NSP2 and NSP5 in the cytoplasm[87]. During assembly, reassortment of gene segments from rotavirus co-infections can give rise to progeny with mixed genomic compositions. Reassortment contributes to rotaviral evolution, with a constraint being that certain gene constellations tend to be favored[88,89].

Defensins

To face and manage the onslaught of pathogens, organisms have developed ways to defend themselves. Antimicrobial peptides, like defensins, can have a broad range of activity and thus are an important part of innate immunity for many organisms[90–92]. Defensins can be found in plants, fungi, invertebrates, and vertebrates. They are generally small (18-45 amino acids), cationic, and amphipathic peptides that are broadly antimicrobial. In mammals, defensins can be separated into three classes; α, β, and θ, based on the disulfide bond linkages of six cysteines[93]. α-defensins have the linkages C1-C6, C2-C4, C3-C5; and β-defensins the linkages C1-C5, C2-C4, C3-C6. θ-defensins are made from two 9-amino acid peptides that are cyclized and have ladder-like linkage of C1-C6, C2-C5, C3-C4[94,95].

Despite sequence variability and different disulfide bond linkages, α- and β-defensins have similar structures. They contain three beta-sheets that have *trans*-oriented disulfide bonds stabilizing the structure, with some β-defensins having an additional N-terminal alpha-helix[96]. In addition to the six invariant cysteine residues, there are a few more residues that are imperative to the structure and function of α-defensins. α-defensins have a salt bridge between an arginine and glutamic acid that is necessary for proteolytic resistance[97,98]. There is also one invariant glycine that is important for proper defensin folding as it is in a “β-bulge” [99,100]. Finally, dimerization of α-defensins via hydrogen bonding between the second β-strands is also very important for their function[101–103].

α-defensins can be further divided into enteric and myeloid defensins based on their expression pattern and gene organization. Myeloid α-defensins were the first

defensins discovered and were originally isolated from rabbit alveolar macrophages[104–106]. Myeloid α-defensins are expressed by neutrophils and are stored in granules which can either be fused with phagolysosomes or secreted during the formation of neutrophil extracellular traps[107]. Human neutrophils are estimated to contain 10 mg/ml (~3 mM) myeloid α-defensins, with the azurophil granules containing a higher local concentration[108,109]. Enteric α-defensins, on the other hand, are constitutively secreted by Paneth cells into the crypts of the small intestine and are also secreted in both the female and male genitourinary tract. Human enteric defensin 5 (HD5) and mouse enteric α-defensin concentrations have been estimated to reach low millimolar concentrations in the lumen of the small intestine, with higher concentrations present in the mucus layer[110,111]. Humans and rhesus macaques have both enteric and myeloid α-defensins, while mice only have enteric α-defensins (cryptins)[90,112]. Humans have four myeloid α-defensins [human neutrophil peptide 1-4 (HNP1-4)] and two enteric α-defensins [human defensin 5 and 6 (HD5 and HD6)][113].

β-defensins are ancestral to α-defensins and more widely distributed between species[90,113]. β-defensins can be found in both monomeric and oligomeric forms, and their expression can be transcriptionally regulated with upregulation during infection via TLR signaling[113]. The human genome encodes around 39 β-defensins, but only a fraction of them have been studied[114]. β-defensins are expressed by mucosal epithelial cells in the gastrointestinal, genitourinary, and respiratory tracts and are important for protecting the skin and mucous membranes. Additionally, a subset of β-defensins are only expressed in the male reproductive tract and could be involved in sperm maturation[114].

θ-defensins are thought to have emerged from α-defensins when primates separated from other mammals, as θ-defensins are only found in orangutans and some Old World monkeys like baboons and the rhesus macaque[115,116]. Humans have θ-defensin pseudogenes that have a premature stop codon in the signal peptide that prevents translation. Peptides have been synthetically produced from human θ-defensin pseudogenes (retrocyclins) and their ability to inhibit HIV has been investigated[117,118].

Defensin binding is not constrained to distinct epitopes like antibodies, instead they bind selectively to many different ligands[119]. This allows defensins to be both antiviral and antibacterial[93]. Initial defensin studies focused on their bactericidal properties. These studies revealed that defensins disrupt and depolarize the bacterial membrane[120,121]. Concurrently, enveloped viruses, like herpes simplex virus (HSV), were shown to be inhibited by α-defensins, while non-enveloped viruses, such as echovirus and reovirus, were not inhibited[108,122]. This bolstered the belief that membrane disruption was the inhibitory mechanism. However, further research showed that while defensin-mediated membrane disruption can inhibit some enveloped viruses, like respiratory syncytial virus, most enveloped viruses are inhibited by other mechanisms[123–125]. Although there are numerous examples of bacterial species and enveloped viruses that can be potently inhibited by α-, β-, and θ-defensins, only α-defensins have been shown to alter non-enveloped viral infections[109,113,126]. Thus far, some members of *Adenoviridae*, *Papillomaviridae*, *Parvoviridae*, and *Polyomaviridae* have been shown to be neutralized by α-defensins[127–135]. From my thesis work, we can now add *Reoviridae* to the list of non-enveloped viruses that contain members that are sensitive to neutralization by α-defensins.

Antiviral Mechanisms of Defensins: There are many steps throughout viral entry where defensins can directly interact with and inhibit the virus. The first step, viral attachment, can be inhibited by defensins binding to the viral attachment protein or the viral receptor. For example, the viral glycoproteins of HSV-1&2 and its cellular receptor, heparan sulfate, can be bound by some α- and θ-defensins to hinder cellular attachment[136,137].

Another way defensins can neutralize viruses is through viral aggregation. Aggregation may occur when defensins neutralize charge-based repulsion of viral capsids, or because oligomerized defensins can bind multiple viruses. The non-enveloped virus, BK polyomavirus, aggregates when treated with HD5. This aggregation blocks attachment and entry into the cell[131]. Aggregation could also reduce total viral titers because aggregated viruses would enter a single cell, instead of the multiple cells had the viruses been dispersed. However, defensin-mediated aggregation does not guarantee inhibition. For example, defensins can aggregate AdV, but this aggregation is neither sufficient nor necessary to inhibit infection[103].

After attachment, the viral genome must cross the host's membrane to initiate infection. Enveloped viruses accomplish this by fusing their membrane to the host's membrane. Defensins can inhibit this process by binding and crosslinking the fusion machinery. This prevents critical conformational changes necessary for fusion. HIV and influenza A virus (IAV) are two examples of enveloped viruses where defensins can inhibit the fusion process by crosslinking either viral glycoproteins or host glycoproteins[138–140]. While non-enveloped viruses do not fuse with the host membrane, they still need to penetrate the membrane. For many non-enveloped viruses, membrane penetration requires "uncoating" of the viral capsid. For example, AdV's endosomal escape relies on

the vertex proteins disassociating, which allows for the release of the membrane lytic protein VI[39]. HD5 inhibits AdV by stabilizing the capsid and preventing the release of the vertex proteins, and as a result, protein VI [128,134,141,142]. This eventually causes the virus to be trafficked to the lysosome where it is degraded. Similarly for HPV, HD5 blocks the complete separation of L1 from the genome and hinders furin-mediated cleavage of L2, resulting in HPV being redirected to the lysosome[129,143,135]. Finally, HD5-mediated neutralization of JC polyomavirus also follows the trend of capsid stabilization followed by improper trafficking[132].

Lastly, defensins can have indirect antiviral activity. They can bind to the host cell and modulate expression of receptors and proteins that are important for viral infection. For example, HNP1 inhibits protein kinase C (PKC). PKC activation is essential for some viruses, like IAV and HIV, and therefore its inhibition by HNP1 results in the inhibition of those viruses[144,145]. Additionally, defensins can function as chemokines and attract immune cells[146,147]. This immunomodulatory effect may have a big influence on viral pathogenesis *in vivo*.

Pro-viral Effects of Defensins: Despite defensins' great breadth of anti-microbial properties, many pathogens can successfully infect in their replicative niche even in the presence of defensins. In this regard, enteric pathogens such as adenovirus and rotavirus are of particular interest for me. Some viruses can even appropriate α-defensins to enhance their infection. For example, in contrast to the antiviral effect human myeloid α-defensins have on HIV-1, HD5 and HD6 enhance HIV infection by increasing attachment to cells[148,149]. AdVs can exhibit varying responses to enteric α-defensins depending on their serotypes. Respiratory HAdVs are generally neutralized by HD5, in contrast, enteric

HAdVs are either enhanced by or resistant to HD5[141,150–152]. Likewise, the more pantropic mouse AdV serotype 1 is neutralized by mouse enteric α-defensins[153], while the fecal-orally transmitted mouse AdVs serotype 2 is enhanced[154]. Given that enteric α-defensins are constitutively secreted in the small intestine, it is likely that fecal-orally transmitted pathogens have evolved mechanisms to either resist or co-opt enteric α-defensins. Moreover, the microbial communities within the gastrointestinal tract are shaped by their differential susceptibility to enteric α-defensins[155–157]. Supporting this hypothesis, rather than kill the enteric bacterial pathogen *Shigella*, HD5 actually promotes its cell binding and facilitates infection[158,159]. These observations suggest that defensin-driven evolution of enteric microbes is a common cross-kingdom occurrence.

In the following chapters the *in vitro* evolution of HAdVs and monkey rotaviruses under α-defensin selective pressure will be explained in greater detail. These directed evolution approaches identified proteins involved in defensin-mediated resistance and enhancement. My investigation into defensins' modulation of these viruses points to increased cellular binding, like what has been described for HIV and *Shigella spp.*, as a possible mechanism of enhancement.

Chapter 2:
Defensin-driven adenovirus evolution*

Introduction

Despite their broad antimicrobial activity, α-defensins are not able to inhibit all non-enveloped viruses. Echovirus, reovirus, and some adenoviruses (AdVs) from both humans and mice are resistant to α-defensin inhibition [108,141,150,154]. However, assigning resistance or sensitivity to α-defensins cannot be broadly applied across all members of each viral family. For example, human AdV (HAdV) infection can either be neutralized by, resistant to, or enhanced by human enteric α-defensin 5 (HD5), depending on serotype [141]. Thus, the naturally occurring diversity of HAdVs is an appealing substrate to identify viral determinants for neutralization and enhancement by defensins.

The icosahedral AdV capsid consists of three major proteins: hexon, penton base (PB), and fiber. A rational design approach identified the vertex proteins, fiber and PB, as determinants of HD5 neutralization [141]. To better delineate neutralization determinants in PB, a series of chimeric viruses were generated using the HD5-neutralized HAdV-5 as a backbone with portions of PB swapped with the corresponding residues from the HD5-enhanced HAdV-64. These constructs also contain a DTET to GYAR mutation in the N-terminal region of fiber, which acts in concert with changes in PB to ablate HD5-dependent neutralization[141]. Infection by a chimera containing the entire HAdV-64 PB was moderately enhanced 2- to 3-fold when incubated with 5 μM or 10 μM HD5 when compared to HAdV-5. If C-terminal residues 288 to 571 of PB are from HAdV-5, then the virus is neutralized by HD5. If they are from HAdV-64 (**C4 Vertex Chimera**), then infection

* Adapted from Diaz K, Hu CT, Sul Y, Bromme BA, Myers ND, Skorohodova KV, Gounder AP, and Smith JG. (2020) Defensin-driven viral evolution. PLOS Pathogens 16(11): e1009018.

is not neutralized but enhanced. Although not exhaustive, additional chimeras were created to probe the contribution of specific variable sequences within the C-terminal half of PB to HD5-dependent neutralization. Collectively, this analysis suggests that complete neutralization of HAdV-5 by HD5 reflects the additive effects of multiple residues in PB.

Nonetheless, nature can create many different solutions to overcome defensin-mediated neutralization. The naturally occurring diversity of HAdVs and other microorganisms' sensitivity to defensins could be due to evolutionary pressure imposed by enteric α-defensins during fecal-oral transmission. To directly test the ability of enteric α-defensins to drive viral evolution and to test if the vertex proteins are the sole determinants of defensin neutralization, a previously described HAdV-5-based "mutator" vector[160] was passaged under the selective pressure of HD5. Over 50 passages, the HD5 IC_{90} used for selection increased 7-fold from ~2.5 μM to ~17.5 μM. Both the initial inoculum and the passaged control samples contained only low frequency (<1%) mutations. In contrast, there were numerous mutations across the viral genome that exceeded 1% frequency in the HD5 selected samples. Of note, two mutations in hexon (I114K and E154K) and a mutation in the hexon chaperone protein, L4-100K (G745D), were fixed by the 15th round of selection, with a third mutation in hexon (E424K) trending towards fixation in passage 50. Each of the hexon mutations introduced positive charge in one of two hypervariable regions (HVRs), HVR1 (I144K and E154K) or HVR7 (E424K), located on the outer face of hexon; therefore, their contribution to HD5 resistance was focused on. The presence of all three hexon mutations resulted in a ~3-fold increase in IC_{50} from the starting population. Viruses engineered with the two mutations in HVR1 but without the mutation in L4-100K was just as resistant to HD5 as viruses with all three

hexon mutations and L4-100K. Taken together, these results indicate an important role for HVR1 and HVR7 in sensitivity of HAdV-5 to neutralization by HD5.

To further explore the potential importance of HVR1 and HVR7 for HD5 interactions, chimeric viruses at these regions between HAdV-5 and HAdV-64 were created. Although virus from genomic constructs containing HAdV-64 HVR1 and HVR7 in the HAdV-5 background was recoverable, the reverse chimeras were not. Placing HAdV-64 HVR1 into HAdV-5 (**Hexon HVR1 Chimera**) increased the HD5 IC_{50} of the virus ~5-fold over HAdV-5, which was also significantly higher than the HD5 IC_{50} of the pool of viruses from round 50 of the selection. In contrast, placing the HAdV-64 HVR7 into HAdV-5 had no effect. Replacing both HVR1 and HVR7 in HAdV-5 resulted in an intermediate phenotype compared to the single HVR changes. Overall, these studies identify HVR1 as a novel determinant for HAdV-5 neutralization by HD5.

While differing in some respects between viruses, a conserved mechanism by which non-enveloped viruses are neutralized by α-defensins has emerged. In essence, stabilization of the capsid by α-defensin binding leads to changes in uncoating and intracellular trafficking, thereby preventing the genome from reaching the nucleus to initiate replication[103,113,128,129,132,134,135,141,161,162]. For enhancement, defensin-mediated receptor-independent binding to the cell surface leading to increased infection has been observed for HIV-1, some AdVs, and *Shigella*[154,159,163]. However, disruption of the epithelial barrier or promoting internalization are still possible mechanism of enhancement[93]. With the interrogation of PB residues and identification of the hexon HVRs that are determinants of neutralization, we sought to better understand the

mechanism behind HD5-mediated neutralization of HAdV and gain insight into its mechanism of enhancement.

Rational design and directed evolution implicated different major capsid proteins as HD5 neutralization determinants, PB/fiber and hexon, respectively. However, the order of addition of virus and defensin to the cells differed between the two approaches. Therefore, this discrepancy could illuminate how defensins interact with those proteins to modulate infection. The HD5 IC_{50} for key viruses was determined by either pre-incubating virus with HD5 and then adding this mixture to cells, as in the assessment of PB chimeric viruses (protocol 1), or by adding the defensin to virus pre-bound to cells, as in the selection for HD5-resistance (protocol 2). The phenotypes of HAdV-5 (Fig. 2-1 A), the directed evolution round 50 pool (Fig. 2-1 B), and hexon HVR1 chimera (Fig. 2-1 C) were largely protocol-independent. The only difference in the phenotype of HAdV-64 (Fig. 2-1 D) was enhancement in protocol 1 compared to resistance in protocol 2. In contrast, the phenotype of the C4 vertex chimera was dramatically protocol-dependent (Fig. 2-1 E), demonstrating that cell binding can alter HD5 sensitivity.

An additional construct combining the changes from the hexon HVR1 and C4 vertex chimeras was created and tested. In both protocols, the hexon HVR1/C4 vertex chimera exhibited an intermediate phenotype. In protocol 1, it was resistant to neutralization by HD5 at all concentrations but not enhanced (Fig. 2-1 F). In protocol 2, it was ~3-fold more HD5-resistant than the C4 vertex chimera but ~2-fold more HD5-sensitive than the hexon HVR1 chimera. Thus, both hexon HVR1 and the vertex are important determinants of viral infectivity in the presence of HD5, but they appear to have additive rather than synergistic effects.

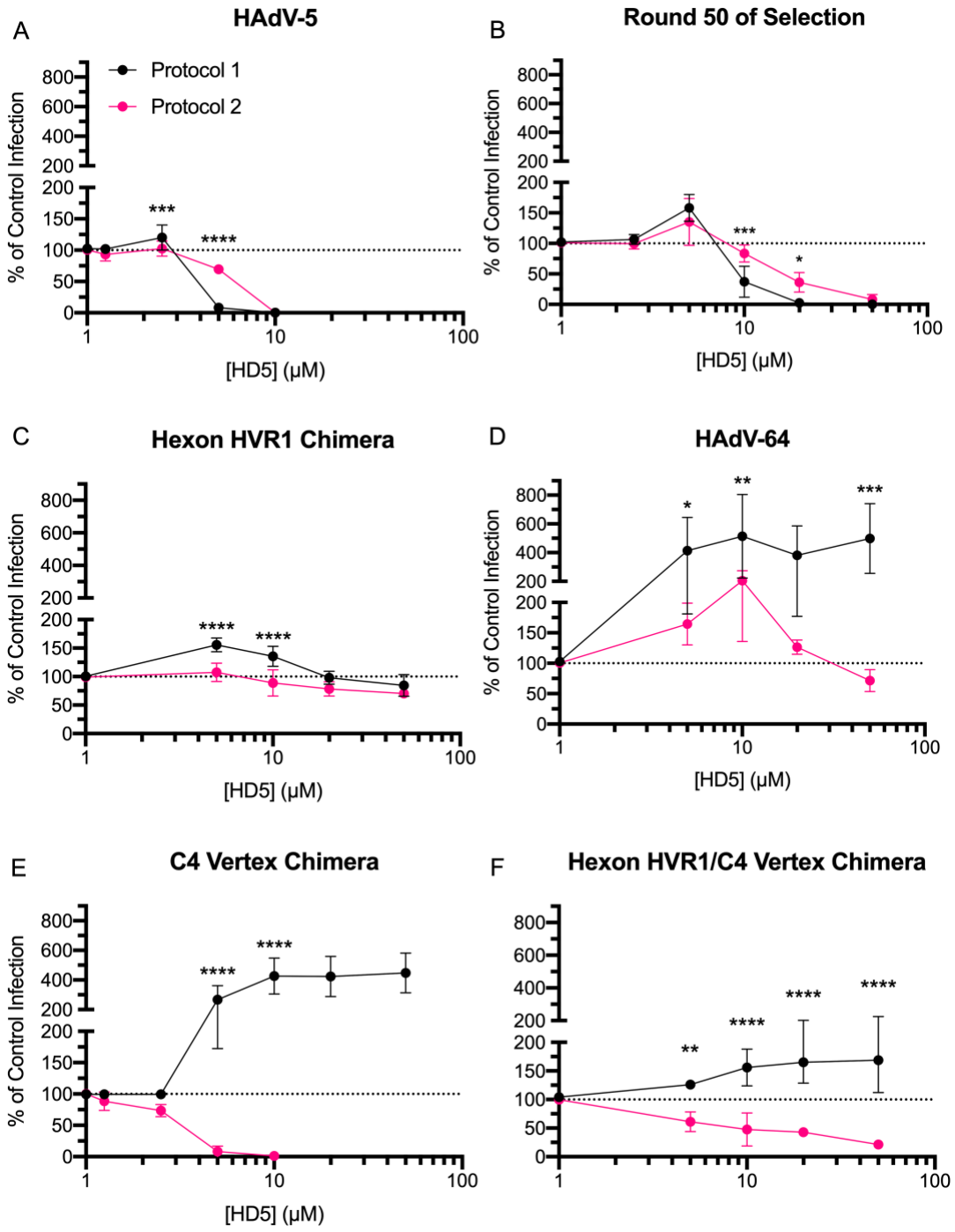

Figure 2-1. Hexon and vertex play different roles during virus-defensin interactions. Purified (A) HAdV-5, (B) virus expanded from round 50 of selection, (C) hexon HVR1 chimera, (D) HAdV-64, (E) C4 vertex chimera and (F) hexon HVR1/C4 vertex chimera were either incubated with HD5 and then added to A549 cells (protocol 1 –black) or bound to A549 cells prior to HD5 addition (protocol 2 –pink). Data are the mean of 3 to 11 independent experiments ± SD. Results of two-way ANOVA with Sidak's multiple comparisons at each HD5 concentration are indicated by asterisks. Data generated by Karina Diaz.

A possible mechanism to avoid neutralization by defensins could be that resistant and/or enhanced viruses bind fewer defensin molecules. Based on previous studies demonstrating a direct interaction between HD5 and HAdV[103,128,141,164], the average number of HD5 molecules bound to the capsid of each virus was quantified. At a concentration of 20 µM, HD5 binds at a high molar ratio to HAdV-5 (7090 +/- 1550 molecules of HD5 per HAdV-5 virion), as shown previously[141], and ~83-fold less to HAdV-64. Interestingly, the C4 vertex chimera bound ~2.3-fold more HD5 than HAdV-5 did, while the hexon HVR1 chimera bound ~5-fold less. Finally, HD5 bound to the combined hexon HVR1/C4 vertex chimera at the same levels as HAdV-5. At lower concentrations (5 µM and 10 µM), HD5 binding to HAdV-5, C4 vertex chimera, and hexon HVR1/C4 vertex chimera was equivalent. Thus, changes in both hexon and the vertex proteins alter the stoichiometry of the HD5-capsid interaction, and the amount of defensin bound to the virion cannot predict the infectivity phenotype.

Results

HD5 binding to the viral capsid increases AdV binding to cells

One possible mechanism for enhanced infection in protocol 1 is an HD5-dependent increase in binding of HAdV to cells, which we have previously demonstrated for HAdV-5[103,141]. To test this hypothesis, I quantified the amount of Alexa Fluor 488 (AF488)-labeled virus bound to cells after pre-incubation with HD5 (Fig. 2-2). As expected, I observed a 1.4- to 2.1-fold increase in HAdV-5 binding to cells that was HD5 dose-dependent. Despite varying levels of HD5 bound to each genotype and regardless of the ultimate effect of HD5 on infection (Fig. 1-1), HD5 enhanced binding of all genotypes to cells to a similar extent. These results are consistent with a model in which

HAdV binding to cells is enhanced by HD5, which results in enhanced infection if the virus is not blocked at a downstream step.

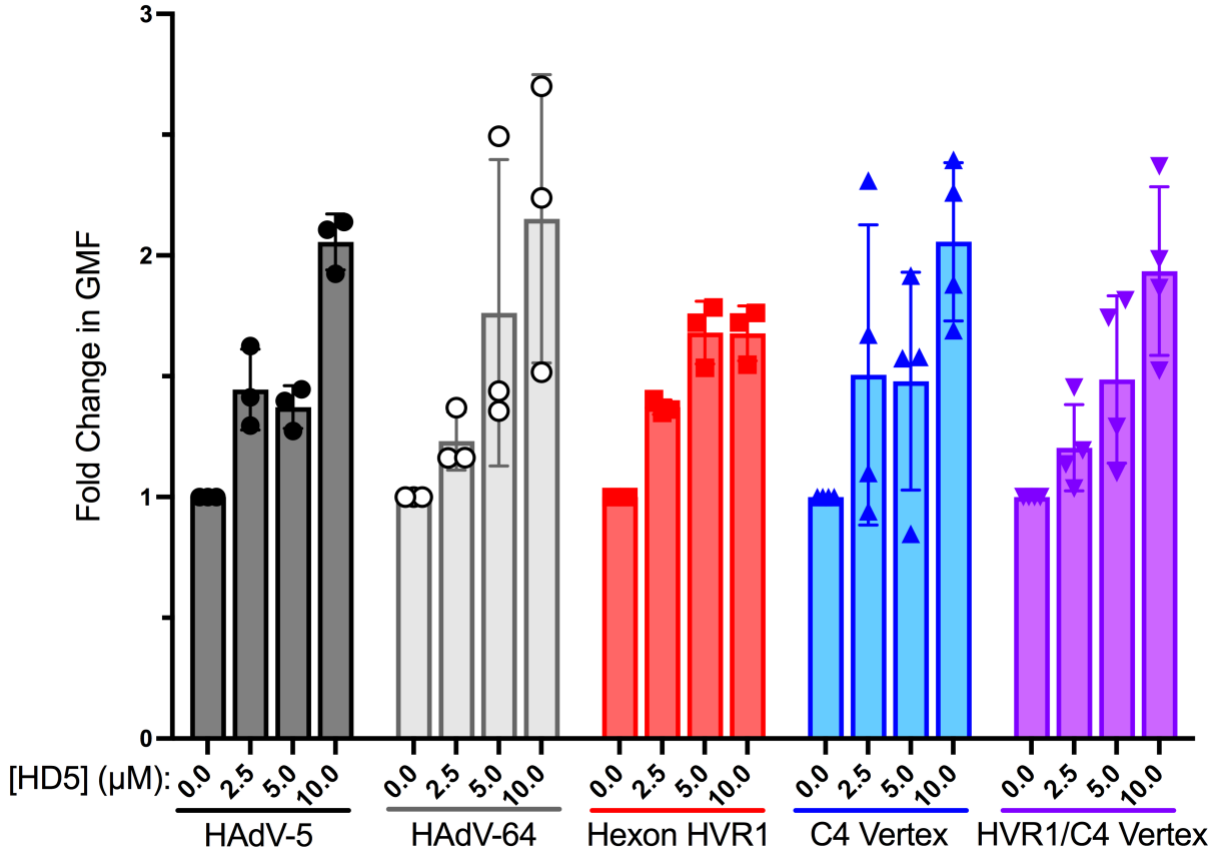

Figure 2-2. HD5 increases the binding of viruses to cells regardless of infection phenotype. AF488-labeled HAdV-5, HAdV-64, and chimeric viruses were incubated with or without HD5 and then allowed to bind to A549 cells in the cold (as in Fig 4, protocol 1). Data are the fold change in geometric mean fluorescence (GMF) of cells bound by the respective labeled virus incubated with the indicated HD5 concentrations relative to no HD5 for each virus. Each point is an independent experiment, and bars are the mean ± SD of 3–4 independent experiments. Differences between each genotype and HAdV-5 at each HD5 concentration are not significant by ordinary two-way ANOVA with Dunnett's multiple comparison test. Flow cytometry data was collected by Jason G. Smith.

The composition of both hexon HVR1 and the vertex proteins influence fiber stability upon HD5 binding

Our prior studies are consistent with a mechanism in which HD5 neutralizes HAdV-5 by stabilizing the capsid and preventing shedding of the vertex proteins[128,141]. Thus, capsid changes could impact the thermostability of the virus in the presence or absence of HD5. I examined this property at pH 7.4 to approximate the neutral pH of the intestinal lumen where HD5 is most abundantly expressed. I first determined the temperature at which 50% of fiber dissociates from the viral capsid (Tm) in the absence of HD5. As expected, all viruses remained intact at 44°C, and fiber was completely dissociated at 50°C (Figs. 2-3 A and 2-3 B). The Tm of the hexon HVR1 chimera was identical to that of HAdV-5 (46°C), while the Tms of the C4 vertex and hexon HVR1/C4 vertex chimeras were similar to each other and warmer than that of HAdV-5 by ~2°C. Thus, amino acid changes in the C4 vertex stabilize the fiber-capsid interaction, while amino acid changes in hexon HVR1 have no effect. I then tested the effect of HD5 on fiber dissociation, when samples were heated to 2°C above the Tm to assure full fiber dissociation in the absence of HD5. Despite their different infection phenotypes and HD5 binding capacities, the fiber of each of these viruses was fully capsid-associated upon incubation with 20 µM HD5 (Fig. 2-3 C). HAdV-5 and C4 vertex chimera fibers were 50% capsid-associated at 5 µM HD5 and had identical HD5-dependent dissociation profiles. The hexon HVR1/C4 vertex chimera required a 2-fold lower HD5 concentration than HAdV-5 to be 50% capsid-associated and was significantly more stabilized than HAdV-5 at both 2.5 µM and 5 µM HD5. In contrast, the hexon HVR1 chimera required at least a 2-fold higher HD5 concentration than HAdV-5 to be 50% stabilized. Overall, the composition of both HVR1

and the vertex influence HD5-mediated fiber stabilization; however, the phenotype of the combination does not mirror the individual contributions of each capsid component.

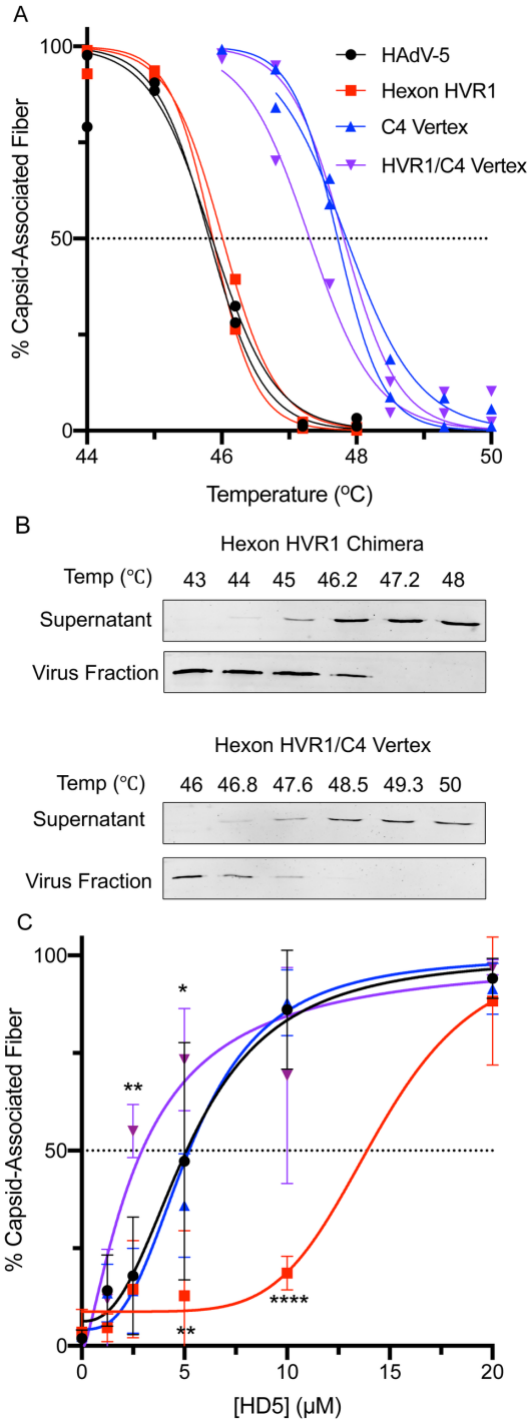

Figure 2-3. Fiber thermostability does not correlate with infection phenotype.

Fig. 2-3 (continued): The percent of fiber that remains capsid associated was determined (A) as a function of temperature in the absence of HD5 or (C) as a function of HD5 concentration for HAdV-5 (black) and hexon HVR1 chimera (red) at 48°C and for C4 vertex chimera (blue) and hexon HVR1/C4 vertex chimera (purple) at 49.3°C. (B) Representative immunoblots from the temperature gradients of hexon HVR1 and hexon HVR1/C4 vertex chimeras are shown. In (A) each point and line is an individual replicate. In (C), each point is the mean ± SD of 3 independent experiments, and the results of two-way ANOVA with Dunnett's multiple comparisons to HAdV-5 are denoted by asterisks.

Neutralization correlates with altered intracellular trafficking

Since the thermostability data do not correlate with infectivity phenotypes, I sought to determine if the mechanism of neutralization seen in protocol 2 agrees with a model whereby HD5 blocks uncoating, alters intracellular trafficking, and prevents the virus from reaching the nucleus. To study the effect of HD5 on intracellular trafficking, I used AF488-labeled viruses and followed protocol 2, binding the virus to cells prior to addition of defensin. At 2 h post-infection (p.i.), samples were stained for LAMP1 to visualize lysosomes and with DAPI to visualize the nucleus, imaged, and analyzed for object-based colocalization. In the absence of HD5, less than 80% of the C4 vertex and hexon HVR1/C4 vertex chimeras reached the nucleus by 2 h p.i. (Figs. 2-4 B and 2-4 D), which is in contrast to >90% nuclear colocalization for HAdV-5 and the hexon HVR1 chimera (Figs. 2-4 A and 2-4 C). Therefore, the C4 vertex and hexon HVR1/C4 vertex chimeras were also examined at 6 h p.i. to account for the slower kinetics of these viruses compared to HAdV-5, which could be a consequence of their higher inherent stability (Fig. 2-3 A).

Overall, subcellular localization correlated with infection phenotype. Consistent with HD5-mediated neutralization in protocol 2 of Fig. 2-1, nuclear colocalization of HAdV-5, the C4 vertex chimera, and the hexon HVR1/C4 vertex chimera were all significantly reduced by HD5 (Figs. 2-4 A, 2-4 B, and 2-4 D). These genotypes generally appeared as

a cluster of peri-nuclear virus in the presence of HD5 (Fig. 2-4 E). However, the hexon HVR1 chimera, which is resistant to HD5 (Fig. 2-1 C), had little change in nuclear colocalization in the presence of HD5 (Fig. 2-4 C). Moreover, virions were evenly distributed across the nucleus even in the presence of HD5 (Fig. 2-4 E). The effect of HD5 on lysosomal colocalization was not as extensive for HAdV-5 as in prior studies [128] and varied little between genotypes, likely due to the use of epifluorescence versus confocal microscopy. Nonetheless, the intracellular trafficking of HAdV-5 and the chimeric viruses inhibited by HD5 in protocol 2 (Fig. 2-4 and [103,134]) is perturbed in a manner similar to that of our prior studies of HAdV-5 following protocol 1[128], resulting in an inability of internalized viruses to reach the nucleus.

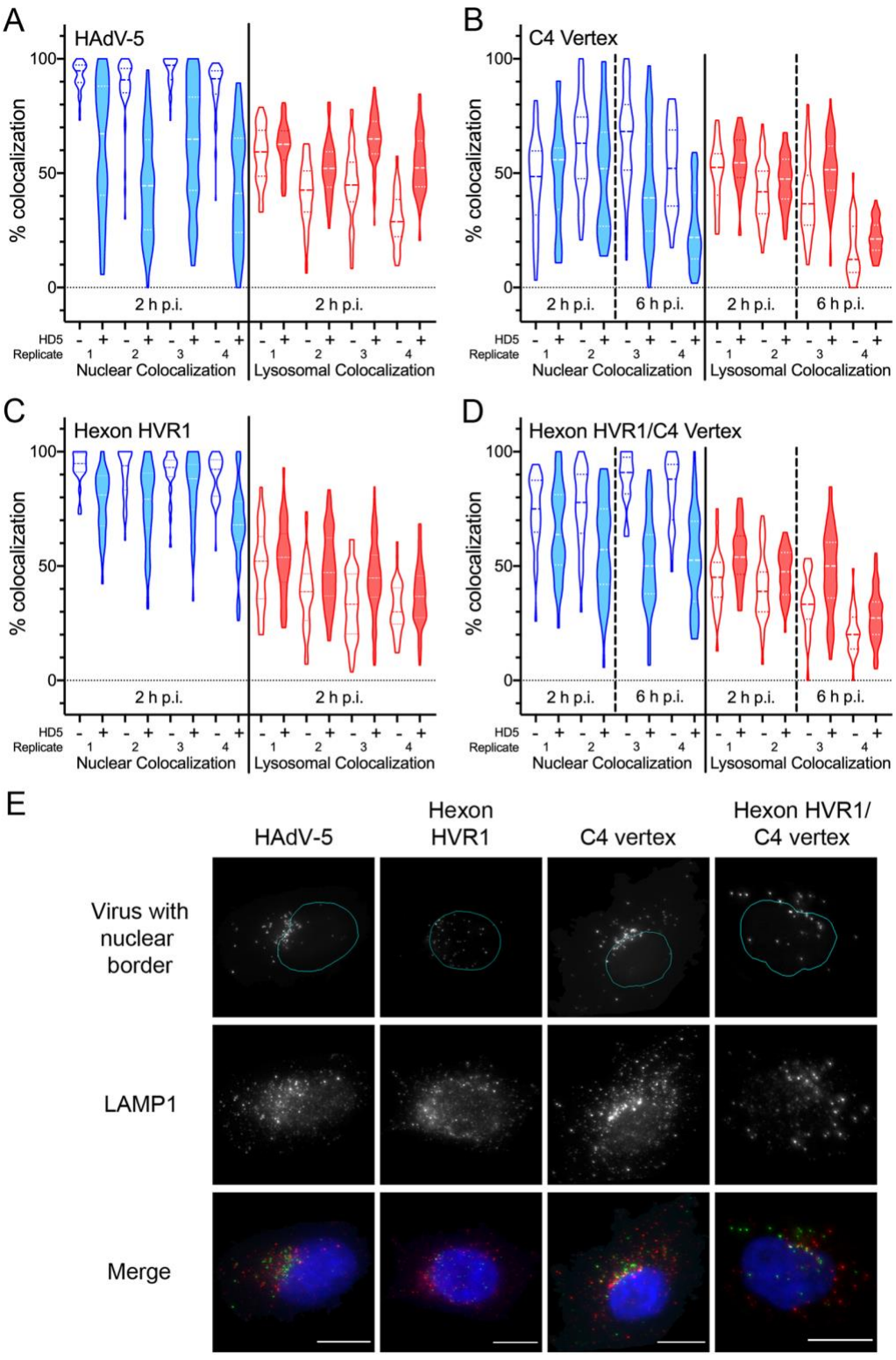

Figure 2-4. HD5 neutralization correlates with a reduction in nuclear localization.

Fig. 2-4 (continued): AF488-labeled HAdV-5 (A), C4 vertex (B), hexon HVR1 (C), and hexon HVR1/C4 vertex (D) were bound to A549 cells in the cold and then incubated with (shaded plots) or without (unshaded plots) 10 μM HD5 (as in Fig 2-1, protocol 2). Cells were then warmed to 37°C and fixed at the indicated times post-infection (p.i.). Images obtained by epifluorescence microscopy were analyzed for percent colocalization of the virus with the nucleus (DAPI, blue) or lysosome (LAMP1, red) on a per cell basis. Violin plots marked with the median value (dashed lines) and interquartile ranges (dotted lines) for 23 to 106 cells for each of four independent experimental replicates are shown. The difference in mean colocalization of virus with the nucleus and with lysosomes in the presence and absence of HD5 was calculated for each replicate for each genotype. For the C4 vertex and hexon HVR1/C4 vertex chimeras, only data from 6 h p.i. was used. The calculated values for each chimera were then compared to HAdV-5 by ordinary ANOVA with Sidak's multiple comparisons test. All comparisons are not significant except for hexon HVR1 nuclear colocalization, where $p = 0.0014$. (E) Representative images of cells at 2 h p.i. (HAdV-5 and hexon HVR1 chimera) or 6 h p.i. (C4 vertex and hexon HVR1/C4 vertex chimera) in the presence of HD5 are shown. In the top panels, nuclear borders from the CellProfiler analysis (cyan) are superimposed on AF488 fluorescence (gray). The merge data includes DAPI (blue), AF488 (green), and LAMP1 (red). Note that the AF488 fluorescence was individually adjusted in these images to account for the differences in brightness between genotypes. Scale bars are 10 μm.

Discussion

Our study provides new insight into the interaction of HD5 with the HAdV capsid. Interestingly, all of the viruses studied herein had similar levels of enhanced epithelial cell binding (Fig. 2-2) despite varied amounts of HD5 bound to their capsids. Defensin-mediated increased cell binding likely occurs by neutralizing the repulsive forces of the electronegative capsid in proximity to the cell membrane. In this regard, charge neutralization by polybrene and other cationic molecules has previously been shown to increase transduction efficiency of HAdV-based vectors[165]. However, the interaction of HD5 with HAdV is not simply charge-dependent, since it requires the hydrophobicity, tertiary structure, and ability to multimerize of HD5[103,141,164]. Thus, variation in surface charge may account for some of the differential binding of HD5 among genotypes, especially in the case of the hexon mutations that arose during selection. But the discrete changes introduced in our chimeras indicate that a more complex interaction occurs. For example, the RGD loop of PB in the C4 vertex chimera is 49 amino acid residues shorter than that of WT HAdV-5 and has a calculated net charge of -1 compared to -10 for WT HAdV-5. The change in fiber (GYAR in C4 vertex vs. DTET in HAdV-5) also introduces positive charge, yet the C4 vertex chimera binds ~2.3-fold more HD5 than does HAdV-5. Interestingly, the dose-dependence of enhanced infection (Fig. 2-1 E) plateaus at an HD5 concentration lower than that required for maximal binding, consistent with higher affinity capsid interactions mediating enhanced infection that may saturate prior to complete occupancy of lower affinity interaction sites required for neutralization.

Increased cell binding appears to be the major driver of enhanced infection of epithelial cells. We define enhancement as ≥2-fold higher infection in the presence of

HD5 than in the absence of HD5. Consistent with this conclusion, enhancement most often occurs when the virus binds HD5 before binding to the cell (protocol 1 in Fig. 2-1). Charge-neutralization by HD5 binding may facilitate prototypical receptor interactions of fiber and PB. Alternatively, HD5 could also bridge interactions between the virus and cellular lipids, glycans, or an unidentified HD5-specific receptor, which could be mediated by defensin bound to hexon. Hexon-mediated cell binding facilitated by host proteins, coagulation factors and lactoferrin, has been previously described[28–31]. Interestingly, both HD5 and lactoferrin interact with HVR1[31]. We also speculate that even in situations where the virus is bound to cells prior to the addition of HD5 (protocol 2), HD5 may promote re-attachment of virions that are bound to a low affinity receptor like sialic acid used by HAdV-64[166]. This may explain the enhanced infection of HAdV-64 in the presence of 10 μM HD5 in protocol 2 (Fig. 2-1D). An alternative model whereby enhancement occurs through increased internalization or more efficient uncoating cannot be formally excluded but is not supported by any of our studies to date. Because *Shigella* is another gastrointestinal pathogen that appropriates HD5 to facilitate infection[158,159], the ability of enteric pathogens to co-opt defensins to promote adhesion may be common.

Despite increased cell binding and the potential for enhanced infection, many HAdV serotypes are nonetheless neutralized by HD5 upon infection of epithelial cells[141]. Our prior studies supported a model where HD5 binds to the fiber and PB proteins at the vertices of the HAdV-5 capsid and stabilizes their interaction[141]. This action blocks uncoating of the capsid during cell entry and restricts release of the membrane-lytic protein VI, which in turn prevents endosome escape and precludes trafficking of the viral genome to the nucleus[128,134]. This mechanism was supported by structural, biochemical,

biophysical, and genetic studies[103,128,141,142,164]. In addition, an HD5-mediated uncoating block for HAdV-5 was directly demonstrated in A549 cells[134]. However, we were unable to account for the extensive HD5 binding to the hexons of HAdV-5 in our cryoEM studies[141]. The results from the directed evolution approach indicate that the HVR1 loop of hexon functions in cooperation with the vertex proteins as a previously unidentified determinant of HD5-mediated neutralization, which is further supported by the recent demonstration of neutralization and enhancement of HAdV-based vectors by HD5 in a mouse model[151]. If either HVR1 or both vertex determinants (four residues near the N-terminus of fiber and the C-terminal half of PB) are derived from a resistant serotype, then neutralization does not occur. Rather, these viruses are either resistant to HD5 (e.g., the hexon HVR1 chimera) or enhanced. This suggests that the functions of the capsid determinants are interrelated and that the infection phenotype reflects the additive effects of enhanced cell binding and the potency of subsequent neutralization. However, if the virus is bound to its cellular receptor and co-receptor prior to HD5 addition (protocol 2 in Fig. 2-1), then HVR1 is the major determinant of neutralization. Thus, the virus-cell interaction functionally replaces the vertex in potentiating HD5 neutralization. Mechanistically, this could occur through receptor-induced conformational changes that lead to exposure of HD5-interacting surfaces in the vertex that are buried in the absence of receptor. Alternatively, the receptor-virus interface could provide a novel target for HD5 binding. However, these interpretations suggest that the virus in protocol 1 either doesn't experience the conformation induced at 4°C in protocol 2 or transitions through it too rapidly for HD5 to exert a neutralizing effect. Moreover, it is unknown how many vertices are receptor-engaged under the conditions of protocol 2. If only a subset are bound, then

blocking uncoating triggered through these vertices may be the key step impeded by HD5 binding[37]. The nature of the HVR1 loop also dictates the Hill slope of the HD5 inhibition curve in protocol 2 (Fig 2-1), suggesting distinct levels of cooperativity and modes of HD5 binding by capsids differing in HVR1 loops. And, C4 vertex-containing viruses are neutralized at a lower HD5 concentration than those with the HAdV-5 vertex, which may be due to the inherently higher thermostability of the C4 vertex (Fig. 2-3A) or to its higher HD5-binding capacity. Although a minimum amount of HD5 binding to the capsid is required for neutralization, there is not a simple correlation between the degree of neutralization and the amount of HD5 bound. Total HD5 bound appears to reflect additive functions of HVR1 and the vertex. However, neither the HAdV-5 nor HAdV-64 vertex binds HD5 to the same extent as the C4 vertex, suggesting altered binding by the artificial interface in the C4 chimera. We also found that fiber stabilization does not directly correlate with the infection phenotypes of the chimeras and that swapping HVR1 also affected the ability of HD5 to stabilize fiber dissociation. Collectively, these findings suggest that our previous model of vertex stabilization mediated only by HD5 interactions with fiber and PB is incomplete.

A model most consistent with our data is that blocking vertex dissociation through HD5 interactions with fiber/PB is insufficient, and a separate hexon-dependent mechanism, perhaps inter- or intra-hexon or hexon-vertex “cross-linking” by HVR1-HD5 interactions, is also required to prevent uncoating. This would account for HD5 density on all four unique hexon positions in the asymmetric unit of the icosahedral capsid in our prior cryo-EM studies[141]. We cannot formally exclude a model where the capsid determinants act cooperatively to coordinate HD5 binding at the vertex, particularly since

the HAdV-5 hexon HVR1 loop is long enough to extend from the peripentonal hexons towards fiber. Although this would explain the relatively greater HD5 density on the peripentonal hexons of HAdV-5[141], in such a model it is harder to rationalize a role for the point mutation that arose in hexon HVR7 in the later rounds of selection or to explain the neutralization of naturally occurring HAdVs from other serotypes that lack long HVR1 loops[141]. Both models are also consistent with the phenotypes of the PB chimeras, where intermediate levels of neutralization result from a subset of the PB changes found in the C4 vertex. Further experimentation and extension of our studies to other HAdV serotypes will be required to resolve these possibilities, which are not mutually exclusive.

In summary, our studies of HD5 interactions with HAdV have generated a few major insights. First, HD5 can act as a selective pressure on the evolution of a non-enveloped virus. Second, HD5 can enhance the binding of HAdV to cells, even if the virus becomes neutralized downstream. Third, hexon is a key contributor to α-defensin interactions with AdV, and although the mechanism behind the HVRs' role in the interaction will require future investigation. Finally, our trafficking studies of viruses inhibited by HD5 under both protocol 1[128] and protocol 2 (Fig. 2-4 and [103,134]) support the conclusion that the outcome of blocking vertex dissociation is to prevent internalized HAdV from escaping the endosomal system and reaching the nucleus. Thus, we have extensively revised the prior model of HD5-mediated neutralization and established the feasibility of this process to shape viral evolution *in vivo*.

Chapter 3:
VP4 is a Determinant of Alpha-Defensin Modulation of Rotaviral Infection†

Introduction

In the previous chapter, I discussed the ability of human enteric α-defensins to select for the evolution of α-defensin-resistant human adenovirus *in vitro*[152]. α-defensin primary sequences, number of isoforms, and activity against specific microorganisms often vary greatly between species, reflecting adaptation to species-specific pathogens[167]. Therefore, α-defensins might influence not only microbial evolution and tissue tropism within a host but also species tropism and zoonotic potential.

Rotavirus infects a broad range of animals and is a leading cause of severe diarrhea in young children. Rotavirus has an 11-segment double-stranded RNA genome that is encapsidated in a triple-layered particle[74], with the outermost layer consisting of the protease sensitive spike protein (VP4) and calcium ion-stabilized trimers of the glycoprotein (VP7). VP4 matures following trypsin cleavage into VP5* and VP8*. VP5* makes up the foot and the stalk of the spike protein and is vital for membrane penetration. VP8* forms the head of the spike protein and is involved in viral attachment to its receptor, which is often a glycan[64]. Because of the segmented nature of the genome, reassortment of gene segments from multiple viruses infecting the same cell can give rise to progeny with mixed genomic compositions. This process contributes to rotaviral evolution and provides a powerful approach to investigate rotaviral genetics, particularly prior to the recent development of a tractable reverse genetics system[168].

---

† Adapted from Hu CT, Diaz K, Yang LC, Sharma A, Greenberg HB, and Smith JG. (2022) VP4 Is a Determinant of Alpha-Defensin Modulation of Rotaviral Infection. JVI 96(7): e02053-21.
Note this manuscript accounts for the correction of figure 5.

Like other fecal-oral pathogens, rotaviruses encounter abundant, constitutively expressed α-defensins in the small intestine. Despite rotaviruses being significant enteric pathogens, the lack of knowledge on their interaction with α-defensins unveils a notable gap in basic rotavirus biology. The only study thus far on the effects of defensins on infection by a *Reoviridae* family member found that reovirus type 3 is resistant to HNP1[108]. Given more recent examples of neutralization of non-enveloped viruses by α-defensins and the potential for enteric α-defensins to influence the evolution of fecal-orally transmitted viruses[109,113,152], we investigated how homologous (from the same species) and heterologous (from different species) α-defensins impact rotaviral infections. We generated a panel of enteric and myeloid alpha-defensins from humans, rhesus macaques, and mice and tested their activity against human (DS-1 and Wa), simian (RRV and SA11), and mouse (EDIM) group A rotaviruses.

Selection and purification of α-defensins for rotaviral studies

The α-defensin repertoire differs between species at both the genetic and protein levels, and there is considerable variability in the primary sequences of α-defensins despite the conservation of fold, disulfide bonding pattern, a salt bridge, and an invariant glycine (Figs 3-1 A and B) [169,170]. Humans have three genes that encode myeloid α-defensins (*DEFA1*, *DEFA3*, and *DEFA4*), but four distinct α-defensin proteins have been isolated (HNP1-4). In the human gut and genitourinary tracts, there is a predominant form of the products (HD5 and HD6) of each of the two enteric α-defensin genes (*DEFA5* and *DEFA6*), although additional cleavage products of HD5 have been identified[110]. Rhesus macaque myeloid (RMAD) and enteric (RED) α-defensins have not been investigated extensively. However, sequence analysis indicates that the 6-9 isoforms that have been

described for each subtype of α-defensin can be further subdivided into two groups (Fig 3-1 A)[171–173]. The mouse is even more complex, with an absence of intact myeloid α-defensin genes and a large number (>20) of enteric α-defensin genes, which vary by strain, leading to abundant expression of ~6 isoforms (called cryptdins, Crps) in the gut[174].

Because an exhaustive analysis of all human, rhesus, and mouse α-defensins was not feasible, we chose a subset for analysis in these studies. HNP1-3 vary by only the first amino acid and are much more abundant in neutrophils than HNP4, so we selected HNP1. HD5 was chosen because it has potent antiviral activity against multiple non-enveloped viruses, unlike HD6. Crp2 was chosen based on our prior analyses with mouse AdVs[153,154]. We chose abundant RMADs that are more (RMAD1) or less (RMAD4) similar in sequence to HNP1. Likewise, we chose REDs that are more (RED3) or less (RED1) similar in sequence to HD5. Due to our focus on an enteric virus, rhesus oral defensins were not included, however they have comparable sequences to RMAD4[172].

Two protocols have been described for the oxidative refolding of synthetic human α-defensins, one using guanidine hydrochloride for HNP4, HD5, and HD6[175] and the other using urea and *N*,*N*-dimethylformamide for HNP1-3[176]. We therefore chose a refolding protocol for the REDs, RMADs, and Crp2 based on sequence similarity to the human defensins. Upon purification by semi-preparative RP-HPLC, analytical RP-HPLC was consistent with high purity and homogeneity (Figs 3-1 C and D), and the measured masses of the refolded species indicated the formation of the expected three disulfide bonds (Fig 3-1 D). Although most of the refolded α-defensins had retention times between 25 and 30 min on the analytical C18 RP-HPLC column, we noted an unusually prolonged

retention time for RED1, which was consistent with prior studies[173]. Thus, we successfully generated purified α-defensins for further study.

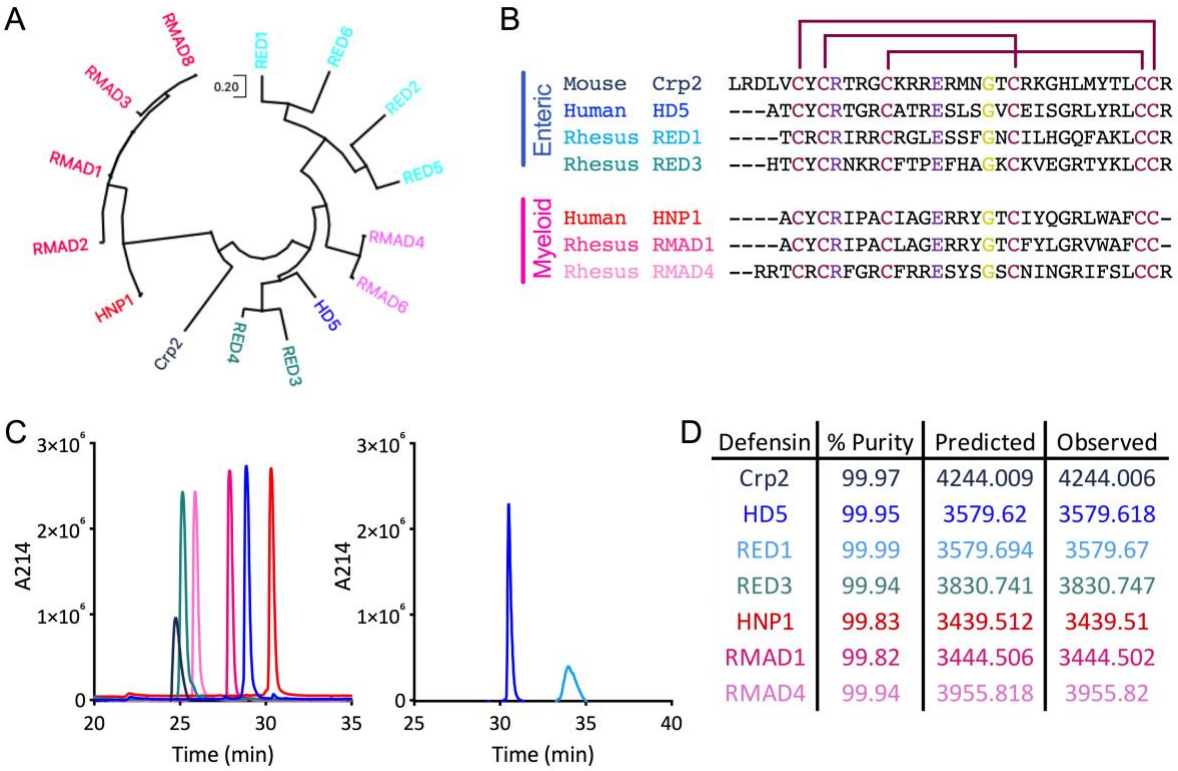

D

Defensin	% Purity	Predicted	Observed
Crp2	99.97	4244.009	4244.006
HD5	99.95	3579.62	3579.618
RED1	99.99	3579.694	3579.67
RED3	99.94	3830.741	3830.747
HNP1	99.83	3439.512	3439.51
RMAD1	99.82	3444.506	3444.502
RMAD4	99.94	3955.818	3955.82

Figure 3-1. Defensin refolding, sequences, and evolutionary relationships. (A) Dendrogram of mature protein sequences of rhesus enteric and myeloid α-defensins, one mouse enteric α-defensin (Crp2), and one each of the human enteric (HD5) and myeloid (HNP1) α-defensins. The evolutionary history was inferred by using the Maximum Likelihood method and JTT matrix-based model[177]. The tree with the highest log likelihood is shown. Initial tree(s) for the heuristic search were obtained automatically by applying Neighbor-Join and BioNJ algorithms to a matrix of pairwise distances estimated using the JTT model and then selecting the topology with superior log likelihood value. The tree is drawn to scale, with branch lengths measured in the number of substitutions per site. Evolutionary analyses were conducted in MEGA X[178]. (B) Amino acid sequence alignment of the mature α-defensin peptides used in this study. Enteric α-defensin names are written in shades of blue, while myeloid α-defensin names are written in shades of pink. Disulfide bond linkages are indicated by maroon lines. Residues that interact through a conserved salt-bridge are colored purple, and the conserved glycine is colored yellow. Dashes represent gaps. For A and B, accession numbers for defensin protein sequences are NP_066290 (HD5), P59665 (HNP1), AAW51365 (RED1), AAW51366 (RED2), AAW51367 (RED3), AAW51368 (RED4), AAW51369 (RED5), AAW51370 (RED6), AAF06312 (RMAD1), P82317 (RMAD2), AAF06313 (RMAD3), AAF06315 (RMAD4), AAF06316 (RMAD6), AAF06314 (RMAD8), and AAI25549 (Crp2). (C) Peptide samples were analyzed individually by RP-HPLC on a C18 column. Peaks are colored as in B. Peptides depicted on the same graph were analyzed sequentially on the same day. (D) Percent purity determined by the analyses in C as well as predicted and observed molecular masses determined by electrospray ionization are listed for each defensin. Peptide purification and analysis in C and D were done by Karina Diaz and Jason Smith.

Results

Rhesus rotavirus (RRV) is resistant to rhesus enteric alpha-defensins but neutralized by rhesus myeloid and human alpha-defensins

We tested the effects of the panel of purified α-defensins on RRV infection starting with the homologous defensins of rhesus macaques (RED1, RED3, RMAD1, and RMAD4). For these experiments, we incubated RRV with each α-defensin on ice before adding the mixture to MA104 cells. Based on our previous studies of α-defensin interactions with mouse and human AdVs[103,128,141,150,152–154,164], we defined three phenotypes of defensin effects on infection relative to control infection in the absence of defensin: neutralization (0% to 49%), resistance (50% to 199%), and enhancement (≥200%). RRV was potently neutralized by both rhesus myeloid α-defensins, RMAD1 (IC_{50} = 9.1 μM, 95% CI = 7.4-11.6 μM, Hill slope = -4.6) and RMAD4 (IC_{50} = 6.0 μM, 95% CI = 5.2-7.0 μM, Hill slope = -2.2), with an almost complete block of infection in the presence of 20 μM defensin (Figs 3-2 C and D). However, RRV was resistant to both rhesus enteric α-defensins, RED1 and RED3, up to the highest concentration tested (40 μM) (Figs 3-2 A and B, solid lines).

To our knowledge, there is only one report describing bactericidal properties of RED1 and RED3[173] and none that have investigated their antiviral capabilities. Therefore, to ensure that RED1 and RED3 are functional, we tested their activity against another non-enveloped virus, human papilloma virus 16 (HPV16). Like prior studies with human defensins[129,135,161,162,164], HPV16 was potently neutralized by both RED1 (IC_{50} = 10.7 μM, 95% CI = 9.4-12.1 μM, Hill slope -2.8) and RED3 (IC_{50} < 5 μM), demonstrating that RED1 and RED3 can be antiviral (Fig 3-2 H).

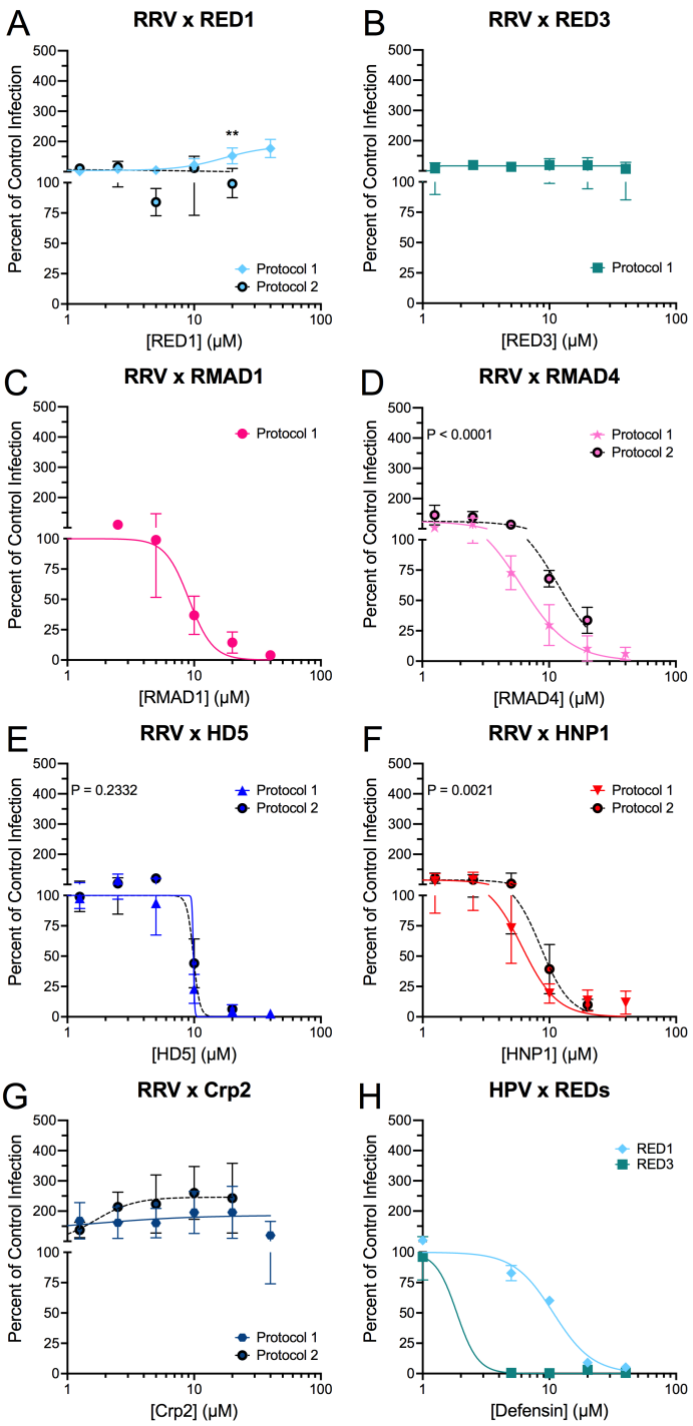

Figure 3-2. RRV is selectively resistant to homologous enteric alpha-defensins. RRV was incubated with the indicated concentrations of (A) RED1, (B) RED3, (C) RMAD1, (D) RMAD4, (E) HD5, (F) HNP1, or (G) Crp2 before infecting MA104 cells (Protocol 1; solid, colored lines). For Protocol 2 (dotted, black lines with filled circles), RRV was bound to cells in the cold prior to defensins being added (A and D-G). (H) HPV16 pseudovirus infection was measured in the presence of RED1 and RED3 following protocol 1.

Fig. 3-2 (continued): Data are normalized to infection in the absence of defensin (control infection) and are the mean ± SD of at least 3 individual experiments.

Next, we tested the effects of heterologous α-defensins from humans and mice on RRV infection. Although HD5 and RED3 cluster together phylogenetically and are 56% identical (Figs 3-1A and 3-1B), RRV is completely neutralized by 20 μM HD5 (IC_{50} = 8.1 μM, lower 95% CI = 7.1 μM, Hill slope = -5.7; Fig 3-2 E, solid line). Similarly, the heterologous myeloid α-defensin, HNP1, strongly neutralizes RRV (IC_{50} = 6.1 μM, 95% CI = 5.4-6.9 μM, Hill slope -3.1; Fig 3-2 F, solid line). Thus, our data are consistent with the hypothesis that selective pressure during fecal-oral transmission among rhesus hosts has pressured RRV to evolve resistance to rhesus enteric α-defensins (RED1 and RED3) but not rhesus myeloid α-defensins or heterologous α-defensins (RMAD1, RMAD4, HD5, and HNP1). The only exception to this trend is the resistance of RRV to mouse Crp2 (up to 40 μM, Fig 3-2 G).

The non-human primate rotavirus SA11 has an infectivity phenotype like that of RRV in the presence of alpha-defensins

SA11 is a widely studied group A rotavirus strain that was originally isolated from the vervet monkey, *Chlorocebus pygerythrus*[179]. A detailed analysis of the sequences and relative expression of α-defensins of *C. pygerythrus*, which is estimated to have diverged from macaques 12 million years ago[180], has not been published. Therefore, we did not examine defensin peptides from this species. Nonetheless, we tested the effects of our panel of defensins on SA11 infection. Like RRV, SA11 was resistant to RED1 and RED3 (Figs 3-3 A and B) and neutralized by RMAD1, RMAD4, HD5, and HNP1 (Figs 3-3 C-F). However, the IC_{50} values of RMAD1, RMAD4, HD5, and HNP1 for SA11 infection were 1.3- to 3.0-fold greater than those for RRV. The Hill slopes for RMAD1 and RMAD4 were

similar to those for RRV; however, they differed for HD5 (-4.7 for SA11 vs -5.7 for RRV) and HNP1 (-1.5 for SA11 vs -3.1 for RRV). And, unlike the resistance of RRV, Crp2 reduced the infectivity of SA11 at 40 μM, although inhibition was less than 40% (Fig 3-3 G). Thus, the effects of α-defensins on RRV and SA11 are comparable but not identical, and the high similarity between RRV and SA11 proteins may facilitate future mapping of viral determinants of α-defensin activity.

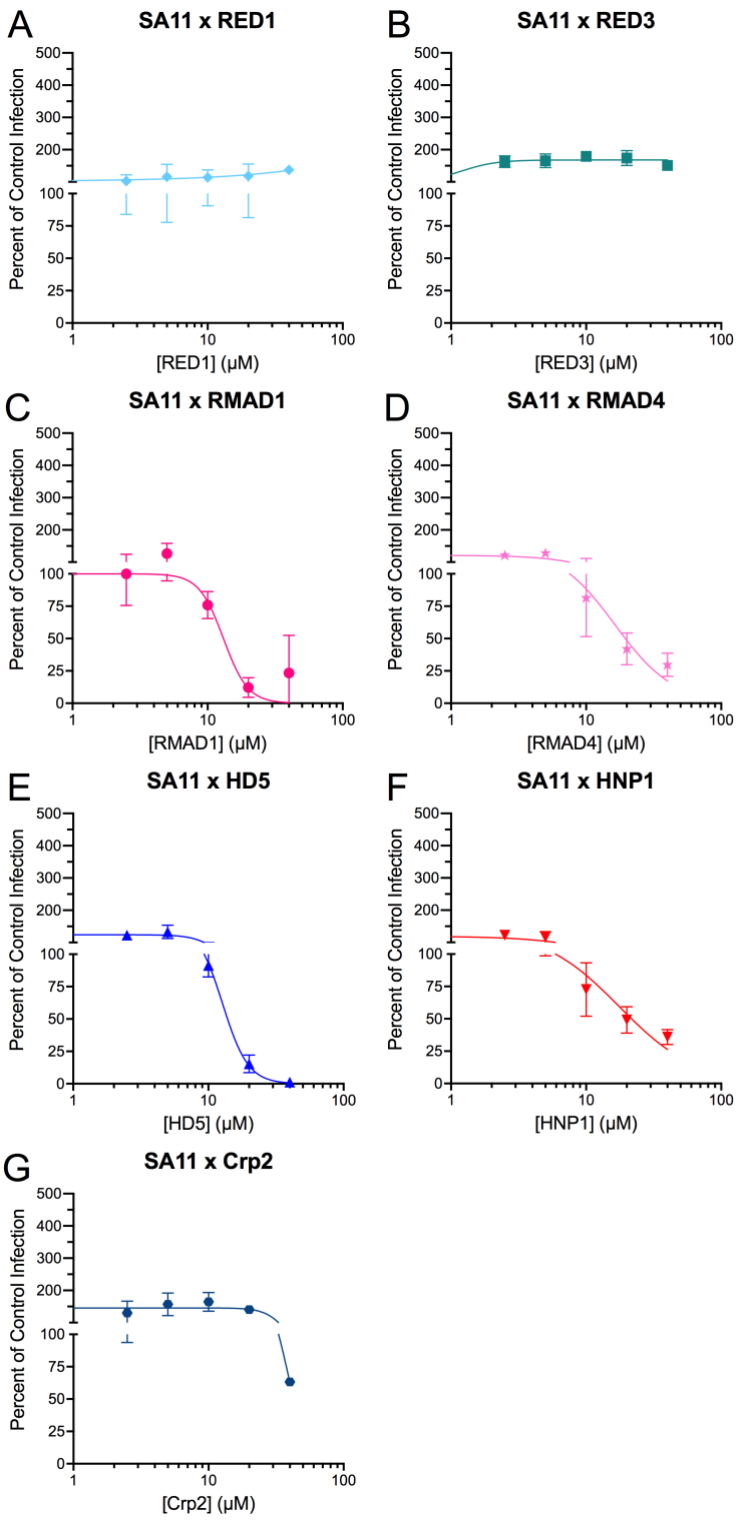

Figure 3-3. SA11 has a similar phenotype to RRV. SA11 was incubated with the indicated concentrations of (A) RED1, (B) RED3, (C) RMAD1, (D) RMAD4, (E) HD5, (F) HNP1, or (G) Crp2 before infecting MA104 cells (Protocol 1). Data are normalized to infection in the absence of defensin (control infection) and are the mean ± SD of at least 3 individual experiments.

Infectivity of mouse and human rotaviruses is either enhanced by or resistant to homologous enteric alpha-defensins

To investigate the generalizability of our finding that group A rotaviruses are resistant to homologous enteric α-defensins but sensitive to myeloid and heterologous α-defensins, we expanded our analyses to both mouse and human group A rotaviruses. Infection by a mouse rotavirus, EDIM, was enhanced in the presence of the homologous enteric α-defensin, Crp2, with 3- to 4-fold increased infection in the presence of >20 μM Crp2 (Fig 3-4 G, solid line) compared to control. This is consistent with the possibility that selective pressure led to EDIM appropriating Crp2 to increase its infectivity. However, among the heterologous α-defensins, EDIM was neutralized by HNP1 (IC_{50} = 12.4 μM, 95% CI = 7.7-22.8 μM, Hill slope = -2.5) and enhanced 2- to 4-fold by all other α-defensins (Figs 3-4 A-F, solid lines).

The prototype strains of two of the more prevalent rotavirus A genogroups that infect humans, DS-1 and Wa, had different phenotypes in the presence of α-defensins. DS-1 resembled EDIM in that it was enhanced by all α-defensins to varying degrees (Fig 3-5, open symbols with dotted lines). The >9-fold increase in infection in the presence of 40 μM HD5 was particularly striking (Fig 3-5 E), and the bi-phasic effect of RED3 was unusual but reproducible (Fig 3-5 B). In contrast, Wa was resistant to HD5, RED1, RED3, RMAD4, and Crp2. Wa was weakly neutralized by RMAD1 (IC_{50} = 10.9 μM, Hill slope = -1.3), and its infectivity was reduced by HNP1 at 40 μM, although inhibition was highly variable and less than 50% for HNP1 (Fig 3-5, filled symbols and solid lines). Thus, a clear distinction between the activity of homologous and heterologous α-defensins, like we observed for RRV, was not apparent for EDIM, DS-1 or Wa.

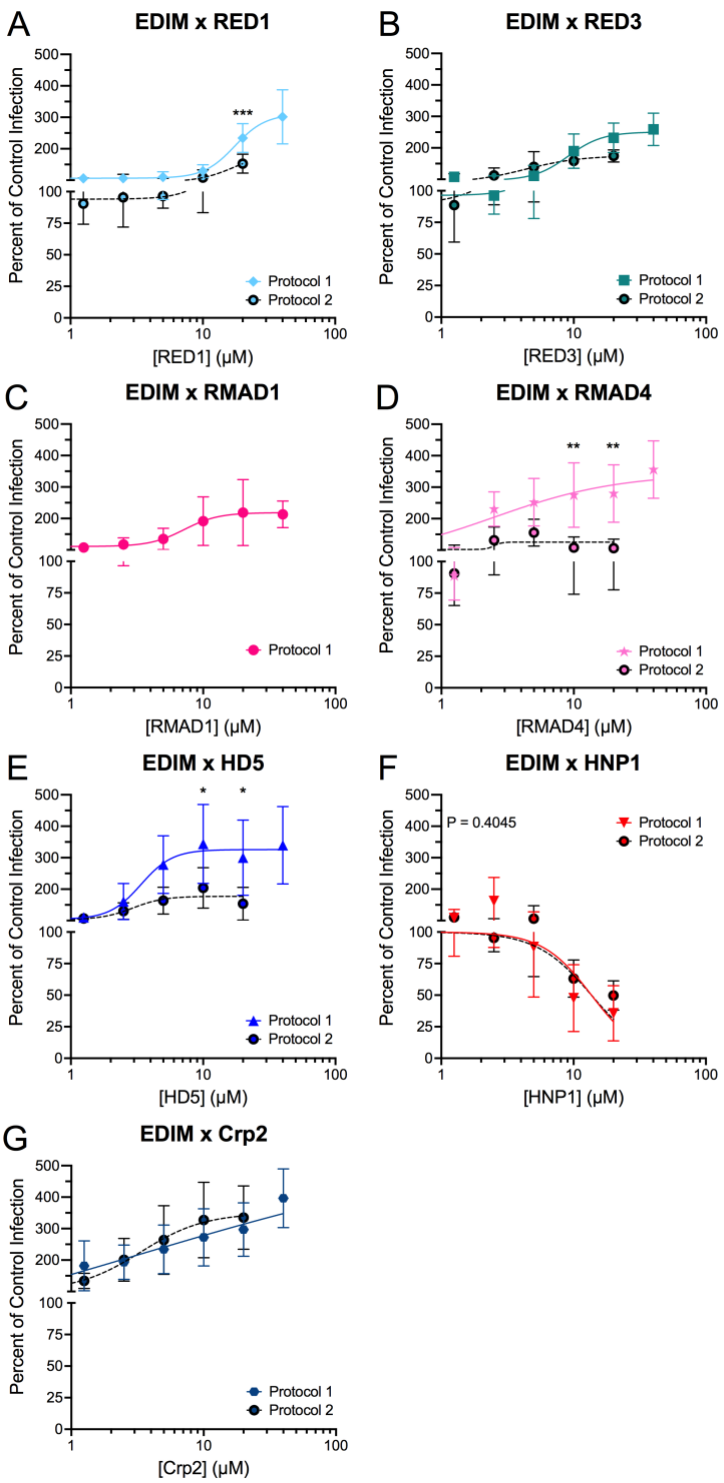

Figure 3-4. EDIM is enhanced by most defensins. EDIM was incubated with the indicated concentrations of (A) RED1, (B) RED3, (C) RMAD1, (D) RMAD4, (E) HD5, (F) HNP1, or (G) Crp2 before infecting MA104 cells (Protocol 1; solid, colored lines). For Protocol 2 (dotted, black lines with filled circles), EDIM was bound to cells in the cold prior to defensins being added (A, B, and D-G). Data are normalized to infection in the absence of defensin (control infection) and are the mean ± SD of at least 3 individual experiments.

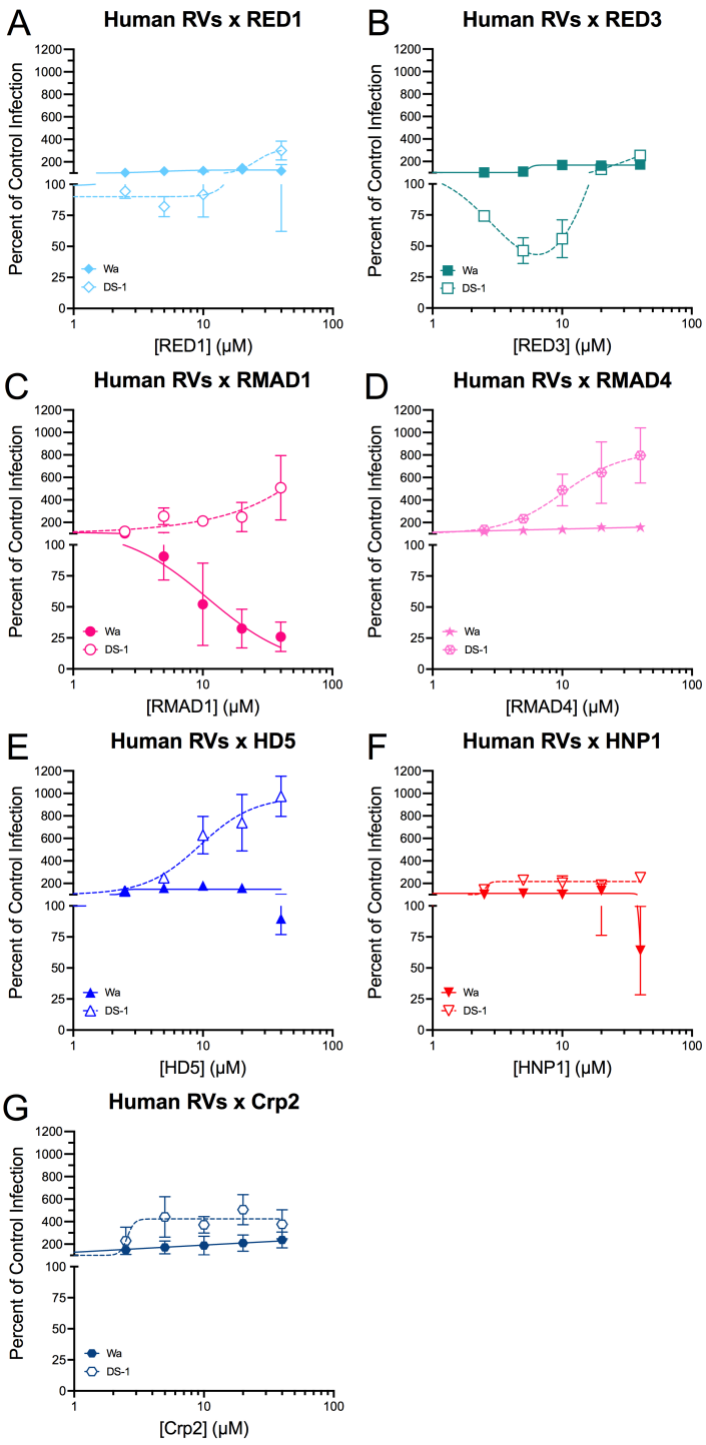

Figure 3-5. DS-1 and Wa have different sensitivities to defensins. DS-1 (open symbols) and Wa (filled symbols) were incubated with the indicated concentrations of (A) RED1, (B) RED3, (C) RMAD1, (D) RMAD4, (E) HD5, (F) HNP1, or (G) Crp2 before infecting MA104 cells (Protocol 1). SA11 (gray "x" symbols), which was the contaminant of our original Wa stock, was assayed concurrently with Wa, and the data are independent of the data in Fig. 3. Data are normalized to infection in the absence of defensin (control infection) and are the mean ± SD of at least 3 individual experiments.

Order of addition does not substantially alter the effects of alpha-defensins on rotaviral infection

We previously found that the order of addition of α-defensin and virus to the cell can have a dramatic effect on the outcome of human AdV infection[152]. The data in the prior sections of this chapter were generated by exposing the virus to defensin before the virus was added to cells (protocol 1). To test if the order of addition affects the outcome of the interaction, we re-examined a subset of the α-defensin/rotavirus combinations by binding the virus to MA104 cells before adding α-defensin (protocol 2). Under these conditions, RRV is less sensitive to the myeloid defensins RMAD4 (Fig 3-2 D, IC_{50} = 11.8 μM in protocol 2 vs. 6.0 μM in protocol 1) and HNP1 (Fig 3-2 F, IC_{50} = 8.5 μM in protocol 2 vs. 6.1 μM in protocol 1). For the enteric defensins, Crp2 became weakly enhancing (Fig 3-2 G), while there were only minor differences between protocol 1 and 2 for RRV infection with RED1 and HD5 (Figs 3-2 A and E).

For human AdV, we found that some enhanced viruses in protocol 1 became neutralized in protocol 2[152]. We therefore compared protocol 1 to protocol 2 for EDIM, which is enhanced by some α-defensins, using most of our α-defensin panel (Fig 3-4, black dotted lines). Neutralization of EDIM by HNP1 was protocol-independent (Figs 3-4 F). In contrast, EDIM was no longer enhanced but became resistant to RED1, RED3, RMAD4 and HD5 under protocol 2 (Figs 3-4 A, B, D, and E). Interestingly, like for RRV, Crp2 enhanced EDIM infection in protocol 2 to an even greater extent than protocol 1 (Fig 3-4 G). Therefore, pre-binding the virus to the cell before adding α-defensins only abrogates defensin-dependent enhancement, although Crp2-mediated enhancement

was unaffected. We did not observe any protocol-dependent changes from an enhanced to a neutralized phenotype, unlike what was observed for human AdVs.

VP4 is a determinant for alpha-defensin activity

To identify a viral determinant for α-defensin activity, we interrogated a previously characterized panel of reassortant viruses between RRV and EW, a wild type murine strain that has not been adapted to cell culture (Fig 3-6 B)[181,182]. As a control, we included a cell culture-adapted derivative of EW, ETD. ETD is enhanced by HD5 and RMAD1, while RRV is neutralized by those α-defensins (Fig 3-6 A). The reassortant viruses D1/5, EA 4-1-2, and B7/2 were all neutralized, like RRV, rather than enhanced, like ETD, by both HD5 and RMAD1 (Fig 3-6 C-E). Because these reassortant viruses have several RRV gene segments in common, we tested an additional virus, D6/2, in which only the VP4 gene segment is derived from RRV. This virus was also neutralized by both HD5 and RMAD1 (Fig 3-6 F); therefore, substituting the RRV VP4 gene segment for that of ETD is sufficient to alter the infection phenotype of the virus in the presence of HD5 and RMAD1. To extend these findings, we tested additional myeloid and enteric α-defensins and found that D6/2 uniformly mimics the RRV phenotype (Fig 3-6 G-H), although the effect of Crp2 on D6/2 was intermediate between the resistance of RRV and the enhancement of EDIM.

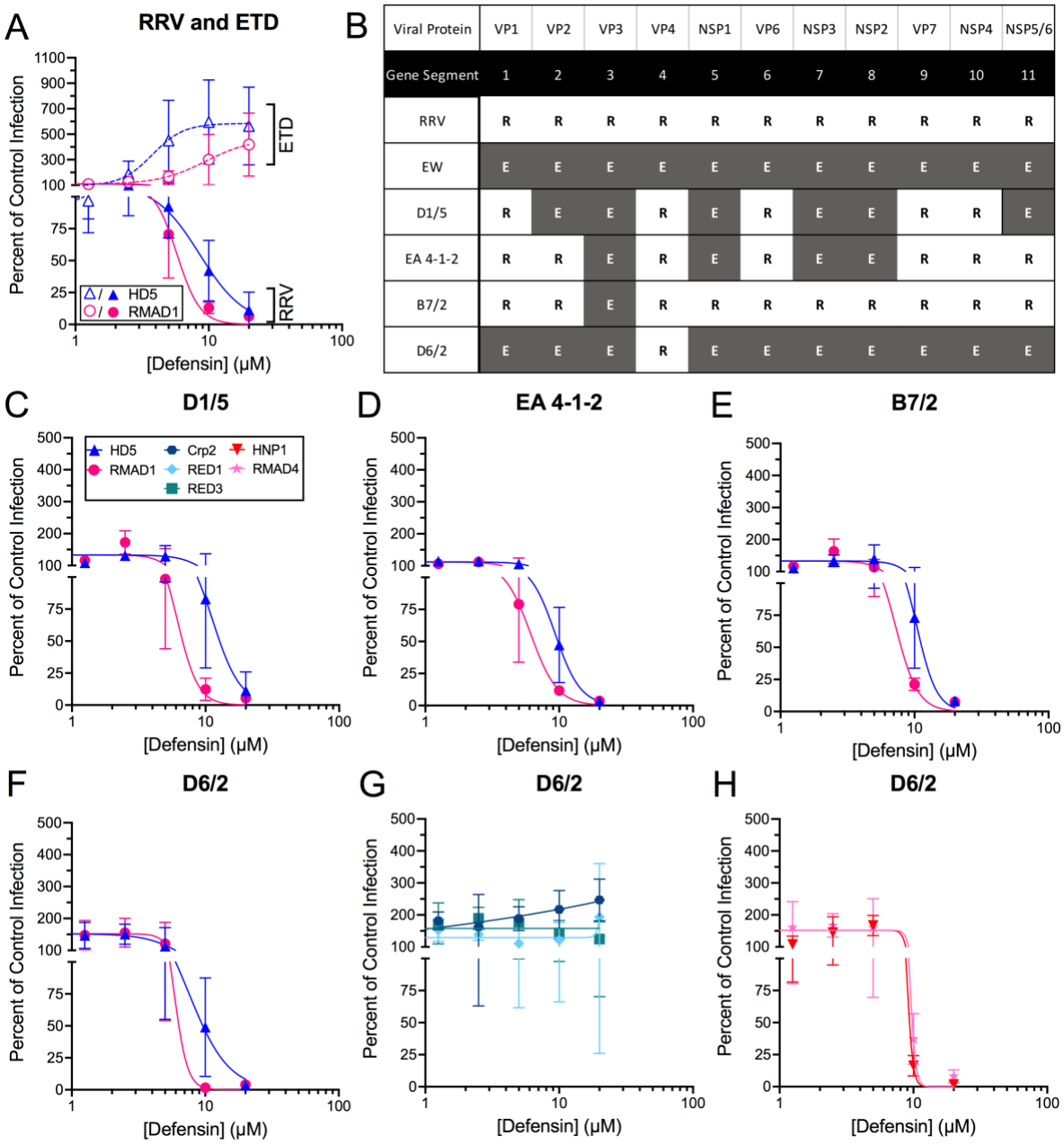

Figure 3-6. VP4 is a determinant of defensin neutralization. (A) ETD, a culture-adapted strain of murine rotavirus EW, (open symbols) and RRV (closed symbols) infection in the presence of HD5 or RMAD1. Note that the RRV data are independent of the data in Fig 2. (B) Genetic composition of reassortant viruses between RRV (R, white boxes) and the murine rotavirus, EW (E, gray boxes). (C-F) Infection of the indicated reassortant viruses in the presence of HD5 or RMAD1. (G) D6/2 infection in the presence of enteric α-defensins, Crp2, RED1, or RED3. (H) D6/2 infection in the presence of myeloid α-defensins, HNP1 or RMAD4. All viruses were incubated with defensins before infecting MA104 cells (Protocol 1). Defensins in C-H are denoted by the key in C. Data are normalized to infection in the absence of defensin (control infection) and are the mean ± SD of at least 3 individual experiments.

An additional reassortant virus was generated by Yiyu Sun that had the simian rotavirus, SA11, backbone with the VP4 encoding gene segment from the mouse rotavirus, EDIM. She observed that infectivity of the reassortant virus was enhanced by the presence of RMAD4 and HNP1, unlike the parental SA11 strain (unpublished, data not shown). In summary, these data strongly support the identification of VP4 as a determinant for neutralization and enhancement for multiple α-defensins.

Discussion:

Enteric α-defensins are important for host immunity against enteric pathogens and influence the composition of the intestinal microbiome[183]. Comparative genetic studies suggest that differences in the primary sequences and number of isoforms of defensins between species reflect adaptation to pathogens during evolution[170]; however, studies that directly compare the effects of heterologous and homologous α-defensins on viral infection are limited. Our approach to investigate a panel of α-defensins from multiple host species led to several important insights. We found that RED1, RED3, RMAD1, and RMAD4 are all capable of inhibiting the infection of at least one type of non-enveloped virus. Prior studies of the antiviral capabilities of rhesus α-defensins identified RMAD4 as having anti-HIV properties while RMAD3 did not[184]; however, both RMAD1, which differs from RMAD3 by only two residues (L22R and G23R), and RMAD4 were largely equivalent in our assays with the exception of Wa being neutralized by RMAD1 and resistant to RMAD4. They were also both comparable to HNP1 for RRV and SA11; however, both RMADs enhanced EDIM/ETD to varying degrees, while HNP1 was neutralizing, and both RMADs were much more enhancing than HNP1 for DS-1. The similar activity of these myeloid α-defensins is remarkable given that RMAD4 differs substantially in linear

sequence from RMAD1 and HNP1 (36.7% identical to each), which are themselves quite closely related (86.7% identical). Among the enteric α-defensins, HD5 and RED3 (56% identical) have different effects on RRV, SA11, and DS-1. Conversely, both REDs were largely equivalent for all viruses despite being only 48.4% identical, and HD5 and Crp2 are 46.9% identical but similarly enhance EDIM infection. Thus, α-defensin antiviral activity cannot be easily predicted by sequence nor the degree of positive charge; however, the activities identified here inform the design of α-defensin mutants to dissect the features of α-defensins that dictate their effects on rotaviral infection.

A key finding of our study is that VP4, the viral attachment and membrane penetrating protein, can dictate the neutralizing activity of α-defensins on rotaviral infection. Although we have not formally excluded a cellular target for α-defensin activity that determines the outcome of infection, the importance of VP4 strongly suggests that defensin binding to the virus and not the cell is critical. Such a mechanism would also be consistent with defensin-dependent mechanisms that we and others have determined for a wide range of non-enveloped viruses[109,113,126,133]. Moreover, like for other non-enveloped viruses, our data show that α-defensins impact rotaviral entry upstream of VP6 translation, which we used to quantify infection. Mechanistically, α-defensins could directly compete with VP4 for receptor binding, although receptor competition has not been documented for other non-enveloped viruses. However, our use of rotaviruses with differing receptor specificities[64], which is mediated by VP8*, argues against receptor competition as a mechanism. Alternatively, defensin-mediated aggregation, although not inherently neutralizing, could have the effect of reducing the total number of cells that are infected; however, this is an unlikely mechanism for neutralization of rotavirus, since

binding RRV to cells prior to the addition of RMAD4, HD5, or HNP1 (protocol 2) did not circumvent aggregation and rescue infection. α-Defensins could also modulate membrane penetration mediated by VP5*, either directly or indirectly, thereby blocking infection. Because VP4 determines the cellular entry pathway and subcellular compartment from which rotavirus escapes into the cytosol[86], defensin-bound VP4 may direct the virus into a non-permissive cellular pathway that does not trigger VP5*-mediated membrane penetration. Alternatively, defensin interactions with the host membrane in a rotavirus-containing compartment could disrupt cellular factors needed to trigger uncoating, such as calcium levels[81,86]. This would effectively convert a permissive pathway into a non-permissive pathway. More directly, α-defensins could perturb the conformational changes in VP5* or block access of VP5* loops to the membrane that are required for membrane penetration[74].

Although our use of viral strains is somewhat broad, one caveat of our studies is that they are limited to MA104 cells. Rotaviral entry remains incompletely understood, cell- and strain-specific entry mechanisms have been reported, and the nature of the membranous compartment that is penetrated by VP5* has not been definitively identified[74,86]. Thus, confirming these findings in other cell types, particularly more relevant intestinal cells, is needed. At the same time, the study of α-defensins as novel inhibitors may provide valuable tools to dissect entry mechanisms. Prior studies of α-defensin interactions with non-enveloped viruses have focused on DNA viruses, where we and others have observed alterations in intracellular trafficking in the presence of defensins that preclude the genomes of AdVs[103,128,134,152], polyomaviruses [132], and papillomaviruses[129,135,161] from reaching the nucleus. Rotavirus is the first non-enveloped

virus that replicates in the cytoplasm to be shown to be neutralized by α-defensins. The intracellular routes of RNA viral genomes to reach their replicative niche are different than those of DNA viruses, and additional studies of rotavirus may reveal novel defensin-dependent mechanisms.

Although our data strongly point to VP4 as a critical determinant for neutralization, we considered other possible mechanisms. The steepness of the Hill slopes of the inhibition curves suggests cooperative binding, which differs between defensin/virus combinations and may reflect the involvement of additional binding partners on the viral capsid. VP7 makes up the facets of the outer layer of the capsid, which become destabilized during internalization in part due to the loss of Ca^{2+} [59]. Thus, α-defensins could block infection by crosslinking or stabilizing VP7 trimers, as has been observed for neutralizing antibodies[59], or by bridging a VP4-VP7 interaction, thereby constraining VP5 and preventing uncoating and membrane penetration. Because there is some evidence that α-defensins function as lectins[109,169] and because VP7 is a glycoprotein, a mechanism that involves both a protein-protein interaction with VP4 and a lectin-glycan interaction with VP7 is plausible. EDIM and RRV VP7 differ not only in sequence but also in N-linked glycosylation. However, the one N-linked glycosylation site on RRV VP7 (N69) is conserved between them and is not surface accessible in intact virus. Thus, involvement of VP7 in the VP4-dependent neutralization mechanism through strain-specific glycans is still formally possible but unlikely.

We also observed that VP4 is a determinant for defensin-mediated enhancement. A likely mechanism for enhanced infection is that the defensin/virus interaction leads to enhanced cell binding. This would in turn lead to increased uptake and infection if the

virus enters a cellular pathway conducive to uncoating and membrane penetration. We have previously reported enhanced cell binding of both mouse and human AdVs, even for defensin/virus combinations that result in neutralized infection (Fig. 2-2)[103,141,152]. Increased cell binding mediated by α-defensins is consistent with the marked loss of enhancement when EDIM is bound to cells prior to the addition of RMAD4 and HD5 (protocol 2) compared to when defensin/virus complexes are added to cells (protocol 1). However, we note that Crp2 still potently enhances EDIM under protocol 2, perhaps due to Crp2 reducing the off-rate of the virus-receptor interaction. Increased association of the virus and cell in the presence of defensin need not be mediated by VP4-receptor interactions but could be a result of defensins bridging the virus and cell through binding to cellular proteins, glycans, or the lipid bilayer. For example, DS-1 has a surface exposed glycosylation site on VP7 (N146), located in the middle of the VP7 trimer, that is not present in the other viruses studied in this paper. A defensin dimer could bind atop the VP7 trimer and bridge defensin-specific receptor interactions. Alternatively, the α-defensin could augment VP5*-dependent membrane penetration, leading to more efficient escape into the cytosol. The nature of α-defensin interactions with cells that enhance viral and bacterial infection remains elusive, and further studies of enhanced rotaviral infection may provide critical insight. Moreover, the mechanisms for enhancement and neutralization are not mutually exclusive. Thus, resistant viruses may contain VP4 proteins to which specific α-defensins cannot bind or could reflect a balance between these putative enhancement mechanisms and one or more of the neutralization mechanisms described above.

Based on our prior studies of mouse and human AdVs and consistent with early studies of α-defensin interactions with non-enveloped viruses, we hypothesized that the resistance of fecal-orally transmitted viruses reflects evolution driven by defensins. By this process, the virus evolves to be resistant to or enhanced by the constitutively expressed enteric α-defensins of its host while remaining susceptible to neutralization by myeloid α-defensins[152,154]. Our analysis of RRV, Wa, and to some extent EDIM and DS-1, supports this hypothesis. Furthermore, the differential effects of HD5 on Wa (G1P[8]), DS-1 (G2P[4]), and animal rotaviruses in combination with variation in HD5 expression could potentially contribute to the epidemiology of human rotaviruses. While human Paneth cells develop during gestation[185], the global variance in the level of HD5 expression is not known, and differences in HD5 mRNA expression in specific populations because of nutritional state, body mass index, and enteropathy have been described[186–188]. Because the relative prevalence of Wa-like versus DS-1-like genotypes varies over time and location in the human population, it is difficult to determine if the resistance of P[8]-containing viruses or enhancement of P[4]-containing viruses by HD5 is consequential. In addition, circulating P[8] (and presumably P[4]) strains have evolved compared to the original Wa P[8] that we studied and may no longer be just resistant to HD5[189]. Furthermore, the variation in HD5 expression combined with the differential effects of HD5 on animal strains could modulate susceptibility to zoonotic rotaviral infection. Finally, HD5 may impact vaccine efficacy. The Rotarix vaccine and one component of the RotaTeq vaccine both contain G1P[8]. The effect of HD5 on the P[5] VP4 of the remaining four components of the RotaTeq vaccine remains to be determined.

Therefore, a more expansive analysis of strains differing by VP4, including clinical isolates, is warranted.

In summary, we examined the effects of α-defensins–homologous and heterologous, enteric and myeloid–on rotaviral infections. We found that many group A rotaviruses are resistant to or enhanced by enteric α-defensins from their host species. Although the exact mechanisms of enhancement and neutralization are yet to be uncovered, identification of VP4 as a determinant for both defensin-mediated neutralization and enhancement in addition to elucidation of the differential activities of α-defensins will focus future efforts to understand the molecular properties of both partners that dictate the outcome of the interaction.

Chapter 4:
Mutations in VP4 drive rotaviral resistance to neutralization by alpha-defensins

Introduction

From our work with HAdV, we know that rational design and directed evolution can identify different determinants of defensin-mediated neutralization (chapter 2)[152]. Up to now our data supports only VP4 being the rotaviral protein influencing the infectivity phenotype upon defensin treatment. However, our approach thus far has used whole gene segment reassortants which are limited by the combinations possible and reassortant recovery. Similar to how hexon was found to be a determinant of neutralization for HAdV via directed evolution[152], perhaps VP7, which makes up the facets of the rotaviral capsid, could be involved in defensin-mediated neutralization or enhancement. Additionally, using a directed evolution approach may uncover which parts of VP4 are important for defensin interactions. VP4 is proteolytically cleaved into VP8* and VP5*, which are involved in cell attachment and membrane penetration, respectively. Knowing which protein fragment and which amino acid residues change under defensin pressure can provide insight into defensin's mechanism of action on rotavirus.

To investigate how defensins can influence the evolutionary trajectory of a rotavirus, we serially passaged a reassortant rotavirus, composed of the gene segments encoding the outer proteins (VP4 and VP7) from RRV and the remaining nine gene segments from SA11, under increasing pressure from rhesus myeloid alpha-defensin 1 (RMAD1). Whole genome sequencing of the virus evolved under RMAD1 pressure

revealed that most of the mutations were in VP8*. Investigation of these mutations revealed that the surface accessible mutations in both the stalk part and the galectin-like domain of VP8* contributed to RMAD1 resistance. Interestingly, we observed that some, but not all, defensin resistance mutations may alter receptor usage. Surprisingly, RMAD1 does not inhibit viral binding to the cells and may promote cellular attachment instead. Our results reemphasize the ability of defensins to drive viral evolution as well as the utility that directed evolution can provide in uncovering the mechanisms by which defensins can modulate rotaviral infection.

Results

Evolution of RMAD1 resistance in a SA11 x RRV reassortant rotavirus.

For selection, we generated a SA11 virus that has the outer layer proteins, VP4 and VP7, originating from RRV (**SR-WT**). This decision was driven in part by the high rescue efficiency of SA11 in the plasmid-based reverse genetics system, which facilitated downstream investigation of mutations that arose during the selection process, as well as a desire to match the outer layer proteins to a neutralizing homologous defensin. SR-WT was passaged 5 times to allow any compensatory mutations that might be needed to accommodate the SA11 VP6 and RRV outer protein interfaces as well as generate a more diverse starting population. The RMAD1 IC_{90} for SR-WT was assessed (Fig 4-1, gray circles; IC_{90}, ~11 μM) and then the virus was serially passaged under approximate RMAD1 IC_{90} pressure. After each passage the infectious titer of the virus was determined so that a similar MOI would be achieved upon each round of passaging. Additionally, its RMAD1 IC_{90} was revaluated every 1 to 2 passages, and the concentration of RMAD1 was adjusted as needed to keep a similar

selective pressure on the evolving viruses (Fig 4-3). Passaging was terminated when the RMAD1 IC_{90} was > 40 µM. This evolution process was repeated for a total of 3 replicates. Replicate 1 was stopped after 13 passages under selective pressure (Fig 4-1 A; IC_{90}, 81 µM), replicate 2 after 9 passages (Fig 4-1 B; IC_{90}, 55.9 µM), and replicate 3 after 8 passages (Fig 4-1 C; IC_{90}, 50 µM). A no defensin pressure (**n.p.**) passaging control was done in parallel with each replicate, and its RMAD1 IC_{90} barely changed (Fig 4-1 D).

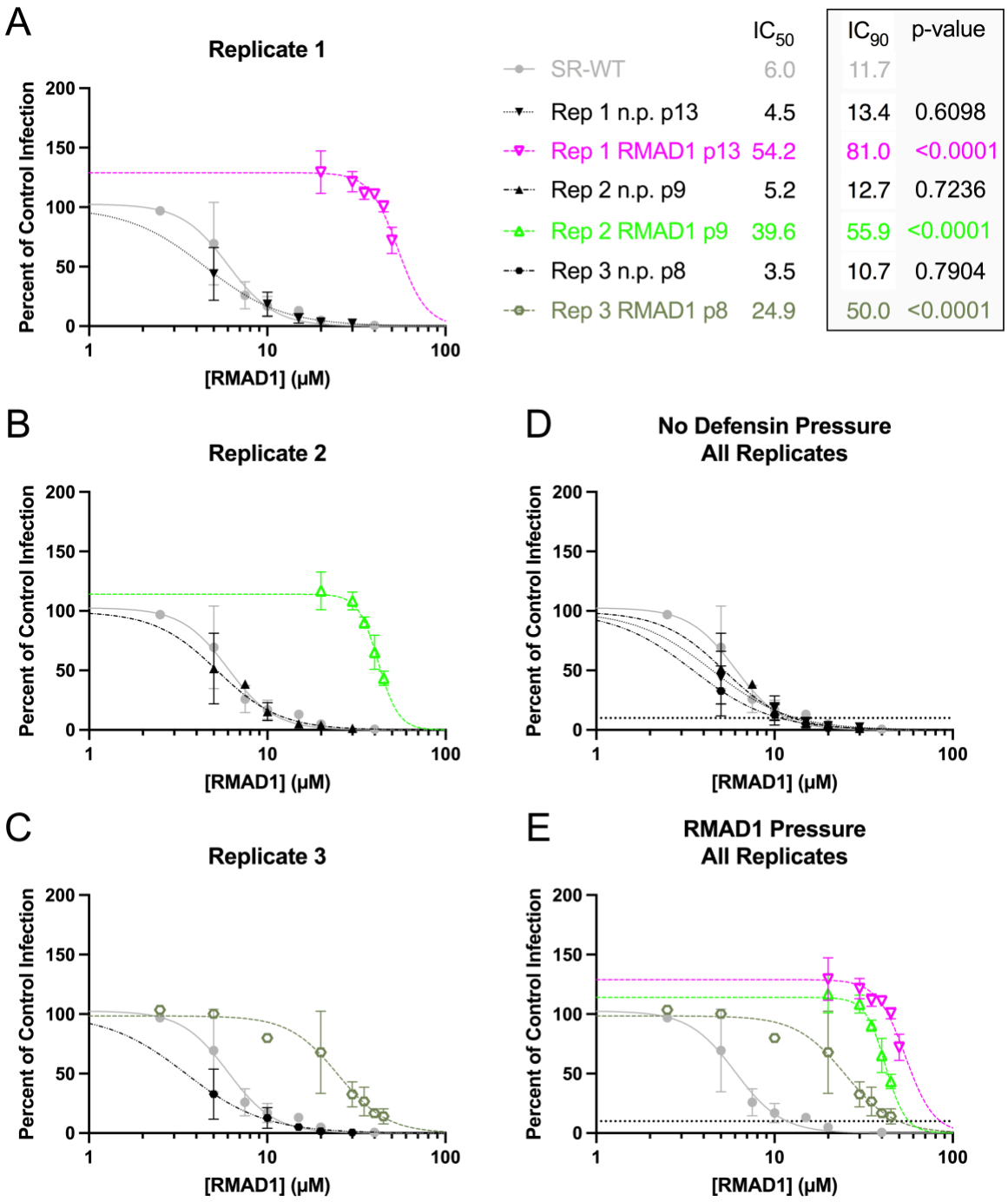

Figure 4-1: Defensin phenotypes of bulk passaged virus versus parental virus. A-C) The effect RMAD1 has on the infectivity of the final passages of the evolution process for both RMAD1 pressure (colored dashed lines, Replicate 1, magenta inverted triangles; Replicate 2, bright green triangles; Replicate 3, camo green hexagons) and no defensin pressure (Replicate 1, black inverted triangles on a dotted line; Replicate 2, black triangles on a dashed line with a single dot; Replicate 3, black hexagons on dashed line with double dots) was evaluated. A parental SR-WT virus is included on each graph for demonstrative purpose.

Fig. 4-1 (continued): D) A compilation of the no defensin pressure's final passage of each replicate plus the parental SR-WT (gray circles) and the first passage of Replicate 1's no defensin pressure (dark gray, inverted triangles). E) A compilation of the RMAD1 pressure's final passage of each replicate plus the parental SR-WT (gray circles). A dotted line at 10% of control infection is added in D and E. Note the SR-WT data is the same on every graph, and panels D and E used the same data that is displayed in panels A-C. For SR-WT, n=2 at 2.5 and 40 μM RMAD1. For Rep 1 RMAD1 p13 at 20 and 50 μM RMAD1, n=2. For Rep 3 RMAD1 p8 at 2.5-10 μM RMAD1, n=1. Data are normalized to infection in the absence of defensin (control infection) and are the mean ± SD of at least 3 individual experiments unless otherwise noted. The P values from comparing the log IC_{90} values between SR-WT and VP4 mutant rotaviruses using the extra sum-of-squares F test is provided.

The lysate of every odd passage, plus the final passage in replicate 3, was whole genome sequenced and compared to the SR-WT p5 starting population for both the RMAD1 pressure and the no defensin pressure (**n.p.**) conditions. Of note, we found most of the high allele frequency (**AF**) mutations in VP4, and surprisingly no mutations in VP7 (Fig. 4-2), consistent with our data from whole gene segment reassortants. At the final passage for the RMAD1 pressure condition, the VP4 mutations L37P (Rep 1 AF, 82%; Rep 2 AF, 82%; Rep 3 AF, 69%), Y155H (Rep 2 AF, 75%), V184A (Rep 1 AF, 98%), and I575L (Rep 3 AF, 77%) were present at high frequency. We also observed that in replicate 2, K187R rose to prominent AF by passage 7 (53%), but then dropped to an almost undetectable AF (2%) by passage 9 (Fig 4-3). Curiously, we also identified VP4 mutations that only arose during the n.p. conditions, such as V78L (Rep 1 n.p. AF, 86%; Rep 2 n.p. AF, 47%) and V93A (Rep 3 n.p. AF, 75%).

Although we found no mutations in proteins besides VP4 that compose the outer layers of the TLP (VP7) or DLP (VP6), mutations unique to RMAD1 pressure also appeared on the innermost capsid proteins (VP1, VP2, and VP3) as well as the non-structural protein NSP1. VP1 is the RNA-dependent-RNA-polymerase. VP2 is the protein that makes up the inner most layer of the capsid. VP3 is the capping enzyme.

And NSP1 is involved in innate immune system antagonism. There were 7 nonsynonymous mutations in VP1 that uniquely appeared under RMAD1 pressure (V173I - Rep 3 AF, 37%; G411A - Rep 1 AF, 17%; Y494C - Rep 3 AF, 40%; R680K - Rep 2 AF, 17%; Y714C - Rep 1 AF, 26%; Y783C - Rep 1 AF, 19%; I894V - Rep 1 AF, 26%), while only one nonsynonymous mutation appeared in VP1 under the n.p. condition (K1047R - Rep 1 n.p. AF, 17%). The VP2 mutations N498D (Rep 1 AF, 18%) and K639R (Rep 1 AF, 23%) appeared under RMAD1 pressure while F785I (Rep 1 n.p. AF, 10%) was observed in the absence of defensin pressure. For VP3, we observed one mutation of note under RMAD1 pressure in replicate 1, I281L (Rep 1 AF, 45%). Finally, unique NSP1 mutants were only found under RMAD1 selective pressure. These mutations were Q128R (Rep 1 AF, 66%), A171T (Rep 2 AF, 30%), and N346D (Rep1 AF, 19%).

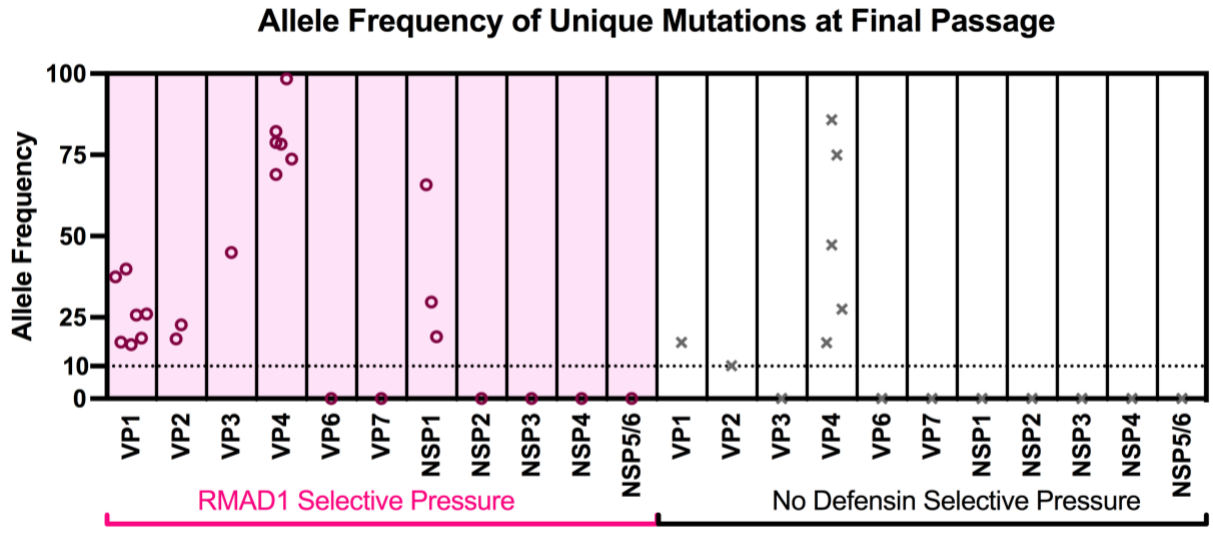

Figure 4-2: Mutations that arose during directed evolution of SR-WT. Unique non-synonymous mutations that arose in each gene segment under RMAD1 pressure (“o”) or no defensin pressure (“x”) at allele frequencies greater than 10% at the final passage in any replicate are depicted. If the same mutation arose in multiple replicates, its allele frequency for each replicate is plotted. Of note, VP4 V184A is included and plotted on both the RMAD1 pressure and no defensin pressure sides.

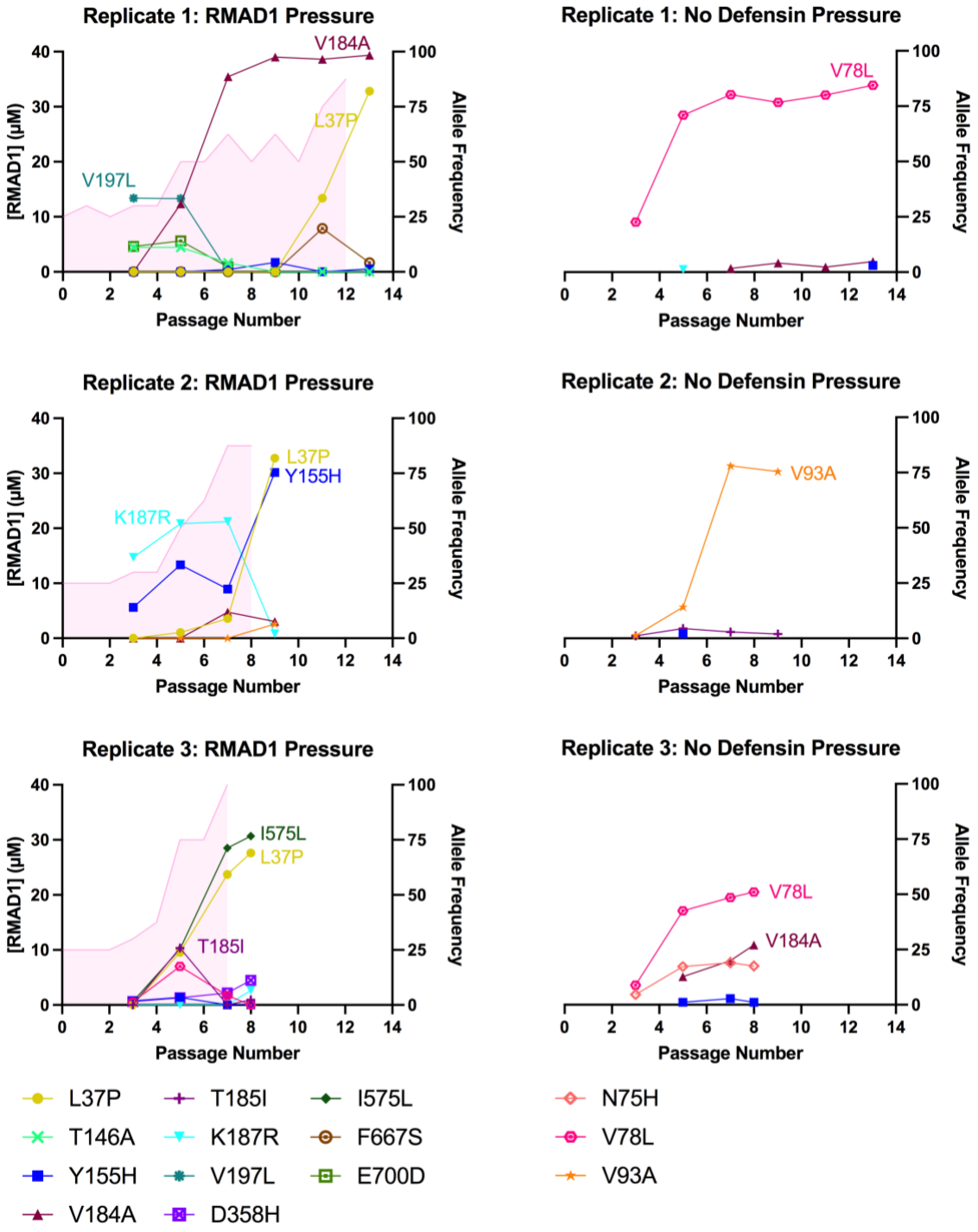

Figure 4-3: VP4 mutations and allele frequencies during the directed evolution of SR-WT. VP4 mutants that reached >10% allele frequency in any replicate, at any passage. Left y-axis, pink shading indicates the concentration of RMAD1 used to generate the next passage. Right y-axis, VP4 allele frequencies. Labeled on the graphs are mutations that reached >25% allele frequency at some point during the passages.

Resistance to RMAD1 confers resistance to RMAD4

We have previously observed that RMAD1 and RMAD4 have similar phenotypes for most rotaviruses (Fig 3-2 to 3-5)[190]. We examined the cross-protectivity of RMAD1 resistance to RMAD4 for the final passage of each replicate. The RMAD4 IC_{50}s for the n.p. replicates were all slightly higher than they were for RMAD1 (Fig 4-1). We observed Rep 1 RMAD1 p13 was enhanced in the presence of RMAD4, which was surprising given that it was only resistant to RMAD1 at the same concentrations (Fig 4-4A and D). Rep 2 RMAD1 p9 was more sensitive to RMAD4 at lower concentrations but then became resistant around 20 µM RMAD4 (Fig 4-4B). Finally, Rep 3 RMAD1 p8 was resistant to RMAD4 at all concentrations tested despite Rep 3 RMAD1 p8 being neutralized by 25 µM RMAD1 (Fig 4-4C and F). All viruses that were evolved under RMAD1 pressure were more resistant to RMAD4 than their n.p. counterparts, indicating that RMAD1 and RMAD4 may have similar, but not identical, mechanisms of action.

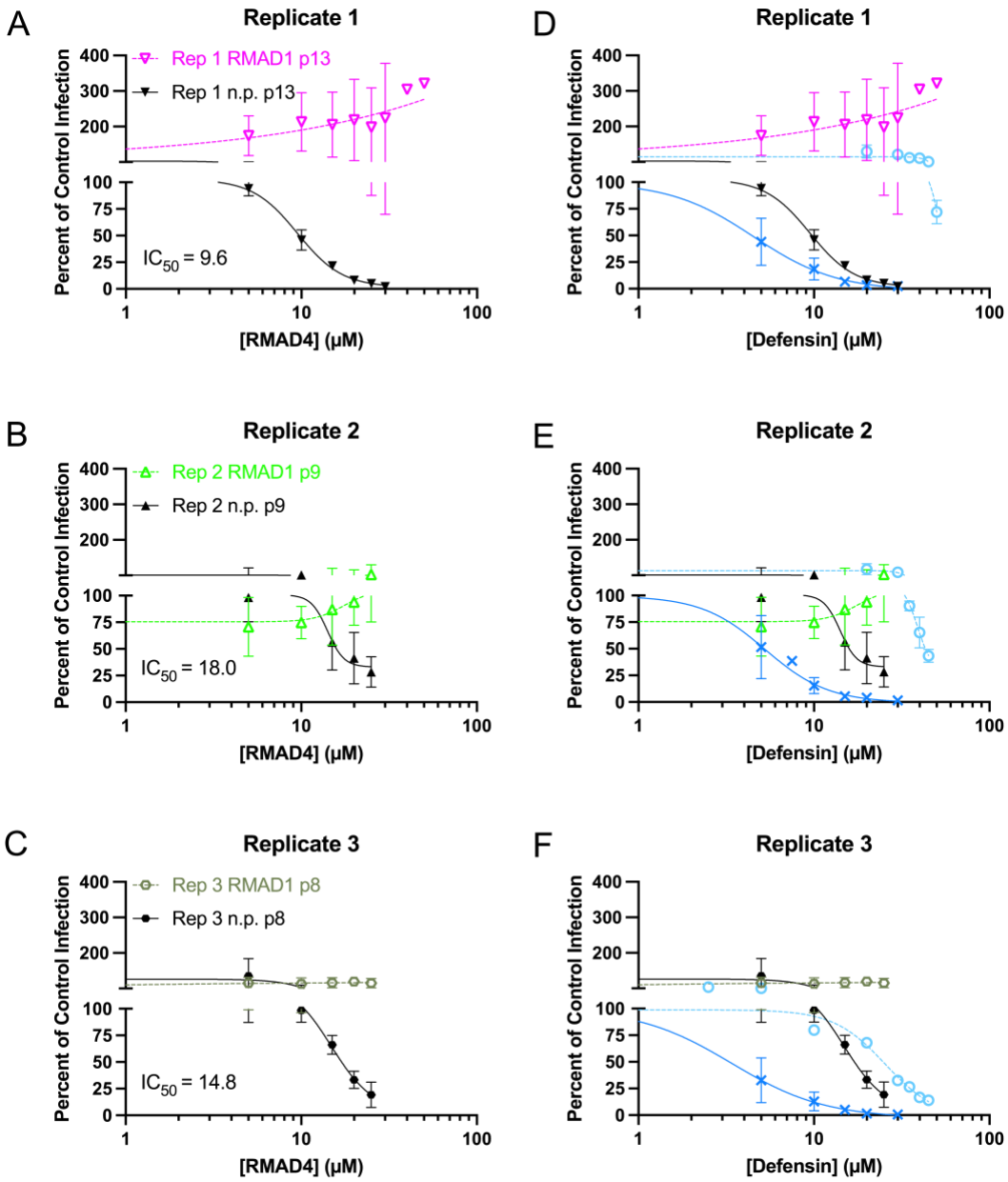

Figure 4-4: Resistance to RMAD1 also confers resistance to RMAD4. The infectivity of the final passages for replicate 1 (inverted triangles, A), replicate 2 (triangles, B), and replicate 3 (hexagon, C) for both RMAD1 pressure (colored dotted lines) and no defensin pressure (black solid lines) were tested under the presence of RMAD4. The IC_{50} values (μM) for the no defensin pressure replicates are indicated on each graph. D-F) Comparison of the infectivity of the final passages for each replicate against RMAD4 (colored same as A-C) or RMAD1 (blue). Rotavirus evolved under defensin pressure are dashed lines with hollow or "O" symbols, viruses passaged without defensin pressure are solid lines with filled or "X" symbols. The data are the same as in A-C and Fig 4-1. Note in A, for 30-50 μM, n=1. In B, Rep 2 n.p. p9 n=2. Data are normalized to infection in the absence of defensin (control infection) and are the mean ± SD of at least 3 individual experiments unless otherwise noted.

Mutations in the head and the stalk, but not the foot, of VP4 can confer RMAD1 resistance

We next wanted to examine the individual contributions of the mutations that arose during RMAD1 selection to defensin resistance. As most of the mutations greater than 50% AF were in VP4, and VP4 is a structural protein that can encounter defensins outside of the cell, we focused our efforts on only examining the VP4 mutants. We generated ten VP4 mutants using an optimized reverse genetics system that had SA11 as the backbone plus VP7 and our mutant VP4 being of RRV origin (Fig 4-5). We examine the single mutants: L37P, Y155H, V184A, and I575L due to their high AF in the final passage. We also examined K187R, as it had reached >50% of the population in replicate 2 passage 7. We generated three double mutants which contained L37P in combination with either Y155H, V184A or I575L. These double mutants represent the two most prominent mutations in each replicate. Finally, we generated two quadruple mutants. The first one combined the VP4 mutations that had the highest allele frequencies of each replicate (**Best 4**: L37P+Y155H+V184A+I575L). We also noted that many of the VP4 mutations arose near the sialic acid binding pocket, therefore we combined all mutations that appeared with >25% AF near the binding pocket to make a **Binding Pocket** mutant (Y155H+V184A+T185I+K187R).

Once rescued, the mutant viruses were passaged once and their sensitivity to RMAD1 assessed. All single mutations except for I575L contributed to RMAD1 resistance (Fig 4-6 A, B). L37P has a less steep hill slope (-1.66) and an IC_{50} of 16 µM. Y155H, V184A, and K187R all have similar IC_{50}s (8.3-8.5 µM), but only V184A had some enhancement at 5 µM RMAD1. The L37P single mutant and L37P+I575L double

mutants were very similar, meaning that the resistance in replicate 3 was probably mostly due to L37P (Fig 4-6 E). Interestingly, the L37P+Y155H and L37P+V184A double mutants were resistant to or enhanced by RMAD1 (Fig 4-6 C) to a greater degree than the individual components added together, indicating possible synergy among these mutations. Furthermore, the L37P+V184A and L37P+Y155H double mutants might be more infectious under the concentrations of RMAD1 assayed than the bulk populations of Replicate 1 RMAD1 p13 and Replicate 2 RMAD1 p9, respectfully (Fig 4-6 E). When the quadruple Best 4 mutant was assessed, it was enhanced by RMAD1 like the L37P+V184A double mutant. Curiously, the Binding Pocket mutant was resistant to RMAD1 up to 20 µM but then is sensitive at 40 µM (Fig 4-6 D, IC_{50}, 21.5 µM). The difference between the phenotypes of these quadruple mutants may be due to the synergistic role L37P plays with the mutations in the binding pocket, since they both contain Y155H and V184A but only the Best 4 contains L37P.

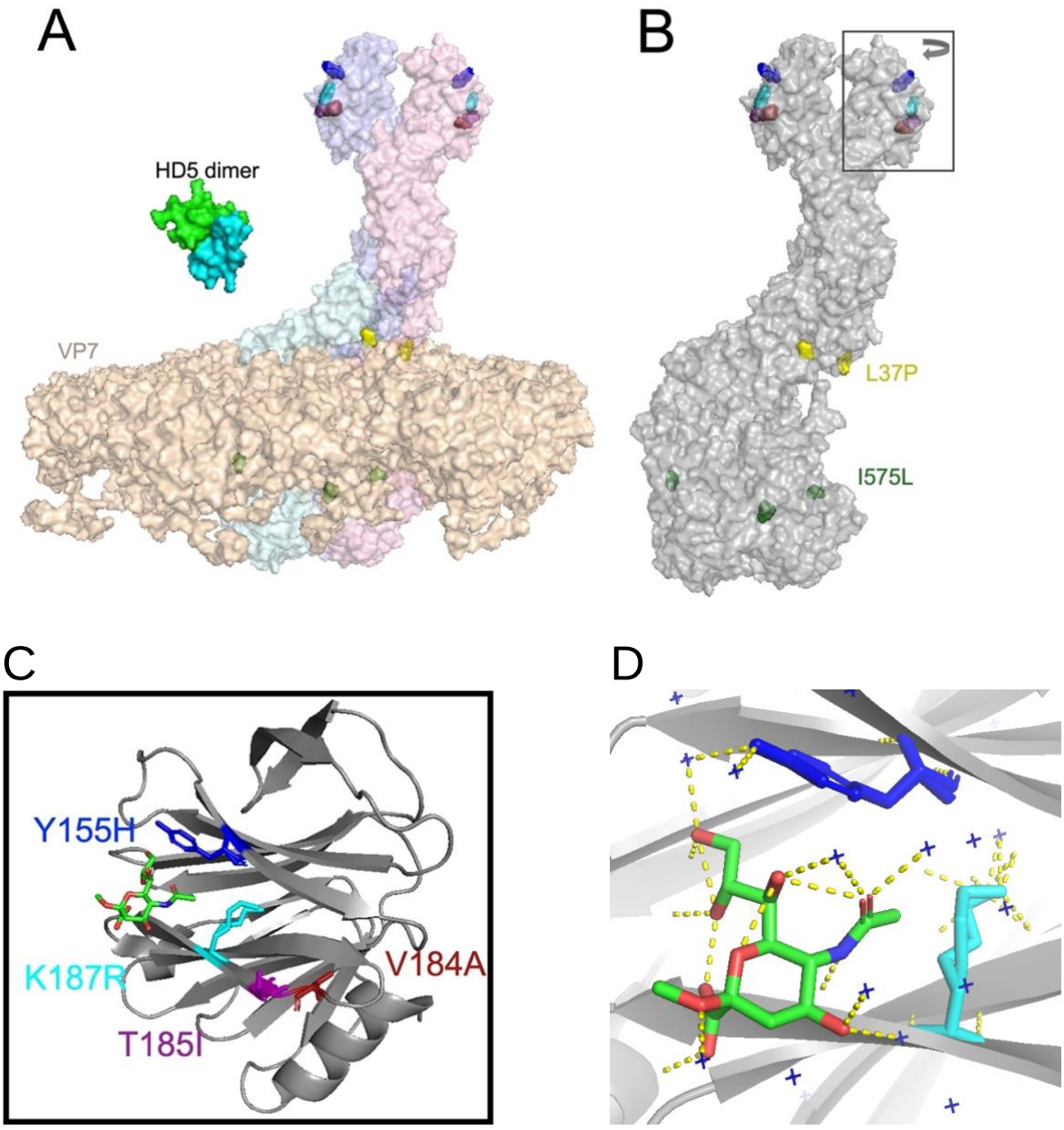

Figure 4-5: Location of VP4 mutations. A) Surface rendering of mature VP5* and VP8* with each monomer depicted with a different pastel color. Surface rendering of VP7, colored in wheat, fits just below L37P, meaning that I575L is not surface exposed in the intestinal lumen. A dimer of HD5 (cyan and green) is depicted for size comparative purposes. B) Mature VP5* and VP8* with a gray rendering with transparency to show the locations of the mutated amino acid residues. C) Box from B zoomed in with a cartoon representation of VP8* with the sialoside, 2-O-methyl-alpha-D-N-acetyl neuraminic acid, in green and the amino acids that became mutated colored with the wild type side chains shown as licorice. D) Water (“+”) mediated hydrogen bond between Y155 and the sialoside. Modified from PDB: 6WXE and 1KQR. Images were generated with PyMOL Molecular Graphics System (Schrodinger LLC, version 2.3.4).

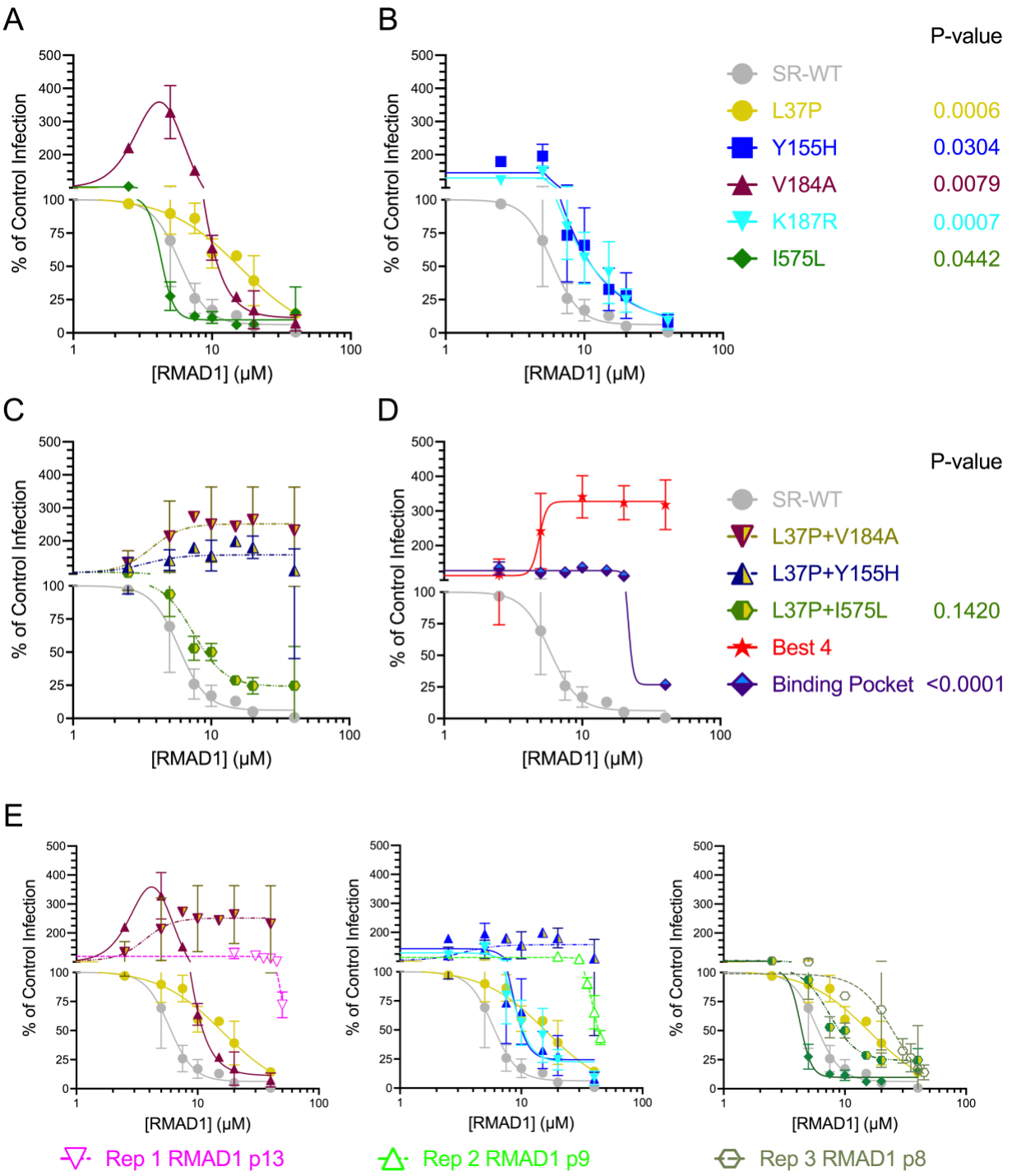

Figure 4-6: Mutations in the head and stalk of VP4, but not the foot, contribute to defensin resistance. A) L37P (yellow circles) and V184A (maroon triangles) have right shifted curves compared to SR-WT (gray circles) while I575L (green diamonds) has a similar RMAD1 sensitivity as SR-WT. B) Y155H (blue squares) and K187R (cyan inverted triangles) are more resistant to RMAD1 than SR-WT.

Fig. 4-6 (continued): C) The double mutants L37P+V184A and L37P+Y155H (maroon and yellow inverted triangles and blue and yellow triangles) are enhanced by or resistant to RMAD1 while L37P+I575L (green and yellow hexagons) has similar RMAD1 sensitivity as SR-WT. D) The quadruple mutants are differentially sensitive to RMAD1. The Binding Pocket mutant is resistant up to 20 µM RMAD1 (aqua and purple diamonds), while the Best 4 is enhanced by higher concentrations of RMAD1 (red stars). E) The RMAD1 sensitivity curves for the final passage, bulk populations of the RMAD1 selection and the individual and double mutants that were present in the respective replicate are compiled together for illustrative purposes. All data is the same as was shown in Fig. 4-1 and A-C of this figure. SR-WT data is the same as in Fig 4-1 and is reprinted on every graph for comparative purposes. Data are normalized to infection in the absence of defensin (control infection) and are the mean ± SD of at least 3 individual experiments.

The Y155H and K187R mutations provide neuraminidase resistance to viruses with RRV VP4

Two of the defensin resistance mutants we identified have been previously studied as part of the nar3 neuraminidase resistant mutant (L37P, K187R, Y267C), with K187R being identified as the cause of neuraminidase resistance[67,83]. Neuraminidase cleaves off terminal sialic acids, which viruses like RRV use for VP8*-mediated cellular attachment. The appearance of a neuraminidase resistance mutation suggested that RMAD1 might inhibit the ability of the virus to use sialic acid as an attachment factor. Therefore, one mechanism of defensin resistance may be for the virus to change its binding preferences and receptor interactions. Adding further support to this hypothesis is that Y155 is involved in stabilizing sialic acid in the binding pocket by a water-mediated hydrogen bond and K187 plays a role in neuraminic acid binding preference (Fig 4-5 D)[191–193]. Therefore, we tested the neuraminidase sensitivity of our panel of mutants to determine whether the defensin resistance mutations altered the viral dependence on sialic acid.

We observed that the infectivity of SR-WT and SA11 was only maximally inhibited 2-fold by treatment of the cells prior to infection with neuraminidase (Fig 4-7,

gray circles and dark gray “X”, same data is reprinted on each graph panel for comparative purposes). We reproduced that K187R makes the virus neuraminidase resistant[67,194], while L37P is not sufficient for neuraminidase resistance (Fig 4-7 A, B). Next, we observed that Y155H is a novel neuraminidase resistance mutation, although its level of resistance may not be as strong as K187R (Fig 4-7 B, blue squares and cyan inverted triangles). We also observed that some of the individual mutants like L37P, V184A, and I575L may make the RRV VP4 containing virus more sensitive to neuraminidase (Fig 4-7 A, maroon triangle at 3.25 mU/mL, yellow circle and green diamond at 25 and 50 mU/mL neuraminidase). Likewise, the L37P+V184A and L37P+I575L double mutants were both inhibited by neuraminidase to a greater extent than SR-WT (Fig 4-7 C). L37P+Y155H was the only double mutant resistant to neuraminidase, and it resembles the Y155H individual mutant (Fig 4-7 C and B). Curiously, the Best 4 mutant is not neuraminidase resistant even though it includes Y155H (Fig 4-7 D). Perhaps the presence of V184A and/or I575L dominate over the resistance effect Y155H has. On the other hand, the Binding Pocket mutant, which contains V184A in combination with Y155H as well as K187R and T185I, is resistant to neuraminidase. Thus, the combination of either two neuraminidase resistant mutations may dominate over V184A or K187R alone may be sufficient to confer neuraminidase resistance regardless of the other mutations present.

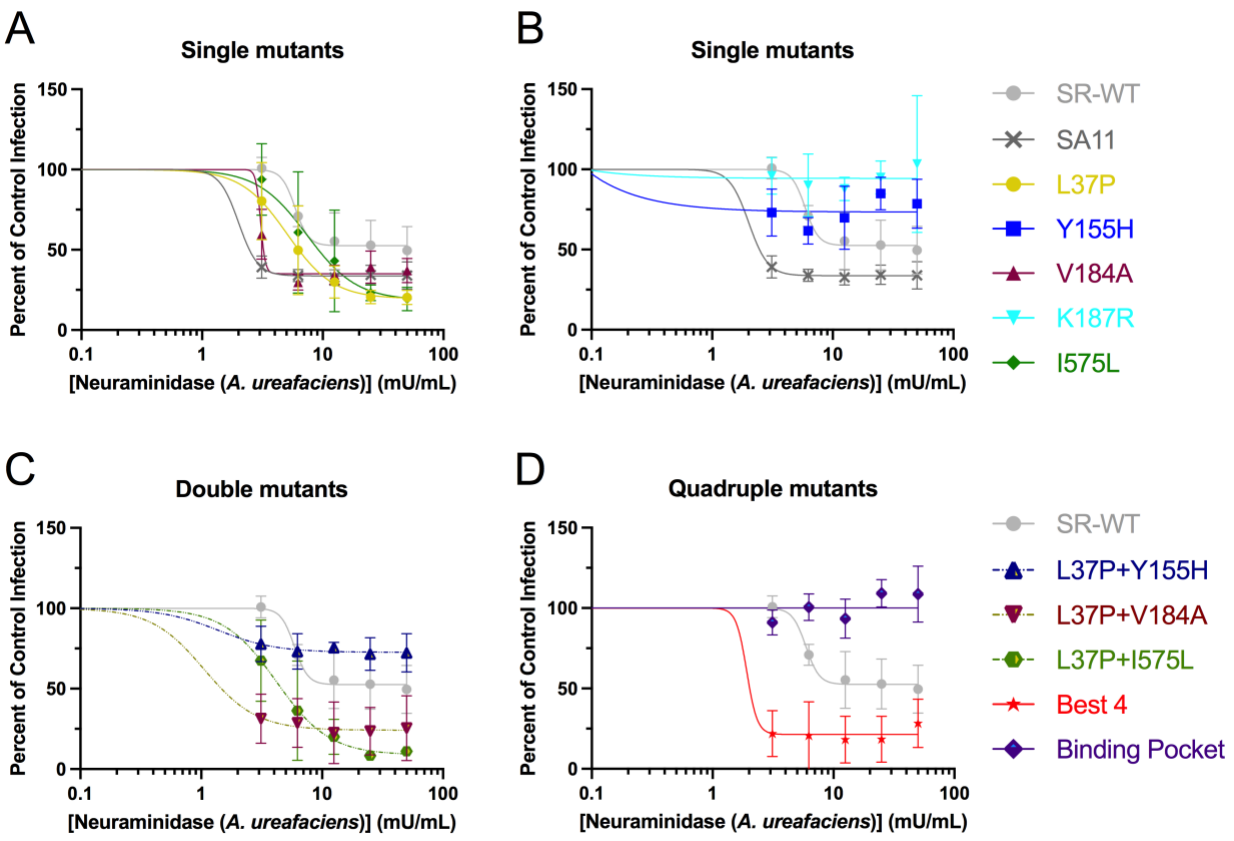

Figure 4-7: Neuraminidase sensitivity of mutant rotaviruses. MA104 cells were treated with the indicated concentration of neuraminidase for 1 h at 37°C prior to the addition of rotavirus. A) L37P (yellow circles), V184A (maroon triangles), and I575L (green diamonds) have similar sensitivities to neuraminidase as SR-WT (gray circles) and SA11 (dark gray "x"). B) Y155H (blue squares), and K187R (cyan inverted triangles) are resistant to neuraminidase treatment. C) The double mutants L37P+V184A and L37P+I575L (maroon and yellow inverted triangles, and green and yellow hexagons) may be more sensitive to neuraminidase than SR-WT or SA11, while L37P+Y155H (blue and yellow triangles) is resistant to neuraminidase treatment. D) The quadruple mutants are differentially sensitive to neuraminidase. The Binding Pocket mutant is completely resistant to neuraminidase treatment (aqua and purple diamonds), while the Best 4 is inhibited by neuraminidase treatment (red stars). SR-WT and SA11, are reprinted on every graph for comparative purposes. Data are normalized to infection in the absence of neuraminidase (control infection) and are the mean ± SD of at least 3 individual experiments.

RMAD1 does not inhibit viral attachment to MA104 cells

While only two of the individual mutations, Y155H and K187R, facilitated infection when the sialic acid receptor was cleaved by neuraminidase, we cannot rule out that defensins could still inhibit rotavirus binding to the cell as a mechanism of neutralization. Furthermore, the maximal infectivity inhibition by neuraminidase we observed was only 50% for wild type viruses. We therefore wanted to determine if defensins can inhibit rotavirus from binding to the cell. SR-WT virus was pre-incubated with RMAD1 or serum-free media before being bound to MA104 cells. Unbound virus was then washed off before we performed RT-qPCR for the NSP1 gene segment. As a control, we also bound SR-WT to neuraminidase treated MA104 cells. While the effectiveness of the neuraminidase treatment on reducing binding varied greatly, we did observe on average about 50% less virus bound to MA104 in the presence of neuraminidase (Fig 4-8), which is comparable to the infectivity data we observed in Fig 4-7. We observed that RMAD1 does not inhibit SR-WT binding to the cells. In fact, RMAD1 may enhance SR-WT binding to cells, even at RMAD1 concentrations greater than the IC_{90} for infection (11.7 µM RMAD1 see Fig 4-1).

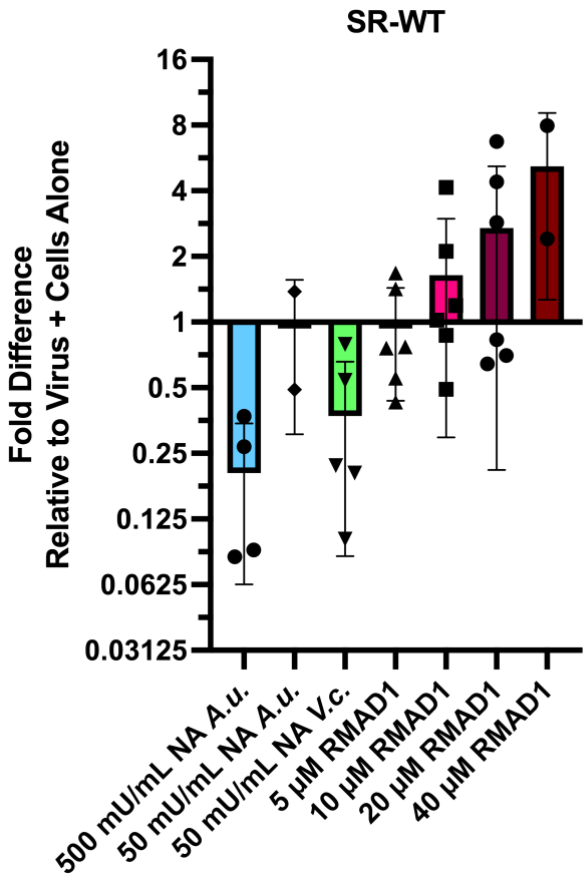

Figure 4-8: Defensin does not inhibit SR-WT virus binding to cells. SR-WT was pre-incubated with various concentrations of RMAD1 and then allowed to bind to MA104 cells in the cold. Unbound virus was washed off and then RNA was collected for RT-qPCR. MA104 were also treated with neuraminidase (NA) from either *Arthrobacter ureafaciens* (*A.u.*) or *Vibrio cholerae* (*V.c.*) as a positive control for reduced viral binding to the cells. $2^{\Delta\Delta Cq}$ values for each replicate are plotted on a Log 2 scale with the mean ± SD represented by the bar graph. 50 mU/mL neuraminidase *V.c.* and 5-20 µM RMAD1 n=6; 500 mU/mL neuraminidase *A.u.* n=4; 50 mU/mL neuraminidase *A.u.* and 40 µM RMAD1 n=2.

As we saw that RMAD1 may increase binding to MA104 cells, we hypothesized that this RMAD1 mediated binding may be primary receptor independent. We therefore combined neuraminidase treated cells with mutant viruses preincubated with RMAD1. We chose to preliminarily examine L37P, K187R, Y155H, L37P+Y155H, and the Best 4 mutants as they encompassed a range of resistance/enhancement by RMAD1 and were either sensitive (L37P and Best 4) or resistant to neuraminidase treatment (K187R, Y155H, and L37P+Y155H). Examining how RMAD1 impacts the infectivity of the viruses in the presence of neuraminidase, we saw SR-WT remained sensitive to both RMAD1 and neuraminidase. However, for L37P, RMAD1 was able to recover the infection level to non-neuraminidase treatment levels. For K187R and Y155H, the neuraminidase treatment did not impact viral infectivity, nor did it impact the RMAD1 activity on this virus. Similarly, for L37P+Y155H we observed that the resistance to RMAD1 was independent of neuraminidase treatment. Curiously, we observed that RMAD1 enhanced the Best 4 viral infection in the presence of neuraminidase, like it did in the absence of neuraminidase, despite the Best 4 virus being sensitive to neuraminidase treatment (Fig 4-9).

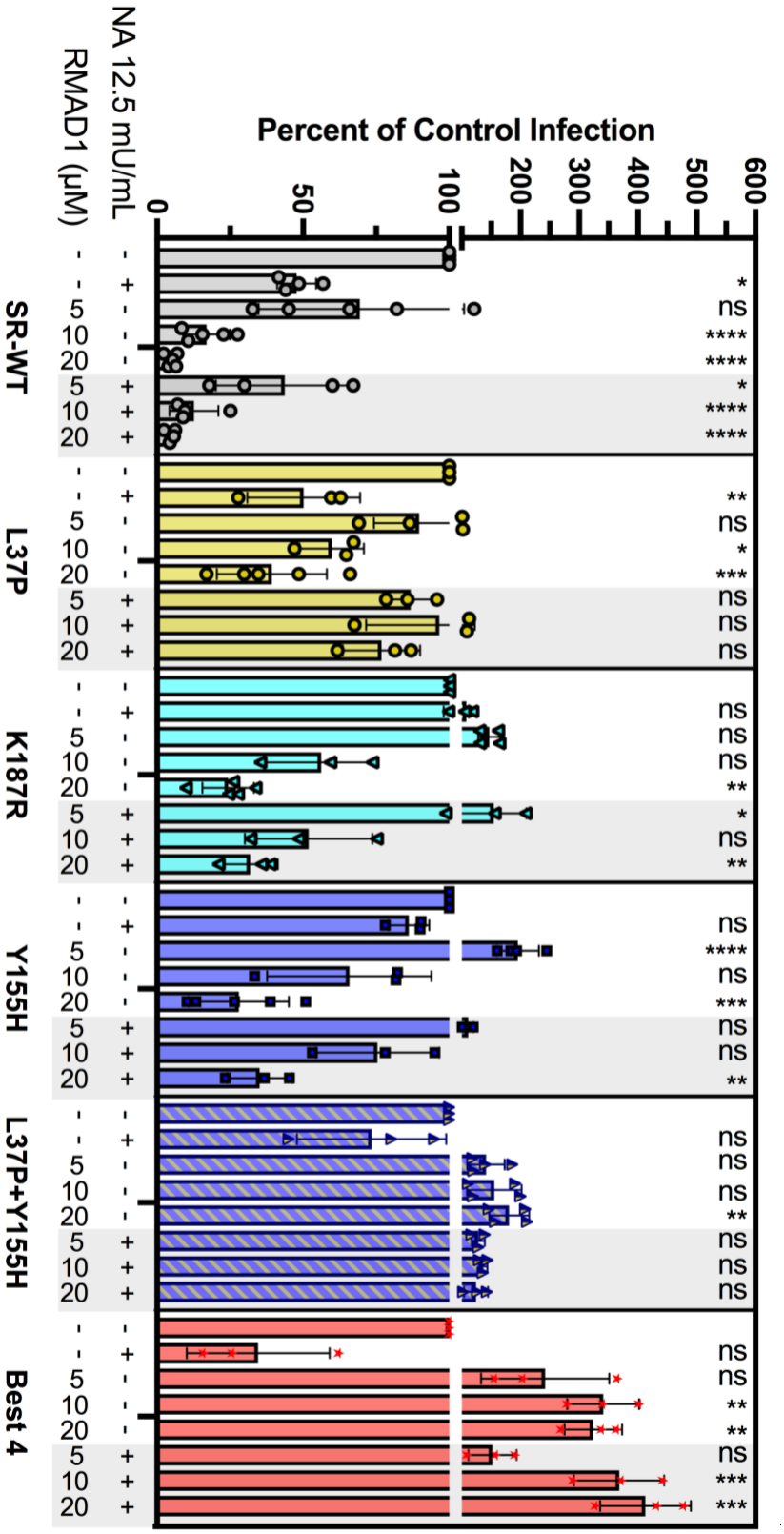

Figure 4-9. L37P containing viruses can use defensin to overcome neuraminidase's block to infection.

Fig. 4-9 (continued): MA104 cells were treated with 12.5 mU/mL neuraminidase (NA) from *A. ureafaciens* or SFM for 1 h before being washed with SFM and the viruses SR-WT, L37P, K187R, Y155H, L37P+Y155H, or the Best 4 added to the cells. These viruses were pre-incubated with the indicated concentration of RMAD1 or SFM for 45 min on ice prior to addition. 20 h p.i. cells were fixed and stained for VP6. Data are normalized to infection in the absence of both neuraminidase and defensin (control infection). Individual replicates are plotted and the mean ± SD are indicated by the bar graphs. For SR-WT n=4; for all other viruses n=3. For the NA treatment in the absence of defensin each point is the average of two wells. The RMAD1 without NA treatment data are the same as Fig 4-6 and reproduced here for comparative purposes. Results of a one-way ANOVA with Dunnett's multiple comparisons test to each control infection are indicated by asterisks. *, P = 0.01 to 0.05; **, P = 0.001 to 0.01; ***, P = 0.0001 to 0.001; and ****, P < 0.0001. Bars marked with a "ns" indicates P>0.05.

Discussion

We serially passaged a SA11 virus that had RRV's VP4 and VP7 under rhesus myeloid alpha-defensin 1 (RMAD1) pressure and observed, like what we saw for HAdV[152], that defensins can drive rotaviral evolution. While myeloid defensins are not constitutively secreted and therefore may not be the main drivers of host range, they can be a useful tool for directed evolution. Our directed evolution approach has given us a better understanding of how RMAD1 interacts with rotavirus and provided insights into possible mechanisms of resistance.

Upon sequencing the evolved viral populations, we observed that most mutations that reached high allele frequencies were in VP4. We mostly saw mutations in VP8*, and specifically near the sialic acid binding pocket; however, there was one VP8* mutation in the stalk of the spike protein (L37P) and one mutation in the foot region of VP5* (I575L). While the I575L mutation did not confer defensin resistance, it begs the question as to why its frequency steadily increased over passages up to 77% AF. I575L is in the part of the foot domain of VP5* that is inserted into the membrane and so an advantageous role in facilitating the rearrangements of VP5* to penetrate the

membrane is not obvious[74]. Alternatively, there is the possibility that bottlenecks during each round of passaging allowed the mutation to increase over each passage.

Likewise, a bottleneck may explain K187R's rapid decrease during the last 2 passages of Replicate 2. K187R had a very similar phenotype to the individual Y155H mutant, and so the idea that Y155H alone is more advantageous for the virus cannot explain K187R's replacement. It is unlikely that the loss of K187R was because it is unable to coexist with Y155H as our binding pocket mutant contained both mutations, albeit within the context of V184A and T185I, and this binding pocket mutant was more resistant to RMAD1 than either individual mutant. However, the rise of Y155H tracks well with the rise of L37P in replicate 2. We did not generate a L37P+K187R double mutant, and so it is still unknown if K187R is functionally equivalent to Y155H in the context of L37P. Further research is needed to determine if the L37P mutation acts synergistically with K187R to provide increased resistance to RMAD1 similar to L37P+Y155H or if a lack of synergy might explain K187R disappearance in the population.

Based on the multiple mutations that arose near the binding pocket for sialic acid, we had hypothesized that defensins could block the attachment of rotavirus to the cells. But, based on our binding assays, we can conclude that RMAD1 does not prevent rotavirus from attaching to cells (Fig 4-8). In fact, the mutant rotaviruses could take advantage of defensin-mediated binding, as we saw that RMAD1 could rescue or enhance the infection of rotaviruses when terminal sialic acids are removed (Fig 4-9). However, RMAD1 may still perturb the wild type rotavirus's ability to bind to sialic acid and potentially lead to non-productive attachment or non-productive entry into the cell.

One hypothesis is that the resistance mutations that arose allow the rotavirus to use different attachment and entry receptors. For example, we saw two mutations in amino acids that are involved in stabilizing the sialic acid molecule in the binding pocket (Y155 and K187) and that these mutations led to the virus becoming neuraminidase resistant. Additionally, previous studies on the nar3 mutant, which contains K187R and L37P, found that the virus can use α2β1 integrin directly for binding[73,86]. It has been proposed that the L37P mutation is sufficient to change the conformation of RRV's VP5 such that it can bind to α2β1 integrin directly[72,86]. As we saw L37P arise in all three replicates, this direct α2β1 integrin interaction may be a key factor in RRV resistance to RMAD1.

However, if L37P is sufficient for attachment to cells using the α2β1 integrin, why then did we observe mutations in the binding pocket? If RMAD1's mechanism of action was to block viral attachment to its sialic acid receptor, then the binding pocket mutations might be redundant to defensin's neutralizing function. The viruses in replicates 1 and 2, which had mutations appear in or around the binding pocket, were more resistant to RMAD1 than replicate 3, and the L37P+V184A and L37P+Y155H double mutant viruses were more resistant to RMAD1 than any of the individual mutations (Figs. 4-1 and 4-6). Potentially, removing or reducing the ability of rotavirus to bind to sialic acid through these mutations increases the likelihood of the rotavirus using the α2β1 integrin or other attachment factors. However, we only observed neuraminidase resistance mutations in one of our three replicates, meaning that neuraminidase resistance is not required for defensin resistance.

Another possibility is that the sialic acid bound VP8* interface is a target for RMAD1 that leads to neutralization. Yet, this mechanism of action cannot fully explain neutralization as defensin incubation pre- and post-cellular attachment did not lead to much of a difference in phenotype (see chapter 3, Fig. 3-2 and 3-4). While we did not do order of addition experiments with RMAD1, for RRV neutralization by RMAD4, we saw that RRV is less sensitive to the myeloid defensin RMAD4 when the virus was pre-bound to cells (Fig 3-2 D, RMAD4 IC_{50} = 11.8 µM in post-attachment to cells vs. 6.0 µM in pre-attachment to cells). Therefore, the receptor attached RRV was not more neutralized by RMAD4.

We also would like to investigate if the replication dynamics are a tradeoff for defensin resistance by examining the growth kinetics of our mutant rotaviruses. This is particularly of interest for the K187R and Y155H containing mutants that are neuraminidase resistant. There have been studies of K187R containing viruses that show that it grows to lower titers than WT RRV[194]. However, the amount those two mutant viruses were diluted by to achieve linear range infection levels was similar to the dilution used for the SR-WT in our studies, indicating comparable infectious titers in my hands. In a similar vein, when staining monolayers of MA104 cells to quantify infection levels, we observed that the wells infected with V184A (and sometimes L37P+V184A) had blotchy or clumpy dispersion of viruses (data not shown), while all other mutants had a uniform distribution of infection like SR-WT. I speculate that V184A may cause viral aggregation based on the distribution of infected cells. It would be interesting to study what the relatively small change of valine to alanine does to the virus's binding

preferences. Does this valine to alanine mutation expand or reduce the spectrum of glycans the rotavirus can bind?

In addition to insights into RMAD1 and rotavirus interaction, we have also shown that RMAD1 resistance is cross-protective for RMAD4. Despite similar overall structure, RMAD1 and RMAD4 differ substantially in linear sequence (36.7% identical). Therefore, it is striking that we saw strong correlation in resistance. In replicate 3, we observed that the bulk viral population was resistant. While we cannot rule out entirely any contribution to the resistance by the I575L mutation, we hypothesize that like what we observed with RMAD1, L37P maybe the main driver of the resistance to RMAD4 for replicate 3. In replicate 2, we saw that the bulk virus may be more resistant to RMAD4 at higher concentrations compared to lower concentrations like 5 μM RMAD4. Interestingly replicate 1's bulk population appears to be enhanced by RMAD4. Further investigation of the individual V184A mutant may reveal if having the A184 alone is sufficient to confer protection and an enhancing phenotype in the presence of RMAD4 or if there is again synergy between P37 and A184 like what we observed for RMAD1. Further investigation into these the mutations that appeared in replicate 1 can serve as a tool to begin to tease apart the distinct mechanisms of action of between these two defensins, especially because this is only the second virus, the other being Wa, that we have observed an appreciable difference in phenotype between these two rhesus myeloid alpha-defensins.

Thus far, we have only focused on examining the VP4 mutations that arose under defensin pressure. However, some VP4 mutations, V78L (Rep 1 n.p. AF 86%; Rep 2 n.p. AF 47%) and V93A (Rep 3 n.p. AF 75%), appeared only in the no defensin

pressure condition. These mutations are present on the head of VP8* but are not near the sialic acid binding pocket. We did not investigate if they conferred any advantage or if these mutations were just a consequence of random bottlenecking that allowed them to reach high allelic frequencies. In addition to VP4, we identified mutations that arose under RMAD1 pressure in VP1, VP2, VP3, and NSP1. What these mutations might contribute to defensin resistance has not been studied, however because our VP4 mutations alone provide defensin resistance, the non-VP4 mutations are not necessary for defensin resistance. We hypothesize that the VP1 and VP3 mutations may play a role in increasing the frequency of mutations. For example, Y494C, which reached up to 40% AF, may be in the proposed “priming loop”[195]. The VP3 mutation is in the ribose 2′-O-MTase domain, which is used to generate the cap-1 on the RNA, however this mutation is not in the catalytic site[196]. We hypothesize that the NSP1 mutations (Q128R (replicate 1; AF=66%), A171T (replicate 2; AF=30%), and N346D (Rep1 AF 19%)) could aid in the antagonism of IRFs[197] and that this hinderance of the innate immune system could lead to better viral titers. The NSP1 mutations could also be involved in counteracting any innate immune activation caused by the defensins. We cannot formally rule out any role of VP7 especially as L37P sits just above where VP7 encapsidates the foot of VP4. One possible mechanism of neutralization by RMAD1 would be to bridge VP4 and VP7 together and thus impede the membrane penetration function of VP5*. However, the lack of mutations in VP7 underscore the importance of VP4 in defensins’ mechanism of action.

In summary, using a directed evolution approach, we identified residues in VP8* that are important for SR-WT’s resistance to RMAD1. These residues also are important

for, at a minimum, other homologous myeloid defensins, pointing to a possible conserved mechanism of action for α-defensins. Most of the VP8* mutations were in the galectin-like domain, with some of the mutations even allowing the viruses to infect independently of terminal sialic acid receptors, however the one VP8* mutation that appeared in all three replicates under defensin pressure, L37P, is located in the stalk of the spike protein. While RMAD1 does not inhibit SR-WT binding to MA104 cells, perhaps the endocytic pathway the virus traffics through during entry, which is determined by the receptor the virus uses, is important for the defensins' ability to inhibit rotaviruses. A few of the mutations that arose during our RMAD1 selection have been previously studied due to their ability to confer neuraminidase resistance, and those past studies provide further support to the idea that entry and trafficking may be perturbed by α-defensins. For example, L37P has been proposed to enable VP5* binding to α2β1 integrin, while the K187R mutation causes rotavirus to escape from late endosomes instead of maturing endosomes[84]. Future investigation into events downstream of viral attachment, such as entry and uncoating, will hopefully enlighten us on where defensins inhibits rotavirus.

Chapter 5: Future Perspectives and Significance

Dissecting alpha-defensin's mechanism of neutralization for rotavirus:

Our investigation of α-defensin effects on rotaviral infection by has led to some insights and many follow up questions. We observed that, in contrast with what we have observed for adenovirus and adeno-associated viruses (AAVs)[133,152], the order of addition of defensin and rotavirus to the cells barely impacted defensin's modulatory effect on the virus. We also identified that the rotavirus spike protein determines whether rotavirus is neutralized, resistant to, or enhanced by defensin. Based on the mutations that arose in VP4 under RMAD1 pressure, we hypothesize that the resistance mutations alter the rotavirus receptor usage which can then lead to different, but still productive, endosomal trafficking.

All studies thus far have pointed to VP4 as being the determinant for receptor usage, entry pathway, and endosomal trafficking, in addition to our discovery of its importance for defensin phenotype. Our directed evolution investigation of rotavirus used a reassortant virus that had an SA11 backbone with RRV's outer-layer proteins, VP4 and VP7. Curiously SA11, which is slightly more resistant to RMAD1 than RRV (Fig. 3-3, SA11 IC_{50} 13 μM; Fig. 3-2, RRV IC_{50} 9 μM; and Fig. 4-1 SR-WT IC_{50} 6 μM), already has a proline at position 37. This slight increase in resistance might be comparable to L37P (Fig 4-6 A, L37P IC_{50} 16 μM, Hill slope -1.7), although the Hill slopes are different. In addition to P37, SA11 has an alanine at its amino acid position 184, however the context of the binding pocket is different in SA11 compared to RRV. In our binding pocket mutant Y155H, V184A, T185I, K187R, those residues are Y155, A184, R185, A187 in SA11. SA11 and RRV's VP4s are 79% identical by sequence

alignment, and their differences in sequence contribute to their glycan preferences and different endocytic pathways. SA11 has a greater affinity towards Neu5Gc compared to RRV which has a greater affinity towards Neu5Ac[64,191]. Additionally, RRV seems to be unusual in terms of entry, being the only virus to enter in a clathrin-independent manner. Once endocytosed, SA11 and RRV may require the same conditions to escape the maturing endosome and enter the cytoplasm, but other viruses like Wa and DS-1 as well as the nar3 RRV mutant, traverse to late endosomes[75]. The difference in glycan and receptor preferences as well as entry and endocytic pathways used may obfuscate any direct comparison between SA11, RRV, and other rotaviruses necessitating the need to expand our mechanistic studies to other rotaviral strains.

As previously mentioned, two of the VP4 mutations that arose under RMAD1 selective pressure (L37P and K187R) have also arisen under neuraminidase pressure. Studies on the impacts that these mutations have on receptor usage, entry, and endosomal trafficking have found that L37P is important for the virus to interact with integrin α2β1[194] and that K187R shifts the entry pathway from being clathrin-independent – like RRV – to being clathrin-dependent. Additionally, K187R changes the viral escape from maturing endosomes – like RRV and SA11 – to late endosomes[75,84]. We would like to expand on these previous studies and investigate all the RMAD1 resistance mutants, with extra scrutiny on the L37P double mutants. What receptors do these mutant rotaviruses use? Does RMAD1 impact what receptors the viruses are attached to? Are the neuraminidase resistant mutants using sub-terminal sialic acids for cellular attachment or relying on other receptors like integrins for attachment and entry[198]? One hypothesis I have is that RMAD1 resistance is dependent on the rotavirus being able to

use integrin α2β1 in the absence of sialic acid binding for entry. To test the dependence on α2β1 integrin for RMAD1 resistance we could combine the RRV VP4 D308A mutant, which fails to bind to integrin α2β1, with our RMAD1 resistance mutants[194,199].

As receptor usage and entry pathways are intimately linked, we also want to examine the entry pathways. Investigation into the trafficking and uncoating events are of particular interest because this step in the non-enveloped viral lifecycle seems to be a common target for α-defensins. Perhaps the normal RRV endocytic pathway promotes α-defensin's neutralizing activity. However, SA11 and Wa are both capable of being neutralized by at least one α-defensin, and these rotaviruses use different entry and endocytic pathways than RRV. Perhaps neutralizing defensin-bound rotaviruses all converge into the same inhibitory pathway. For these studies, we can take advantage of the ability to fluorescently label and track rotavirus TLPs and DLPs[81,85]. Recombinant TLPs can be made by recoating a DLP with recombinant VP4 and VP7, and each component can be fluorescently labeled and still lead to DLP delivery into the cytoplasm. In combination with controls such as the RRV VP4 V391D mutant that cannot escape the endosome[200] and using mAb 159 to stabilize RRV VP7 trimers and inhibit uncoating[59,201], we hope to untangle if defensin inhibits membrane penetration, uncoating of rotavirus, or productive endosomal trafficking.

Alpha-defensins as drivers of evolution:

We had hypothesized that gastrointestinal pathogens are resistant to their host's enteric α-defensins due to selective pressure. Our studies on the impact homologous and heterologous α-defensins have on rotaviral infection bolstered our hypothesis. Additionally, our directed evolution approaches with HAdV-5 and a reassortant monkey

rotavirus show that α-defensins can drive the evolution of non-enveloped viruses. A previous study using θ-defensins, and more specifically retrocyclin, showed that HIV-1 can evolve resistance to its inhibitory effect, although the resistance developed slower than the authors had expected[202]. While directed evolution of HIV-1 and HAdV-5 under the pressure of retrocyclin and HD5, respectively, have shown that viral structural proteins became more positively charged, we did not observe that to be the case for rotavirus as only one mutation introduced a positive charge (Y155H)[152,202]. Additionally, for AAV1, one surface-exposed amino acid was determined to switch the phenotype from HD5 resistance to HD5 neutralization, and curiously the neutralizing amino acid was positively charged while the amino acid that allowed for resistance was negatively charged[133]. So, while resistance could be driven by increase in positive charge on the viral proteins reducing the amount of cationic defensin bound, this is not universally true and other dynamics are probably at play.

The ability of defensins to drive evolution leads to an interesting question in terms of epidemiology. For example, Wa and DS-1 should inhabit the same replicative niche in humans. However, Wa is resistant to HD5 while DS-1 is enhanced. These viral strains are thought to have originated from different animals; Wa-like viruses being of porcine origin, while DS-1 like viruses being of bovine origin[203]. Thus far our studies have not included bovine or porcine rotaviruses, but we would like to expand our studies to include those viruses as well as compare the similarities and differences between human, porcine, and bovine enteric α-defensins. If bovine enteric α-defensins are more similar to human enteric α-defensins, this could mean the barrier to cross into humans

could be lower and may explain the prevalence of bovine G10P[11] viruses found in neonates[89,204].

Commonalities in alpha-defensin mediated enhancement:

Defensin-mediated, viral receptor-independent binding to the cells could explain enhancement of HIV-1[148,163,205], some serotypes of HAdV and mouse adenovirus[141,154], and potentially rotavirus as well (Fig 4-9). Increased attachment can even be more broadly the mechanism of defensin-mediated enhancement as α-defensins can promote the attachment of *Shigella* to cells[159,206]. While it hasn't been investigated yet, we have proposed that this defensin-mediated enhanced binding to cells could expand the cellular tropism for some viruses in addition to increasing cellular attachment.

Significance:

Defensins are a vital part of the vertebrate innate immune system. Their effectiveness in restricting a broad range of microorganisms is impressive, especially given their small size. Studying how immune defenses, like defensins, vary across species and their effectiveness against various viral infections is important for our understanding of the evolution, transmission, and zoonotic potential of viruses. The barriers that prevent cross-species transmission are not completely known, but α-defensins could partly dictate viral tropism.

Researching how α-defensins alter the pathogenesis and evolution of viruses can also be important for the improvement of vaccines. While the production of defensins is expensive, and thus not conducive for use as a therapeutic, the defensin-virus interactions and the mechanism behind inhibition could elucidate targets for small molecule inhibitors. Additionally, because defensins can be both pro- and antiviral, they

are an important factor to consider when choosing a viral strains to be used in vaccines. Using defensins as an adjuvant[119,151,207] to promote a better adaptive immune response is one area that could be further explored. Finally, accounting for the natural variability of enteric defensin expression globally could aid in ensuring vaccine effectiveness.

Chapter 6: Supplement

Generation of recombinant triple-layered rotavirus particles: The next steps to investigate defensin modulation of rotavirus are to study how defensins impact rotaviral trafficking and if defensins perturb uncoating. For these studies, we would like to use fluorescently labeled recombinant triple-layered particles (rcTLP), which can be singly, doubly, or even triply labeled[208,85,81]. My initial efforts to make this tool involved purifying recombinant VP7, purifying RRV DLPs, enriching VP4, and performing a recoating reaction (sans labeling).

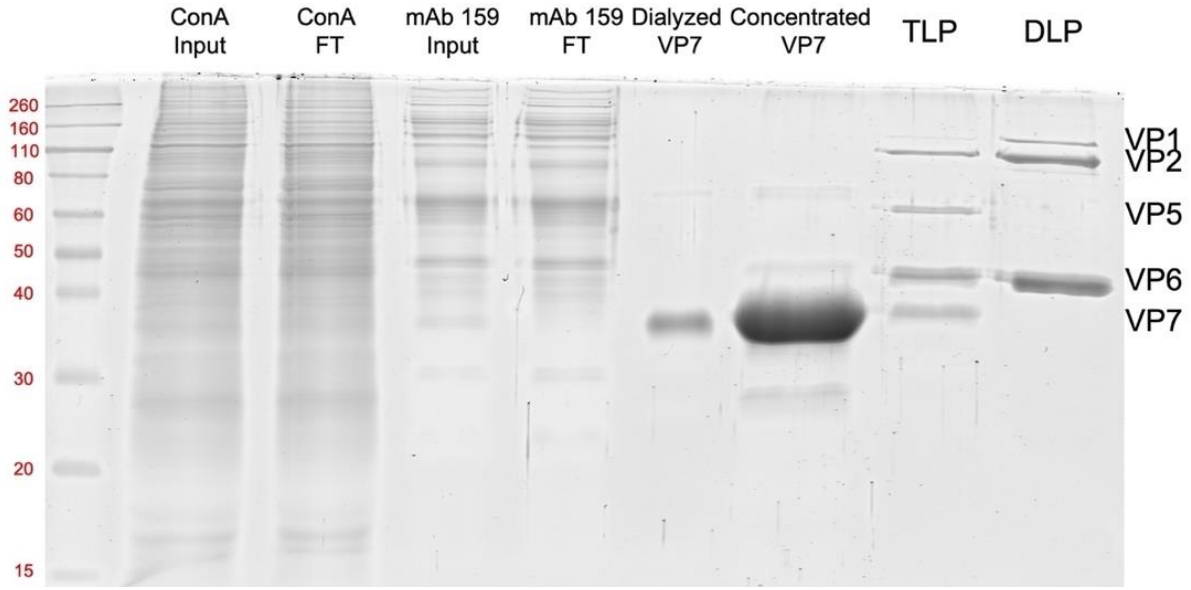

Figure 6-1: Successful VP7, TLP and DLP purification.
Recombinant VP7 was purified from Sf-9 cells using a concanavalin A column (ConA) and an antibody column (mAb 159). A total protein stain of the input and the flow through (FT) from each column, as well as the purified recombinant VP7 (~37 kDa) and purified TLP and DLP.

I successfully purified recombinant VP7, as well as RRV TLPs and DLPs. Recombinant VP7 was produced by infecting Sf-9 cells with a recombinant baculovirus that expresses RRV VP7, and VP7 was subsequently secreted into the media by infected cells. VP7 is a glycoprotein allowing us to first enrich for it using a lectin column

(concanavalin A). Then we used an antibody affinity column that's epitope is trimeric VP7. As these trimers are stabilized by calcium, we eluted off monomeric VP7 by chelating away Ca^{2+} by adding EDTA. TLPs and DLPs from RRV were purified by density gradient ultracentrifugation of the viral lysate over $CsCl_2$ gradients (Fig 6-1).

My attempts to purify VP4 were not as fruitful, due in part to it being very sensitive to proteases[209]. Recombinant VP4 was produced using a baculovirus expressing RRV VP4 and infecting Sf-9 cells, which were then harvested and lysed to release the recombinant VP4. Initial purification attempts involved using hydrophobic, anion exchange, and size exclusion columns sequentially to purify VP4; however, when I examined the fractions by total protein stain and western blot, we did not get pure VP4. Upon consulting Tobias Herrmann in the laboratory of Stephen C. Harrison at Harvard Medical School, I attempted to purify VP4 using an optimized protocol he developed that just employed the anion exchange column. This would reduce the overall purification time and hopefully minimize the time VP4 was at room temperature or exposed to proteases. While I was unable to get pure, uncleaved VP4, I did enrich for uncleaved VP4 (Fig 6-2).

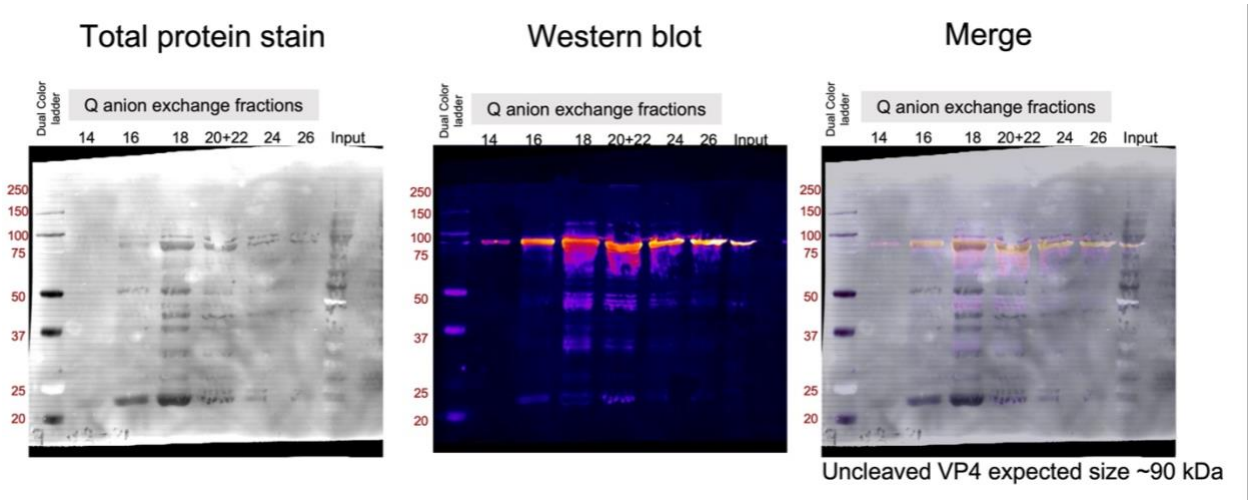

Figure 6-2: Enrichment of VP4.

Fig. 6-2 (continued): A fluorescent total protein stain (AzureRed) and a western blot (probed with an anti-RRV VP5* antibody, HS-2[210]) were done sequentially on a PVDF membrane loaded with the Q anion exchange column fractions. Uncleaved VP4 is 86 kDa and VP8* is 28 kDa[211]. On virions VP5* is 60 kDa; however, trypsin cleavage of recombinant VP4 can produce three fragment sizes (approximately 28, 30, 32 kDa) depending on which arginine is used[212,209].

I performed one recoating reaction using my purified VP7, purified DLP, and enriched VP4. Prior studies optimizing the recoating reaction show that infectious rcTLPs can be obtained when using crude recombinant baculovirus-infected cell lysate as the source of VP7 and VP4[208]. Comparing the infectivity of purified TLP and purified DLP to the recoated rcTLP, I observed that the rcTLP appears to be as infectious as natively produced TLPs (Fig 6-3).

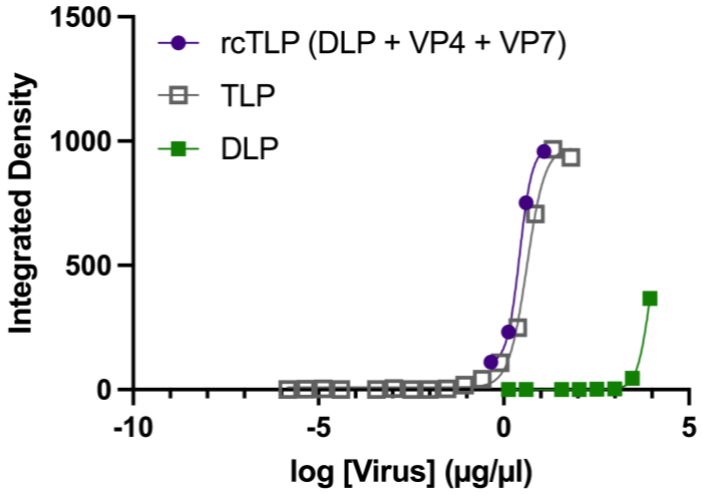

Figure 6-3: rcTLP is as infectious as TLPs purified from cellular lysate.
The rcTLP (purple circles), TLP (gray squares), and DLP (green squares) viruses were serially diluted and used to infect MA104 cells. The integrated density of total well fluorescence of stained VP6 was measured. Both rcTLP and TLP were more infectious than DLPs. n=1

The next steps to make this rcTLP tool useful for our planned trafficking studies is to fluorescently label the DLP, VP7, and VP4 with Atto dyes prior to the recoating reaction. For the purposes of our studies, we might only need to label the DLP and VP7 to interrogate which endosomal compartment the virus is in and if the virus has

uncoated. Future efforts to purify recombinant VP4 will involve using a refrigerated FPLC machine and potentially using a size exclusion column after the anion exchange column to separate uncleaved VP4 from cleaved VP5* and other protein products. However, purification instead of enrichment of VP4 may not be necessary, as I was able to obtain infectious rcTLPs using enriched VP4.

Chapter 7: Materials and Methods

Adenoviral Experiments

Cell lines: HEK 293 cells overexpressing human β5 integrin (293β5)[141] and A549 cells (ATCC) were maintained in Dulbecco's modified Eagle's medium (DMEM) with 10% fetal bovine serum (FBS), penicillin, streptomycin, L-glutamine, and non-essential amino acids (complete media).

HD5: Partially purified (89%) linear peptides (UniProtKB: ATCYCRTGRCATRESLSGVCEISGRLYRLCCR) were synthesized (LifeTein, Somerset, NJ), oxidatively folded, and purified by reverse-phase high-pressure liquid chromatography (RP-HPLC)[164]. Fractions containing the correctly folded species were lyophilized, resuspended in deionized water, and quantified by absorbance at 280 nm as described[164]. Purity (>99%) and mass were verified by analytical RP-HPLC and MALDI-TOF mass spectrometry. HD5 was stored at -80°C.

Adenoviruses: An E1/E3-deleted, replication-defective HAdV-5 vector containing a CMV promoter-driven enhanced green fluorescent protein (eGFP) reporter gene cassette was used as the parent construct for all of the novel chimeras created for these studies, which were generated by recombineering in BACmids [141,213]. The C1 chimera was previously referred to as "PB/GYAR"[141]. Designs of chimeras C2-C14 are depicted in Fig. 3. Hexon chimeras were created by replacing either HVR1 (bp 19247 to 19336 in HAdV-5, NCBI: AC_000008.1), HVR7 (bp 20090 to 20203), or both HVR1 and HVR7 in the HAdV-5 *hexon* ORF with the corresponding sequences from HAdV-64 HVR1 (bp 18196 to 18243, GenBank: EF121005.1) and HVR7 (bp 19027 to 19161). The combined hexon HVR1/C4

vertex chimera was created by replacing the HAdV-5 HVR1 with that of HAdV-64 in the C4 chimera. A previously described E3 deleted, replication-competent HAdV-64 virus containing a CMV-eGFP ORF was also used to study the effects of HD5 on infection of a virus with a WT HAdV-64 capsid[214]. The fidelity of all BACmid constructs was verified by Sanger sequencing of the recombineered region and by restriction digest of the entire BACmid. In addition, the BACmids of HAdV-64, chimera C1, and chimera C4 were sequenced in their entirety by whole genome sequencing.

To produce virus, 293β5 cells were transfected with viral genomes released from the BACmids by *Pac* I endonuclease digestion. Following amplification over several passages in 293β5 cells to generate sufficient inoculum, approximately eight to ten T175 flasks of 293β5 cells were infected at a multiplicity of infection of ~3. Upon development of complete cytopathic effect, virus was precipitated from the supernatant in 8% polyethylene glycol (PEG)[215]. Virus was then purified from cell lysates and the PEG precipitate using a CsCl gradient as previously described[134]. Purified virus was dialyzed against three changes of 150 mM NaCl, 40 mM Tris, 10% glycerol, 2 mM $MgCl_2$, pH 8.1, snap frozen in liquid nitrogen, and stored at -80°C. The viral particle concentration was determined by Qubit fluorometric quantification (ThermoFisher) against a DNA standard (1 µg = 2.34E+10 virions). Genomic DNA was isolated from purified virus using the GeneJET genomic DNA purification kit (Thermo Fisher), and the fidelity of the changed regions was verified by Sanger sequencing. For biochemical assays, viral protein concentration was determined by Bio-Rad Protein Assay with a bovine serum albumin standard.

Binding of Adenovirus/HD5 to Cells: Viruses were labeled using AF488 carboxylic acid, tetrafluorophenyl ester (Thermo Fisher Scientific) as previously described[128]. Labeling appeared to have no effect (C4 vertex), less than a 2-fold effect (HAdV-5, hexon HVR1, and hexon HVR1/C4 vertex), or a 3-fold (HAdV-64) effect on the infectivity of the viruses on A549 cells. To normalize the amount of each virus used for binding and trafficking studies, we used epifluorescence microscopy to quantify the amount of virus internalized by cells at 2 h p.i. for a dilution series of each virus. Because each virus was labeled to a different level of brightness, the absolute shift in GMF of cells bound to each virus varied.

Similar amounts of AdV5.eGFP, HAdV-64, and the chimeric viruses were incubated with 0, 2.5, 5, and 10 µM HD5 on ice in 60 µl SFM. A549 cells (1.0×10^5 cells/sample) were trypsinized and incubated in suspension on ice in PBS containing 0.2% sodium azide to prevent endocytosis. The virus-defensin complexes were added to the cells (final volume of 100 µl/sample), incubated on ice for 45 min, washed twice with cold PBS to remove unbound virus, and fixed with 1% paraformaldehyde. Samples were analyzed on a BD FACS Canto II, and GMF values for the AF488 signal of the entire cell population were calculated using FlowJo v10.7.1.

Quantification of subcellular localization and image analysis: To measure the percentage of virus in the nucleus or lysosomes in the presence or absence of HD5, A549 cells were seeded at 3.5×10^4 cells/mL on glass coverslips at least 24 h prior to infection. AF488-labeled AdV5.eGFP and chimeric viruses were diluted in SFM to achieve similar numbers of visible labeled virions/cell (30 – 100, depending on genotype and replicate), as described above. Virus was bound to cells in 50 µL SFM at 4°C for 1 h in the dark.

Unbound virus was removed by two washes of cold SFM, and samples were then incubated with or without 10 μM HD5 in SFM at 4°C in the dark. After 1 h, coverslips were shifted to 37°C and incubated for the amount of time (2 h or 6 h) indicated in Fig. 8. Note that samples incubated for a total of 6 h were incubated for 2 h in SFM and for the remaining 4 h in complete media. After incubation, coverslips were washed with PBS, fixed for 15 min in 2% PFA at RT, washed with PBS, and then incubated for 20 min at RT in permeabilization buffer (20 mM glycine, 0.5% Triton-X 100, PBS). Cells were sequentially stained with mouse anti-human CD107a antibody (BD #555798) at 1:200 and with goat anti-mouse IgG AF594 (Thermo Fisher Scientific #A11005) at 1:1000 in antibody staining buffer (1% BSA and 0.05% Tween-80 in PBS) for 1 h at RT. The nucleus was then labeled using 500 ng/mL DAPI for 5 min, and coverslips were mounted with ProLong Gold (Life Technologies #P36930).

Z-series of images spanning the entirety of the cells were obtained by epifluorescence microscopy using a Keyence BZ-X710 microscope in high resolution mode with a 100X objective. A maximum intensity z-profile of each field of view was generated using CellProfiler version 3.1.9[216]. CellProfiler was also used for colocalization analysis. Briefly, DAPI fluorescence was smoothed by a Gaussian filter, and nuclei were identified upon application of thresholding by the Otsu method. Nuclear border propagation guided by fluorescence in the Alex Fluor 594 channel, after application of Otsu thresholding, was used to define cell borders. Speckles were enhanced in the AF488 and AF594 channels, and a robust background thresholding was applied to identify virions and lysosomes, respectively. These objects were then shrunk and expanded to uniform circles with diameters of 2 pixels (virions) and 3 pixels (lysosomes) based on the

distribution of dimensions of the raw objects. For quality control, the identified objects were visually inspected and manually adjusted, as needed. Object-based colocalization was then used to identify virions overlapping with lysosomes or the nucleus in each cell. Cells containing fewer than 10 virions were excluded from analysis.

Thermostability Assay: To measure the capsid association of fiber, 250 ng of purified virus was incubated on ice with or without the indicated concentrations of HD5 for 45 min in SFM containing 0.05% BSA, 150 mM NaCl, and 10 mM HEPES pH 7.5. Samples were heated in a thermocycler at the indicated temperatures for 10 min and loaded onto a discontinuous gradient containing 400 µl of 30% Histodenz and 200 µl of 80% Histodenz in 20 mM tris pH 7.4. Samples were centrifuged as described above. Fractions were collected as follows: 90 µl from the top (supernatant), 2 middle fractions of 150 µl, and then 90 µl (virus band). The supernatant and band fractions were reduced with DTT, heated to 95°C for 5 min, separated by SDS-PAGE (12% tris-glycine gel), transferred to nitrocellulose, and probed by immunoblot for fiber using the 4D2 monoclonal antibody (ThermoFisher) and an AF647-conjugated secondary antibody. Blots were imaged and quantified as described above to determine the fraction of total fiber in each sample that was present in the virus band fraction. Prism 8.3.0 was used for non-linear regression analysis to calculate Tm and HD5 concentrations resulting in 50% fiber dissociation in Fig. 2-3.

Rotaviral Experiments

α-defensin peptides: Peptides (see Fig 3-1B for sequences) were synthesized by CPC Scientific (Sunnyvale, CA). Most peptides (HD5, Crp2, RMAD4, RED1, and RED3) were initially dissolved at 2 mg/mL in 8 M GuHCl, 12 mM reduced glutathione, and 1.2

mM oxidized glutathione in water and were then diluted with 0.25 M $NaHCO_3$ in water to a final concentration of 0.5 mg/mL peptide, 2 M guanidine hydrochloride, 3 mM reduced glutathione, 0.3 mM oxidized glutathione, and 0.19 M $NaHCO_3$, pH 8.3. However, HNP1 and RMAD1 were initially dissolved at 0.5 mg/mL in 50% *N*,*N*-dimethylformamide (DMF), 4 M urea, 6 mM reduced glutathione, and 0.6 mM oxidized glutathione in water and were then diluted with 0.2 M $NaHCO_3$ in water to a final concentration of 0.25 mg/mL in 25% *N*,*N*-dimethylformamide (DMF), 2 M urea, 3 mM reduced glutathione, 0.3 mM oxidized glutathione, and 0.1 M $NaHCO_3$, pH 8.1. Note that the ratio of reduced to oxidized glutathione was inadvertently adjusted to 5:1 for one preparation each of HNP1 and RMAD1, although this did not affect the final product. After overnight incubation at RT, peptides were purified by reverse-phase high-pressure liquid chromatography (RP-HPLC) over an acetonitrile gradient using a Hichrom Prevail C18 column (5 µm, 22 x 250 mm) or a Waters Delta-Pak C18 column (5 µm, 19 x 300 mm, 300 Å). Fractions containing the correctly folded species were lyophilized, resuspended in water, quantified by UV absorbance at 280 nm using calculated molar extinction coefficients [217], adjusted to approximately 1 mM with water, and stored in aliquots at 80°C. For all peptides except RED1, the correctly folded species was found in a distinct peak with a shorter retention time than unfolded or partially folded intermediates. However, the RED1 chromatogram was more complex, and the correctly folded species was identified in a peak with an intermediate retention time. Purity was assessed by analytical RP-HPLC performed with an Agilent Zorbax 300SB-C18 column (5 µm, 2.1 x 250 mm) or a Thermo Scientific Acclaim 120 C18 column (5 µm, 4.6 x 100 mm, 120 Å). Formation of three disulfide bonds was verified by electrospray ionization mass spectrometry (ESI-MS) in high resolution

mode on a Thermo Scientific LTQ Orbitrap or Orbitrap Elite mass spectrometer. Average yield of purified defensins from 20-59 mg of partially purified (81.0-86.3%), synthesized peptide was ~15%.

Cells: Monkey kidney epithelial MA104 cells were a kind gift from Monica McNeal of Cincinnati Children's Hospital Medical Center (Cincinnati, OH) and HeLa cells were purchased from the American Type Culture Collection. Cells were propagated in DMEM supplemented with 0.1 mM non-essential amino acids, 100 units/mL penicillin, 100 µg/mL streptomycin, 4 mM L-glutamine, and 10% fetal bovine serum (complete DMEM). HPV16 pseudovirus (PsV) encapsidating an eGFP reporter plasmid was produced via transfection and maturation as previously described [135].

Baby hamster kidney T7 cells (BHK-T7) were a gift from Ursula Buchholz (NIAID, NIH)[218]. The MA104 N*V cells were a gift from Ken Mellits (University of Nottingham). BHK-T7 and MA104 N*V cells were adapted from Glasgow MEM and Medium 199, respectively, to complete DMEM over 4 passages. BHK-T7 cells were propagated in complete DMEM supplemented with 2 mg/mL G-418 for every other passage. MA104 N*V cells were propagated in complete DMEM supplemented with 3 µg/mL puromycin and 3 µg/mL blasticidin every other passage. Hybridoma 159 cells were a gift from Stephen Harrison (Harvard University) and grown in RPMI 1640 media supplemented with 10% FBS.

Rotaviruses: Rhesus rotavirus (RRV), simian rotavirus (SA11), and epizootic diarrhea of infant mice (EDIM) were kind gifts from Monica McNeal. Human rotavirus isolate DS-1 was generously gifted by Mary Estes of Baylor College of Medicine (Houston, TX). Human rotavirus isolate Wa was obtained from ATCC (VR-2018). ETD and reassortant viruses

D1/5, EA 4-1-2, B7/2, and D6/2 were previously described [181,182]. All rotaviruses were stored at -80°C.

To create stocks of rotaviruses, the inoculum was trypsin-activated by incubation for 45-60 min at 37°C with 10 µg/mL type IX-S EDTA-free porcine trypsin (Sigma-Aldrich) and then added to a monolayer of MA104 cells. After incubation for 1 h at 37°C, the inoculum was removed, and the media was replaced with serum-free DMEM containing 0.5 µg/mL type IX-S EDTA-free porcine trypsin. The culture was harvested after incubation for 3-7 d at 37°C, upon the appearance of complete cytopathic effect. Cells were lysed by three freeze-thaw cycles and centrifuged to remove cell debris. Viral lysate was stored in aliquots at -80°C.

Rotavirus verification: The identity of each RRV, SA11, Wa, DS-1, EDIM, ETD, D1/5, EA 4-1-2, B7/2, and D6/2 virus stock was verified by isolating viral genomic RNA (Thermo Scientific GeneJet Viral DNA and RNA Purification Kit), amplifying gene segment 9 (VP7) for all viruses as well as gene segment 4 (VP4) for the reassortant viruses and DS-1 by RT-PCR (Promega GoScript Reverse Transcriptase) using sequence-specific primers followed by end point PCR, and Sanger sequencing. Primers used for amplification and sequencing are listed in Table 1.

Whole genome sequencing was also performed on SA11 and Wa. Viral RNA was extracted from viral lysates using Quick RNA Viral Kits (Zymo Research) and treated with TURBO DNase (ThermoFisher Scientific) to remove any remaining host DNA. Following DNase treatment, viral RNA was reverse transcribed into cDNA using SuperScript IV Reverse Transcriptase (ThermoFisher Scientific) and random hexamers

(Integrated DNA Technologies) for first strand synthesis, and Sequenase 2.0 (ThermoFisher Scientific) for second strand synthesis. The resulting cDNA was cleaned with Ampure XP magnetic beads (Beckman Coulter) and used to generate sequencing libraries using DNA Prep with Enrichment Kits (Illumina). Sequencing libraries were pooled and delivered to the NGS core lab at the University of Washington's Clinical Virology Lab, where they were sequenced using NextSeq and NovaSeq instruments (Illumina) generating 100-150 bp single-end reads.

The raw read data was then trimmed using Trimmomatic to remove adapter sequences and low-quality reads. Variant calling and data visualization were performed using the Reference-based Analysis of Viral Alleles (RAVA) pipeline developed by the Greninger Lab (https://github.com/greninger-lab/lava/tree/rava), using the GenBank sequences for Rotavirus A Strain SA11-5N and Rotavirus A strain Human-tc/USA/Wa/1974/G1P8 as references (Table 2).

Table 1: Primers used to verify the identity of rotaviruses

Viruses	Seg-ment	RT and PCR Primers	Sequencing Primers
B7/2, D1/5, D6/2, EA 4-1-2	4	GGCTATAAAATGGCTTCGCTCATTTATAG GGTCACATCCTCTAGAAATTGCTTACAG	GCTAATGCTTCCCAAACACAATGG
DS-1	4	TATGCTCCAGTTAACTGGGGAC GGCTGATAATGACCTAACATACACC	TATGCTCCAGTTAACTGGGGAC
EDIM	4	GGCTATAAAATGGCTTCACTCATTTATAGAC GGTCACATCCTCTAGACACTGC	CGTACCTACACATTGTTCGG CAGAGATCTCTTTCAAACCAGCG GTGCCGTCCAACGATAACTATC AGCGTCAGAGAAGTTCATTCCG GAAGAGTAGTATGCCTGACCTGC
ETD	4	GGCTATAAAATGGCTTCACTCATTTATAGAC GGTCACATCCTCTAGACACTGC	CGTACCTACACATTGTTCGG
RRV	4	GGCTATAAAATGGCTTCGCTCATTTATAG GGTCACATCCTCTAGAAATTGCTTACAG	GCTAATGCTTCCCAAACACAATGG CGTATACACGAGATGGAGAGGAGG AACGACAGTTGGGTGAACTTAGAG GTCACTGAAGCTTCAGAGAAGTTC GTAGTACTTAGTGGTCACATTCGG
B7/2, D1/5, EA 4-1-2, RRV	9	GGCTTTAAAAGAGAGAATTTC GGTCACATCATACAATTCTAA	TTCCGTCTGGCTAGCGGTT
D6/2, EDIM, ETD	9	GGCTTTAAAAGAGAGAATTTC GGTCACATCATACAGCTGTAA	TTCCGTTTGGCTAGCGGTT
DS-1	9	GGCTTTAAAAGAGAGAATTTC GGTCACATCATACAAATCTGA	TTCCGTCTGGCTAGCGGTT
SA11	9	GGCTTTAAAAGAGAGAATTTC GGTCACATCATACAATTCTAA	TTCCGTTTGGCTAGCGGTT
Wa	9	GGCTTTAAAAGAGAGAATTTC GGTCACATCATACAATTCTAA	TTCCGTCTGGCTAACGGTT

Table 2: Accession numbers used to align rotaviral sequences				
Segment	Virus	Accession Number	Virus	Accession Number
1	SA11	DQ838636	Wa	JX406747
2	SA11	DQ838631	Wa	JX406748
3	SA11	DQ838641	Wa	JX406749
4	SA11	DQ838602	Wa	JX406750
5	SA11	KX548939	Wa	JX406751
6	SA11	DQ838646	Wa	JX406752
7	SA11	DQ838606	Wa	JX406753
8	SA11	DQ838611	Wa	JX406754
9	SA11	DQ838616	Wa	JX406755
10	SA11	DQ838621	Wa	JX406756
11	SA11	DQ838626	Wa	JX406757

Rotavirus reverse genetics plasmids: SA11 plasmids collection (pT7-SA11-VP1, pT7-SA11-VP2, pT7-SA11-VP3, pT7-SA11-VP4, pT7-SA11-VP6, pT7-SA11-VP7, pT7-SA11-NSP1, pT7-SA11-NSP2, pT7-SA11-NSP3, pT7-SA11-NSP4, and pT7-SA11-NSP5) was acquired from Addgene Takeshi Kobayashi (Research Institute for Microbial Diseases, Osaka University, Japan)[168]. The RRV plasmid collection (pT7-RRV-VP1, pT7-RRV-VP2, pT7-RRV-VP3, pT7-RRV-VP4, pT7-RRV-VP6, pT7-RRV-VP7, pT7-RRV-NSP1, pT7-RRV-NSP2, pT7-RRV-NSP3, pT7-RRV-NSP4, and pT7-RRV-NSP5) were a kind gift from Susana López (Institute of Biotechnology, UNAM, Mexico). pCMVScript-NP868R-(G4S)4-T7RNAP (C3P3G1) was a gift from Philippe H Jaïs (EUKARŸS SAS).

The mutant VP4 plasmids were generated using Q5 quick-change mutagenesis. The primers were designed using agilent.com's primer program for Quikchange II. Primers used are listed in Table 3. 100 ng of template wild type pT7-RRV-VP4 or template mutant pT7-RRV-VP4 was added to a 50 µl total reaction that contained 1 unit Q5 High-

Fidelity DNA Polymerase (NEB), 1X Q5 buffer, 0.2 mM dNTPs, and forward and reverse mutagenesis primers at a final concentration of 0.05 µM each. DNA was denatured at 98°C for 30 seconds, then 12 cycles of 98°C for 10 seconds, 55°C for 30 seconds, and 72°C for 162 seconds was done before the final extension at 72°C for 2 min. 5 µl of the PCR reaction was run on a 1% TAE gel to check for amplification, the remaining sample was treated with 20 units of DpnI for 1 h at 37°C to digest template DNA. QIAquick PCR purification was done adhering to the manufacturer's protocol. 5 µl was used to transform 25 µl of subcloning efficiency DH5-alpha competent cells (Thermo Scientific).

Table: 3. Quick-change mutagenesis primers

Amino acid mutation(s)	**Nucleotide Mutation**	**Primer F 5'-->3'; Primer R 5'-->3'**
L37P	T110C	CGCAAAATGTCACTATTAATCCAGGTCCTTTTGCTCAAACAG; CTGTTTGAGCAAAAGGACCTGGATTAATAGTGACATTTTGCG
Y155H	T463C	AACTACACAAAATGGAAGCTATTCACAACACGGACCATTACAATC; GATTGTAATGGTCCGTGTTGTGAATAGCTTCCATTTTGTGTAGTT
V184A	T551C	TCCGAATGCGACCACTAAGTACTACTCAACTACA; GTGGTCGCATTCGGAGTTTCTCCATTATATGT
K187R	A560G	GAAACTCCGAATGTGACCACTAGGTACTACTCAACTACAAATTAT; ATAATTTGTAGTTGAGTAGTACCTAGTGGTCACATTCGGAGTTTC
I575L	A1723C	CCGACGCAGCTTCTTCACTTTCAAGAGGAGCATCT; AGATGCTCCTCTTGAAAGTGAAGAAGCTGCGTCGG
V184A, T185I, K187R	T551C; C554T; A560G	GGAGAAACTCCGAATGCGATCACTAGGTACTACTCAACTACAAATTATGATTC; GAATCATAATTTGTAGTTGAGTAGTACCTAGTGATCGCATTCGGAGTTTCTCC

All plasmids, except for the VP4 encoding ones, were purified using the Qiagen plasmid midiprep kit following manufacture's protocol. The VP4 encoding plasmids were purified using the Qiagen plasmid miniprep kit and nanopore sequenced (Plasmidsaurus).

Plasmid-based rotavirus reverse genetic system: A master mix of the pT7-SA11-VP1, pT7-SA11-VP2, pT7-SA11-VP3, pT7-SA11-VP6, pT7-RRV-VP7, pT7-SA11-NSP1, pT7-SA11-NSP2, pT7-SA11-NSP3, pT7-SA11-NSP4, pT7-SA11-NSP5, and C3P3G1 was generated where 1X master mix contained of 400 ng each of all rotavirus pT7 plasmids,

except pT7-NSP2 and pT7-NSP5 which were added at 1200 ng, and 800 ng of the plasmid C3P3-G1. 400 ng of the wild type or mutant pT7-RRV-VP4 was added to the 1X master mix prior to transfection.

$5x10^4$ BHK-T7 cells/mL were seeded into each well of 12-wells plate (1 mL/well) in the absence of G-418. Forty-eight hours later, each well was washed with 800 µl of fresh complete DMEM medium. To the rotavirus pT7 plasmid mixture described above, 125 µl of warmed Opti-MEM was added followed by 14 µl of MIRUS TransIT-LTI. This transfection mixture was gently pipetted up and down to mix and then incubated at RT for 20 min before adding to the BHK-T7 monolayer dropwise. The cells were incubated at 37°C for 16-18 h and then washed once with serum-free DMEM (SFM) and then 800 µl SFM was added to each well. 24 h later, 200 µl of $2.5x10^4$ MA104 N*V cells/mL in SFM was seeded over the MA104 cells. Approximately 1 h after adding MA104 N*V cells, type IX-s EDTA-free porcine trypsin was added to each well to a final concentration of 0.5 µg/mL. The sample was incubated at 37°C until cytopathic effects (CPE) were observed at which time the lysate was harvested (~3-5 days). If no CPE was observed by 12 days, the remaining cells on the monolayer were scrapped off and the lysate was harvested. Harvested transfected cells were snap frozen in liquid nitrogen and thawed at 37°C three times then 300 to 500 µl of p0 virus was activated with trypsin and passaged into a T25 of MA104 cells.

Defensin sensitivity assay and quantification of viral infection: Rotavirus was activated with 10 µg/mL type IX-S EDTA-free porcine trypsin for 45 min to 1 h at 37°C. For protocol 1, RV or HPV PsV was diluted to a concentration that was 2-fold more concentrated than what was predetermined to yield 50%-80% of maximal signal for

inhibition studies and 15-30% of maximal infection for enhancement studies in the absence of defensin. The viruses were then diluted 2-fold into SFM or defensin and incubated on ice for 45 min in serum-free DMEM (SFM). The mixture (35 or 50 µL) was then added to a well containing a confluent monolayer of MA104 (for rotavirus) or HeLa (for HPV PsV) cells in clear bottom, black wall 96-well plates (Perkin-Elmer) that had been washed twice with SFM. For protocol 2, Rotavirus or HPV PsV was diluted to a concentration that was predetermined to yield 50%-80% of maximal signal for inhibition studies and 15-30% of maximal infection for enhancement studies in the absence of defensin. 35 or 50 µl of RV was added to a well of MA104 cells and incubated while rocking for 1 h at 4°C. The cells were then washed twice with cold SFM, 35 or 50 µL defensin in SFM was added, and samples were incubated while rocking for 45 min at 4°C. For both protocols, samples were then incubated for 2 h at 37°C, with the 35 µl samples rocked constantly. After the incubation, samples were washed with SFM, and incubated for an additional 20-24 h with 100 µl/well complete DMEM. For HPV PsV samples, total monolayer fluorescence of each well was quantified with a Typhoon 9400 (GE Healthcare) variable mode imager.

Rotavirus samples were fixed with 2% paraformaldehyde in phosphate buffered saline (PBS) for 20 min at RT, washed twice with PBS, and then permeabilized and quenched with 20 mM glycine, 0.5% Triton X-100 in PBS for 20 min at RT. Cells were stained with a 1000-fold dilution of a primary anti-rotavirus antibody in 0.05% Tween-80/1% bovine serum albumin (BSA) in PBS for 1 h at RT. The antibody used in chapter 3 was produced in rabbits using an inoculum of mostly double layered Wa, SA11, and ST3 particles and was a kind gift from Monica McNeal [219]. The antibody used in chapter

4 was a primary mouse anti-rotavirus antibody (Santa Cruz Biotechnology sc-101363). Cells were washed three times with 0.05% Tween-80 in PBS and stained with a 1000-fold dilution of Alexa Fluor 488-conjugated goat anti-rabbit antibody (Fisher Scientific and Life Technologies) or Alexa Fluor 594-conjugated goat anti-mouse antibody (Invitrogen) in 0.05% Tween-80/1% BSA in PBS for 1 h at RT. Cells were washed once with 0.05% Tween-80 in PBS and then twice with PBS. Total monolayer fluorescence of each well was quantified with either a Typhoon 9400 (GE Healthcare) or Sapphire (Azure) variable mode image. For all samples, Fiji (version 2.1.0/1.53c) was used to quantify background-subtracted total monolayer fluorescence [220]. Data are shown as a percent of control infection in the absence of defensin.

Rotavirus directed evolution: SA11+RRV: VP4, VP7 was passaged 4 times in T-25 flasks and once in a T-75 flask containing MA104 cells. SA11+RRV: VP4, VP7 p5 was diluted to a concentration that was predetermined to yield 80% of maximal signal for the no defensin pressure condition. For the RMAD1 pressure condition, the viral dilution was about 9-fold more concentrated than in the no defensin condition such that it would have a similar level maximal signal as the no defensin condition after being incubated at its IC_{90} RMAD1. SA11+RRV: VP4, VP7 p5 was activated with 10 µg/mL type IX-S EDTA-free porcine trypsin for 1 h at 37°C and then was pre-incubated, on ice, with SFM or RMAD1 diluted in SFM at its IC_{90} (10 µM first round of selection) for 45 min. Two wells of a 24-well plate of MA104 cells were washed twice with SFM before adding 200 µl of the SA11+RRV:VP4, VP7 p5 plus RMAD1 or the no defensin control virus. The plate was incubated for 2 h at 37°C with rocking. Samples were washed with SFM, and 500 µl of SFM containing 0.5 µg/mL type IX-S EDTA-free porcine trypsin added to each well and

the samples were put back at 37°C until complete cytopathic effects were observed, typically 2-4 d p.i. Viral lysates were harvested, snap frozen in liquid nitrogen and thawed 3 times, and the cell debris removed by centrifugation. An aliquot was used to determine the infectious titer the virus on a 96 well plate and then the RMAD1 sensitivity of both the RMAD1 pressure condition and the no defensin pressure condition was assayed at least every other passage.

The viruses were then passaged again in a 24-well plate of MA104 cells. The no defensin pressure condition was passaged at its ~80% maximal infection concentration. The RMAD1 pressure condition was diluted to be 9-fold more concentrated than the dilution it would need to reach ~80% maximal infection, and the concentration of RMAD1 adjusted as needed to keep the virus under the approximate IC_{90} pressure. Additionally, the RMAD1 pressured condition virus was diluted to its 80% maximal infection concentration and added to a well of MA104 cells in the absence of defensin to qualitatively see the viral replication kinetics in the absence of defensin. Note that this virus was not harvested for further examination. Each passage was harvested and reassessed as above until the RMAD1 IC_{90} was determined to be 40 µM RMAD1 or greater for the RMAD1 pressure condition.

Next Gen Sequencing of Rotavirus Evolution Mutants: Viral RNA was extracted from all viral lysates using Quick RNA Viral Kits (Zymo Research) and treated with TURBO DNase (ThermoFisher Scientific) to remove any remaining host DNA. Following DNase treatment, viral RNA was reverse transcribed into cDNA using SuperScript IV Reverse Transcriptase (ThermoFisher Scientific) and random hexamers (Integrated DNA Technologies) for first strand synthesis, and Sequenase 2.0 (ThermoFisher Scientific) for

second strand synthesis. The resulting cDNA was cleaned with Ampure XP magnetic beads (Beckman Coulter) and used to generate sequencing libraries using DNA Prep with Enrichment Kits (Illumina). Sequencing libraries were pooled and delivered to the NGS core lab at the University of Washington's Clinical Virology Lab, where they were sequenced using NextSeq and NovaSeq instruments (Illumina) generating 100-150 bp single-end reads.

The raw read data was then trimmed using Trimmomatic to remove adapter sequences and low-quality reads. Variant calling and data visualization were performed using the Reference-based Analysis of Viral Alleles (RAVA) pipeline developed by the Greninger Lab (https://github.com/greninger-lab/lava/tree/rava), using the genome sequences of the original unpassaged viruses as the reference sequences.

Neuraminidase Sensitivity Assays: Rotavirus was activated with 10 µg/mL type IX-S EDTA-free porcine trypsin for 1 h at 37°C. Rotavirus was then diluted to a concentration that was predetermined to yield 60%-80% of maximal signal in the absence of NA. While the rotaviruses were activating, a confluent monolayer of MA104 cells in a clear bottom, black wall 96-well plates (Perkin-Elmer) was washed twice with SFM and then 50 µl/well of a dilution series of *A. ureafaciens* neuraminidase (Sigma-Aldrich), diluted in SFM, was added and incubated at 37°C for 45 min. NA was removed from the wells and 50 µl of activated rotavirus added. The virus was allowed to infect for 2 h at 37°C. After the incubation, samples were washed with SFM, and incubated for an additional 20-24 h with 100 µl/well complete DMEM before being fixed and stained as above in the quantification of rotaviral infection.

For the combination of RMAD1 and NA, SR-WT, L37P, K187R, or Best 4 rotaviruses were activated with 10 µg/mL type IX-S EDTA-free porcine trypsin for 1 h at 37°C and diluted to a concentration that was two-fold more concentrated than the dilution that would yield 60%-80% of maximal signal in the absence of NA and defensin. The viruses were then diluted two-fold with SFM or RMAD1 and incubated on ice for 45 min. The MA104 cells were washed twice with SFM and then treated with 50 µl of 12.5 mU/mL NA (*A. ureafaciens*) or SFM and were incubated at 37°C for 45 min. NA was removed from the wells and 50 µl of rotavirus added. The virus was allowed to infect for 2 h at 37°C. After the incubation, samples were washed with SFM, and incubated for an additional 21 h with 100 µl/well complete DMEM before being fixed and stained as above in the quantification of rotaviral infection.

Rotaviral binding assay: MA104 cells were treated with trypsin EDTA (Corning), after the cells had lifted off the plate, the trypsin was quenched with complete DMEM and then the cells were pelleted and washed twice in SFM. MA104 cells were normalized to $1x10^7$ cells/mL in SFM containing 0.2% sodium azide to inhibit endocytosis. 50 µl aliquots of cells ($5x10^5$ cells/sample) were put on ice to cool. For the NA treated samples, *Vibrio cholerae* NA (Sigma-Aldrich) and *A. ureafaciens* NA were diluted in SFM to 100 mU/mL and then 50 µl added to MA104 cells. The cells were treated with NA for 1 h at 37°C, with vortexing every 10 min. After NA treatment, the cells were spun down, NA removed and then resuspended in 50 µl cold SFM containing 0.2% sodium azide. SA11-RRV: VP4, VP7 p5 was activated with 10 µg/mL type IX-S EDTA-free porcine trypsin for 1 h at 37°C. Using undiluted virus for the binding assay led to a linear range readout in the qPCR. RMAD1 was diluted in SFM containing 0.2% sodium azide to 4X the final concentration

such that the concentration indicated on the graph reflects the concentration of the defensin on the cells. 30 µl of virus was incubated with 30 µl RMAD1 on ice for 45 min. Then 50 µl of the complexed virus and defensin was added to 50 µl of cells on ice for 1 h and agitated every 5 min. After incubation, an unwashed sample containing just virus and cells was stored on ice while 800 µl cold SFM containing 0.2% sodium azide was added to eat tube, gently vortexed and then the cells spun down at 4°C. The supernatant was discarded and the cells were washed two more times as above. After final wash, cells were resuspended in 100 µl SFM containing 0.2% sodium azide and then RNA was extracted from all samples using Quick RNA Viral Kits (Zymo Research). 18 µl of RNA was then treated with TURBO DNase (ThermoFisher Scientific) to remove host DNA. Following DNase treatment, viral RNA was reverse transcribed into cDNA using SuperScript IV Reverse Transcriptase (ThermoFisher Scientific) and SA11's NSP3 specific primers (See Table 4) for first strand synthesis, and Sequenase 2.0 (ThermoFisher Scientific) for second strand synthesis. DNA was cleaned up using Zymo DNA Clean and Concentrator-5 kit and then a 10-fold dilution of cDNA into water was done. qPCR was performed using Sso advanced Universal SYBR (Bio-Rad) and the primers listed in table 4 following the manufacturers protocol. The $2^{(-\Delta\Delta Ct)}$ value was calculated by subtracting the Ct value of virus in the absence of treatment minus the Ct value of the unwashed sample from the Ct value of RMAD1 or NA treated samples minus the Ct value of the unwashed sample.

Table 4: Rotavirus Binding Assay Primers	
RT Primers	
TnP7SA11seg7F	5′-TCGTCGGCAGCGTCAGATGTGTATAAGAGACAGGGCATTTAATGC-3′
TnP5SA11seg7R	5′-GTCTCGTGGGCTCGGAGATGTGTATAAGAGACAGGGCCACATAACG-3′
qPCR Primers	
SA11NSP3qPCR2F	5′-GTGATGGACGATTCTGGTGTTA-3′
SA11NSP3qPCR2R	5′-GTATCAGCAAGCCAGTTTCTATTTC-3′

Supplemental Methods:

Rotavirus triple layered particle (TLP) and double layered particle (DLP) purification: Lysate from 10 T-182 flasks of MA104 cells infected with RRV was frozen at -80°C and then thawed overnight at room temperature. Lysate was pelleted in an Allegra X-15R at 3500 rpm for 20 min at 4°C. The supernatant was stored on ice while the pellet was resuspended in 2 mL of cold 20TNC (20 mM Tris pH 8.0, 100 mM NaCl, 1 mM $CaCl_2$). Resuspended pellet was then sonicated on ice for 5 second intervals at 20% Amp for a total of 15 seconds. Then 2 mL of freon (1,1,2-Trichlor-1,2,2,-triflouroethane) was added and mixed by inverting. The mixture was centrifuged at 1000xg for 10 min at 4°C, and the aqueous phase transferred to a new tube. The freon extraction was repeated on the aqueous phase and then the aqueous phase was combined with the viral lysate's supernatant. The combined supernatants were centrifuged in a Ti45 at 45 krpm for 1 h at 4°C, and the resulting pellets combined and resuspended in 3 mL 20TNC. These pellets were sonicated as before and freon extracted three times and then put over a continuous CsCl gradient. The gradient was made from 1.45 g/mL to 1.26 g/mL $CsCl_2$ in 20TNC and poured into SW 55 ti Ultra-clear tubes (13x51 mm). Virus was centrifuged in a SW 55 Ti rotor at 50 krpm for 2 h 24 min and the DLP and TLP bands were collected. DLPs and TLPs were then dialyzed three times against 600 mL 20TNC in a 7000 MWCO dialysis

cassette. Purified DLPs and TLPs were stored at 4°C. If just DLPs are needed, add 5 mM EDTA to viral lysate and use 20TNE (20 mM Tris pH 8.0, 100 mM NaCl, 1 mM EDTA) instead of 20TNC throughout, apart from dialysis, which should be done into 20 mM Tris pH 8.0, 100 mM NaCl.

Insect cell culture and baculoviruses: The baculoviruses encoding RRV VP4, RRV VP4^{V391D}, and RRV VP7 were a generous gift from Stephen C. Harrison (Harvard University). *Spodoptera frugiperda* Sf-9 cells were obtained from Expression System and cultured in ESF 921 medium in shake flasks at 27°C in a non-humidified, non-CO_2 atmosphere and shaken at 130 rpm. Cell concentration and viability were assessed by hemocytometer counting with cell viability evaluated by trypan blue dye exclusion. Cells were split when the density reached 6-8x10^6 cells/mL and seeded at 0.75-1x10^6 cells/mL.

mAb159 purification: Hybridoma 159 cells seeded into 10 T-225 flasks at 60-90% confluency with RPMI 1640 media supplemented with L-glutamine and 10% Low IgG FBS (Thermo Fisher A3381901). 7 days later, the supernatant was harvested, and cells were removed by centrifugation at 4°C. Supernatant was frozen and stored at -80°C.

Purification of mAb 159 was accomplished on an Amersham Biosciences AKTA FPLC system using a 1 mL HiTrap protein G HP column (Cytiva 17-0404-03) and following the manufacturers guidelines. In brief, hybridoma 159 supernatant was filtered through a 0.45 µm filter and then binding buffer (0.02 M sodium phosphate buffer, pH 7.0) was added at a ratio of 125:100 binding buffer to supernatant. 10 column volumes of binding buffer were pumped over the column at a flow rate of 1 mL/min. Then the diluted hybridoma 159 supernatant was pumped over the column at a flow rate of 4 mL/min. The

column was then washed with 10 column volumes of binding buffer. The antibody was eluted off the column with 5 column volumes of 0.1 M glycine-HCl, pH 2.7. Fractions of 0.45 mL were collected into 1.5 mL tubes that contained 50 µl of 1 M Tris-HCl, pH 9.0 to allow the pH of the final samples to be approximately neutral. Pooled fractions were dialyzed into PBS in a 20,000 MWCO slide A lyzer cassette. Protein concentration was measured with a Bradford assay (Bio-Rad). Antibody aliquots were stored at -80°C.

mAb159 column generation: A 1 mL HiTrap protein G HP column was equilibrated with 6 column volumes of 50 mM Tris, pH 7.5 + 150 mM NaCl. Purified mAb159 (1641 µg) was bound to the column 1 mL at a time and allowed to incubate for 10 min at RT after each addition (2.5 mL added in total). The column was washed with one column volume of 50 mM Tris pH 7.5 + 150 mM NaCl, and then one column volume of 200 mM triethanolamine pH 8.9 was added. Next, one column volume of 50 mM dimethyl pimelimidate dihydrochloride in 200 mM triethanolamine pH 8.9 was injected and the injection syringe was kept on the column and the bottom plugged. The crosslinking solution was allowed to incubate for 60 min at room temperature. After incubation, the column was washed with one column volume of 200 mM triethanolamine pH 8.9, and then blocked using one column volume of 100 mM ethanolamine pH 8.9. Unbound antibody was removed with 1.5 column volumes of 0.1 M glycine + 2 M urea. The column was then washed with 4 column volumes of 50 mM Tris pH 7.5 + 150 mM NaCl. The mAb 159 column was stored at 4°C in PBS + 0.02% sodium azide.

Concanavalin A column packing: 25 mL of concanavalin A agarose (G-Biosciences #786217) was packed sequentially into a 25 mL XK 16/20 column. 100TNC buffer (100 mM Tris pH 8.0, 100 mM NaCl, 1 mM $CaCl_2$) was used during the packing process. The

concanavalin A column was stored upright at 4°C in ConA Storage Buffer (100 mM sodium acetate pH 6.0, 1 M NaCl, 1 mM $CaCl_2$, 1 mM $MnCl_2$, 1 mM $MgCl_2$, 20% ethanol) when not in use.

Purification of VP7[74]: Recombinant VP7 was expressed in Sf9 cells using the Bac-to-Bac expression system. 2.4 L of 2×10^6 Sf9 cells/mL were infected with passage 4 baculovirus containing VP7 where the baculovirus makes up 2% of the flask volume. 72 h p.i. the cells were removed from the supernatant by centrifuging at 3200 rpm for 20 min at 4°C. Benzamidine was added to the supernatant to a concentration of 2.5 mM and sodium azide was added to a final concentration of 0.02% of the total volume. The Concavalin A resin column was equilibrated with 2 column volumes of 100TNC (100 mM Tris pH 8.0, 100 mM NaCl, 1 mM $CaCl_2$). The supernatant was filtered through a 0.45 µm filter before being loaded onto the Concavalin A resin column using an Amersham Biosciences AKTA FPLC system. The column was washed with 4 column volumes of 100TNC before the VP7 was eluted using 100TNC + 0.8 M α-methyl-mannose. The pooled fractions containing VP7 were then loaded onto the mAb 159 column that had been equilibrated with “Buffer A” (20 mM Tris pH 8.0, 50 mM NaCl, 0.1 mM $CaCl_2$). Recombinant VP7 was eluted using 25 column volumes of “Buffer B” (20 mM Tris pH 8.0, 50 mM NaCl, 1 mM EDTA). Eluted VP7 was collected into tubes that contained 20 mM Tris pH 8.0, 50 mM NaCl, 5 mM $CaCl_2$ at half the fraction volume. Pooled fractions were dialyzed into 0.1 HNE (2 mM HEPES pH 7.5, 10 mM NaCl, 1 mM $CaCl_2$) and then concentrated to 1.43 mg/mL using Amicom Ultra 10,000 MWCO. Aliquoted recombinant VP7 was flash-frozen with liquid nitrogen, and stored at −80 °C.

VP4 enrichment: Recombinant VP4 was expressed in Sf9 cells using the Bac-to-Bac expression system. 1.2 L of $2x10^6$ Sf9 cells/mL were infected with passage 4 baculovirus containing VP4 (26 mL baculovirus/1 L Sf9 cells). Cells were harvested when the viability had dropped to 75%, approximately 3 d p.i.. Cells were pelleted and then resuspended in 80 mL lysis buffer (75 mM Tris-HCl pH 8.0, 100 mM NaCl, 5 mM EDTA, 7.5% glycerol). After a freeze thaw, the suspension was sonicated three times on ice for 2 min 30 seconds with 1 second pulses at 40% amp, and the sample was put on ice for 5 min between each round of sonication. Sample was clarified by centrifuging in a Beckman 45 Ti rotor at 30 krpm for 1 h at 4 °C. VP4 was precipitated overnight at 4 °C from the supernatant by adding 0.24 g ammonium sulfate per mL solution. Pellet the VP4 precipitate in a Beckmann 45 Ti rotor at 30 krpm for 30 min at 4 °C. Discard supernatant and resuspend the pellet in a total of 60 mL cold 20 mM Tris pH 8.0, 1 mM EDTA, and 0.1X HALT protease inhibitors. Sample was then Dounce homogenized and the homogenate centrifuged in a Beckmann 45 Ti rotor at 30 krpm for 30 min at 4 °C. Supernatant was diluted with cold 20 mM Tris pH 8.0, 1 mM EDTA, 1 mM PMSF to a total of 900 mL, this is to ensure that the conductivity of the sample is below the Q column's start buffer (20 mM Tris pH 8.0, 10 mM NaCl, 1 mM EDTA), and then loaded using an Amersham Biosciences AKTA FPLC system onto a 5 mL Q Sepharose column (Cytiva) that was equilibrated with the Q column's start buffer. Elute VP4 off the column with a gradient from 20 mM Tris pH 8.0, 10 mM NaCl, 1 mM EDTA to 20 mM Tris pH 8.0, 150 mM NaCl, 1 mM EDTA. VP4 containing fractions were pooled, buffer exchanged into HNE (20 mM Hepes pH 7.5, 100 mM NaCl, 1mM EDTA) with 0.1 mM PMSF, and concentrated to 16.5 mg/mL using a 10 kDa MWCO Amicon-Ultra centrifugal filter. Enriched VP4 was snap

frozen with liquid nitrogen and stored at -80 °C. Q Sepharose column was stored in 20% EtOH at 4 °C.

Recoating of DLPs to make TLPs[81]: 2 µg of purified RRV DLPs were recoated by adding recombinant RRV VP7 in a stoichiometry excess of 2 and recombinant RRV VP4 in a stoichiometry excess of 40. A 0.5 mL Zeba spin desalting column was equilibrated in TN0.1E (20 mM Tris pH 8.0, 100 mM NaCl, 0.1 mM EDTA). Recombinant VP4 was diluted two-fold in TN0.1E and then buffer exchanged using the Zeba column. 2 µg of purified RRV DLPs and approximately 40-fold excess recombinant VP4 were diluted in 1 M sodium acetate pH 5.2 such that the final concentration is 100 mM sodium acetate pH 5.2, this mixture was incubated at room temperature for 1 h. Recombinant VP7, in about 2-fold excess, was mixed with a volume of 10 mM $CaCl_2$ in 20 mM Tris pH 8.0, as well as more 1 M sodium acetate pH 5.2, and added to the DLP+VP4 mixture such that the final concentrations would contain 1 mM $CaCl_2$ and 100 mM sodium acetate pH 5.2. DLP+VP4+VP7 mixture was then incubated for 1 h at room temp before being quenched with 2.22 µl of Tris pH 8.

Statistical analysis

Chapter 2: Statistical analysis was performed using Prism 8.3.0. Specific analyses are indicated in the figure legends. For all tests, not significant (ns), P > 0.05; *, P = 0.01 to 0.05; **, P = 0.001 to 0.01; ***, P = 0.0001 to 0.001; ****, P < 0.0001.

Chapter 3: Statistical analysis and non-linear regression of log-transformed data were performed using GraphPad Prism 9.2.0. Hill slopes are best fit values. For enhanced or resistant infection data, results of ordinary two-way ANOVA with Sídák's multiple comparisons test, with individual variances computed for each concentration, comparing protocol 1 and protocol 2 from 1.25-20 μM defensin are indicated by asterisks: P > 0.05; *, P = 0.01 to 0.05; **, P = 0.001 to 0.01; ***, P = 0.0001 to 0.001; ****, P < 0.0001. Unmarked comparisons within the specified analysis range are not significant. For neutralized infection data, log IC_{50} values between protocol 1 and protocol 2 were compared using the extra sum-of-squares F test, and the P value of the comparison is given.

Chapter 4: Statistical analysis and non-linear regression of log-transformed data were performed using GraphPad Prism 9.5.1. Hill slopes are best fit values. For neutralized data in Fig. 4-1, the log IC_{90} values between SR-WT and VP4 mutant rotaviruses were compared using the extra sum-of-squares F test, and the P value of the comparison is given. For neutralized data in Fig. 4-6, the log IC_{50} values between SR-WT and VP4 mutant rotaviruses, except V184A, were compared using the extra sum-of-squares F test, and the P value of the comparison is given. To compare V184A to SR-WT, each individual replicate's IC_{50} value was calculated using a non-linear regression with the top value constrained to 100 (additionally, values greater than 100 were excluded from the analysis)

and the bottom value constrained to 0. A Mann Whitney t-test comparing the log IC_{50} values between V184A and SR-WT was done, and the P value of the comparison is given. In Fig. 4-9 an ordinary one-way ANOVA with Dunnett's multiple comparisons test, with a single pooled variance, was performed to compare each virus to the level of infection in the absence of both neuraminidase and defensin. The P values are indicated by asterisks as follows: *, P = 0.01 to 0.05; **, P = 0.001 to 0.01; ***, P = 0.0001 to 0.001; and ****, P < 0.0001. Bars marked with a "ns" indicates P>0.05.

Copyright Permissions

Chapter 1: Figure 1-2 was modified and reprinted with permission from PLOS Pathogens: Long CP, McDonald SM (2017) Rotavirus genome replication: Some assembly required. PLoS Pathog 13(4): e1006242.

Chapter 2: “Defensin driven adenoviral evolution” was modified and reprinted with permission from PLOS Pathogens: Diaz K, Hu CT, Sul Y, Bromme BA, Myers ND, Skorohodova KV, Gounder AP, and Smith JG. (2020) Defensin-driven viral evolution. PLOS Pathogens 16(11): e1009018.

Chapter 3: “VP4 is a determinant of alpha-defensin modulation of rotaviral infection” was modified and reprinted with permission from the Journal of Virology: Hu CT, Diaz K, Yang LC, Sharma A, Greenberg HB, and Smith JG. (2022) VP4 Is a Determinant of Alpha-Defensin Modulation of Rotaviral Infection. JVI 96(7): e02053-21.

References

(1) Greber, U. F. Adenoviruses – Infection, Pathogenesis and Therapy. *FEBS Lett.* **2020**, *594* (12), 1818–1827. https://doi.org/10.1002/1873-3468.13849.

(2) Greber, U. F.; Flatt, J. W. Adenovirus Entry: From Infection to Immunity. *Annu. Rev. Virol.* **2019**, *6* (1), 177–197. https://doi.org/10.1146/annurev-virology-092818-015550.

(3) GBD 2016 Diarrhoeal Disease Collaborators. Estimates of the Global, Regional, and National Morbidity, Mortality, and Aetiologies of Diarrhoea in 195 Countries: A Systematic Analysis for the Global Burden of Disease Study 2016. *Lancet Infect. Dis.* **2018**, *18* (11), 1211–1228. https://doi.org/10.1016/S1473-3099(18)30362-1.

(4) Jonas, R. A.; Ung, L.; Rajaiya, J.; Chodosh, J. Mystery Eye: Human Adenovirus and the Enigma of Epidemic Keratoconjunctivitis. *Prog. Retin. Eye Res.* **2020**, *76*, 100826. https://doi.org/10.1016/j.preteyeres.2019.100826.

(5) Radke, J. R.; Cook, J. L. Human Adenovirus Infections: Update and Consideration of Mechanisms of Viral Persistence. *Curr. Opin. Infect. Dis.* **2018**, *31* (3), 251–256. https://doi.org/10.1097/QCO.0000000000000451.

(6) Lion, T. Adenovirus Infections in Immunocompetent and Immunocompromised Patients. *Clin. Microbiol. Rev.* **2014**, *27* (3), 441–462. https://doi.org/10.1128/CMR.00116-13.

(7) Alcamo, A. M.; Wolf, M. S.; Alessi, L. J.; Chong, H. J.; Green, M.; Williams, J. V.; Simon, D. W. Successful Use of Cidofovir in an Immunocompetent Child With Severe Adenoviral Sepsis. *Pediatrics* **2020**, *145* (1), e20191632. https://doi.org/10.1542/peds.2019-1632.

(8) Ganapathi, L.; Arnold, A.; Jones, S.; Patterson, A.; Graham, D.; Harper, M.; Levy, O. Use of Cidofovir in Pediatric Patients with Adenovirus Infection. *F1000Research* **2016**, *5*, 758. https://doi.org/10.12688/f1000research.8374.2.

(9) Davison, A. J.; Benkő, M.; Harrach, B. Genetic Content and Evolution of Adenoviruses. *J. Gen. Virol.* **2003**, *84* (Pt 11), 2895–2908. https://doi.org/10.1099/vir.0.19497-0.

(10) Gallardo, J.; Pérez-Illana, M.; Martín-González, N.; San Martín, C. Adenovirus Structure: What Is New? *Int. J. Mol. Sci.* **2021**, *22* (10), 5240. https://doi.org/10.3390/ijms22105240.

(11) Reddy, V. S.; Nemerow, G. R. Structures and Organization of Adenovirus Cement Proteins Provide Insights into the Role of Capsid Maturation in Virus Entry and Infection. *Proc. Natl. Acad. Sci.* **2014**, *111* (32), 11715–11720. https://doi.org/10.1073/pnas.1408462111.

(12) Bergelson, J. M.; Cunningham, J. A.; Droguett, G.; Kurt-Jones, E. A.; Krithivas, A.; Hong, J. S.; Horwitz, M. S.; Crowell, R. L.; Finberg, R. W. Isolation of a Common Receptor for Coxsackie B Viruses and Adenoviruses 2 and 5. *Science* **1997**, *275* (5304), 1320–1323. https://doi.org/10.1126/science.275.5304.1320.

(13) Tomko, R. P.; Xu, R.; Philipson, L. HCAR and MCAR: The Human and Mouse Cellular Receptors for Subgroup C Adenoviruses and Group B Coxsackieviruses. *Proc. Natl. Acad. Sci.* **1997**, *94* (7), 3352–3356. https://doi.org/10.1073/pnas.94.7.3352.

(14) Stasiak, A. C.; Stehle, T. Human Adenovirus Binding to Host Cell Receptors: A Structural View. *Med. Microbiol. Immunol. (Berl.)* **2020**, *209* (3), 325–333. https://doi.org/10.1007/s00430-019-00645-2.

(15) Persson, B. D.; Reiter, D. M.; Marttila, M.; Mei, Y.-F.; Casasnovas, J. M.; Arnberg, N.; Stehle, T. Adenovirus Type 11 Binding Alters the Conformation of Its Receptor CD46. *Nat. Struct. Mol. Biol.* **2007**, *14* (2), 164–166. https://doi.org/10.1038/nsmb1190.

(16) Gaggar, A.; Shayakhmetov, D. M.; Lieber, A. CD46 Is a Cellular Receptor for Group B Adenoviruses. *Nat. Med.* **2003**, *9* (11), 1408–1412. https://doi.org/10.1038/nm952.

(17) Marttila, M.; Persson, D.; Gustafsson, D.; Liszewski, M. K.; Atkinson, J. P.; Wadell, G.; Arnberg, N. CD46 Is a Cellular Receptor for All Species B Adenoviruses except Types 3 and 7. *J. Virol.* **2005**, *79* (22), 14429–14436. https://doi.org/10.1128/jvi.79.22.14429-14436.2005.

(18) Wang, H.; Li, Z.; Liu, Y.; Persson, J.; Beyer, I.; Möller, T.; Koyuncu, D.; Drescher, M. R.; Strauss, R.; Zhang, X.-B.; Wahl, J. K.; Urban, N.; Drescher, C.; Hemminki, A.; Fender, P.; Lieber, A. Desmoglein 2 Is a Receptor for Adenovirus Serotypes 3, 7, 11, and 14. *Nat. Med.* **2011**, *17* (1), 96–104. https://doi.org/10.1038/nm.2270.

(19) Burmeister, W. P.; Guilligay, D.; Cusack, S.; Wadell, G.; Arnberg, N. Crystal Structure of Species D Adenovirus Fiber Knobs and Their Sialic Acid Binding Sites. *J. Virol.* **2004**, *78* (14), 7727–7736. https://doi.org/10.1128/jvi.78.14.7727-7736.2004.

(20) Nilsson, E. C.; Storm, R. J.; Bauer, J.; Johansson, S. M. C.; Lookene, A.; Ångström, J.; Hedenström, M.; Eriksson, T. L.; Frängsmyr, L.; Rinaldi, S.; Willison, H. J.; Domellöf, F. P.; Stehle, T.; Arnberg, N. The GD1a Glycan Is a Cellular Receptor for Adenoviruses Causing Epidemic Keratoconjunctivitis. *Nat. Med.* **2011**, *17* (1), 105–109. https://doi.org/10.1038/nm.2267.

(21) Haisma, H. J.; Boesjes, M.; Beerens, A. M.; van der Strate, B. W. A.; Curiel, D. T.; Plüddemann, A.; Gordon, S.; Bellu, A. R. Scavenger Receptor A: A New Route for Adenovirus 5. *Mol. Pharm.* **2009**, *6* (2), 366–374. https://doi.org/10.1021/mp8000974.

(22) Stichling, N.; Suomalainen, M.; Flatt, J. W.; Schmid, M.; Pacesa, M.; Hemmi, S.; Jungraithmayr, W.; Maler, M. D.; Freudenberg, M. A.; Plückthun, A.; May, T.; Köster, M.; Fejer, G.; Greber, U. F. Lung Macrophage Scavenger Receptor SR-A6 (MARCO) Is an Adenovirus Type-Specific Virus Entry Receptor. *PLoS Pathog.* **2018**, *14* (3), e1006914. https://doi.org/10.1371/journal.ppat.1006914.

(23) Khare, R.; Reddy, V. S.; Nemerow, G. R.; Barry, M. A. Identification of Adenovirus Serotype 5 Hexon Regions That Interact with Scavenger Receptors. *J. Virol.* **2012**, *86* (4), 2293–2301. https://doi.org/10.1128/JVI.05760-11.

(24) Maler, M. D.; Nielsen, P. J.; Stichling, N.; Cohen, I.; Ruzsics, Z.; Wood, C.; Engelhard, P.; Suomalainen, M.; Gyory, I.; Huber, M.; Müller-Quernheim, J.; Schamel, W. W. A.; Gordon, S.; Jakob, T.; Martin, S. F.; Jahnen-Dechent, W.; Greber, U. F.; Freudenberg, M. A.; Fejer, G. Key Role of the Scavenger Receptor MARCO in Mediating Adenovirus Infection and Subsequent Innate Responses of Macrophages. *mBio* **2017**, *8* (4), e00670-17. https://doi.org/10.1128/mBio.00670-17.

(25) Greber, U. F.; Suomalainen, M. Adenovirus Entry: Stability, Uncoating, and Nuclear Import. *Mol. Microbiol.* **2022**, *118* (4), 309–320. https://doi.org/10.1111/mmi.14909.

(26) Parker, A. L.; Waddington, S. N.; Nicol, C. G.; Shayakhmetov, D. M.; Buckley, S. M.; Denby, L.; Kemball-Cook, G.; Ni, S.; Lieber, A.; McVey, J. H.; Nicklin, S. A.; Baker, A. H. Multiple Vitamin K-Dependent Coagulation Zymogens Promote Adenovirus-Mediated Gene Delivery to Hepatocytes. *Blood* **2006**, *108* (8), 2554–2561. https://doi.org/10.1182/blood-2006-04-008532.

(27) Parker, A. L.; McVey, J. H.; Doctor, J. H.; Lopez-Franco, O.; Waddington, S. N.; Havenga, M. J. E.; Nicklin, S. A.; Baker, A. H. Influence of Coagulation Factor Zymogens on the Infectivity of Adenoviruses Pseudotyped with Fibers from Subgroup D. *J. Virol.* **2007**, *81* (7), 3627–3631. https://doi.org/10.1128/jvi.02786-06.

(28) Waddington, S. N.; McVey, J. H.; Bhella, D.; Parker, A. L.; Barker, K.; Atoda, H.; Pink, R.; Buckley, S. M. K.; Greig, J. A.; Denby, L.; Custers, J.; Morita, T.; Francischetti, I. M. B.;

Monteiro, R. Q.; Barouch, D. H.; van Rooijen, N.; Napoli, C.; Havenga, M. J. E.; Nicklin, S. A.; Baker, A. H. Adenovirus Serotype 5 Hexon Mediates Liver Gene Transfer. *Cell* **2008**, *132* (3), 397–409. https://doi.org/10.1016/j.cell.2008.01.016.

(29) Kalyuzhniy, O.; Di Paolo, N. C.; Silvestry, M.; Hofherr, S. E.; Barry, M. A.; Stewart, P. L.; Shayakhmetov, D. M. Adenovirus Serotype 5 Hexon Is Critical for Virus Infection of Hepatocytes in Vivo. *Proc. Natl. Acad. Sci. U. S. A.* **2008**, *105* (14), 5483–5488. https://doi.org/10.1073/pnas.0711757105.

(30) Johansson, C.; Jonsson, M.; Marttila, M.; Persson, D.; Fan, X.-L.; Skog, J.; Frängsmyr, L.; Wadell, G.; Arnberg, N. Adenoviruses Use Lactoferrin as a Bridge for CAR-Independent Binding to and Infection of Epithelial Cells. *J. Virol.* **2007**, *81* (2), 954–963. https://doi.org/10.1128/JVI.01995-06.

(31) Persson, B. D.; Lenman, A.; Frängsmyr, L.; Schmid, M.; Ahlm, C.; Plückthun, A.; Jenssen, H.; Arnberg, N. Lactoferrin-Hexon Interactions Mediate CAR-Independent Adenovirus Infection of Human Respiratory Cells. *J. Virol.* **2020**, *94* (14), e00542-20. https://doi.org/10.1128/JVI.00542-20.

(32) Shayakhmetov, D. M.; Eberly, A. M.; Li, Z.-Y.; Lieber, A. Deletion of Penton RGD Motifs Affects the Efficiency of Both the Internalization and the Endosome Escape of Viral Particles Containing Adenovirus Serotype 5 or 35 Fiber Knobs. *J. Virol.* **2005**, *79* (2), 1053–1061. https://doi.org/10.1128/jvi.79.2.1053-1061.2005.

(33) Cuzange, A.; Chroboczek, J.; Jacrot, B. The Penton Base of Human Adenovirus Type 3 Has the RGD Motif. *Gene* **1994**, *146* (2), 257–259. https://doi.org/10.1016/0378-1119(94)90302-6.

(34) Albinsson, B.; Kidd, A. H. Adenovirus Type 41 Lacks an RGD Alpha(v)-Integrin Binding Motif on the Penton Base and Undergoes Delayed Uptake in A549 Cells. *Virus Res.* **1999**, *64* (2), 125–136. https://doi.org/10.1016/s0168-1702(99)00087-8.

(35) Meier, O.; Greber, U. F. Adenovirus Endocytosis. *J. Gene Med.* **2004**, *6* (S1), S152–S163. https://doi.org/10.1002/jgm.553.

(36) Greber, U. F.; Willetts, M.; Webster, P.; Helenius, A. Stepwise Dismantling of Adenovirus 2 during Entry into Cells. *Cell* **1993**, *75* (3), 477–486. https://doi.org/10.1016/0092-8674(93)90382-Z.

(37) Burckhardt, C. J.; Suomalainen, M.; Schoenenberger, P.; Boucke, K.; Hemmi, S.; Greber, U. F. Drifting Motions of the Adenovirus Receptor CAR and Immobile Integrins Initiate Virus Uncoating and Membrane Lytic Protein Exposure. *Cell Host Microbe* **2011**, *10* (2), 105–117. https://doi.org/10.1016/j.chom.2011.07.006.

(38) Nemerow, G. R.; Stewart, P. L. Insights into Adenovirus Uncoating from Interactions with Integrins and Mediators of Host Immunity. *Viruses* **2016**, *8* (12), 337. https://doi.org/10.3390/v8120337.

(39) Wiethoff, C. M.; Wodrich, H.; Gerace, L.; Nemerow, G. R. Adenovirus Protein VI Mediates Membrane Disruption Following Capsid Disassembly. *J. Virol.* **2005**, *79* (4), 1992–2000. https://doi.org/10.1128/JVI.79.4.1992-2000.2005.

(40) Cassany, A.; Ragues, J.; Guan, T.; Bégu, D.; Wodrich, H.; Kann, M.; Nemerow, G. R.; Gerace, L. Nuclear Import of Adenovirus DNA Involves Direct Interaction of Hexon with an N-Terminal Domain of the Nucleoporin Nup214. *J. Virol.* **2015**, *89* (3), 1719–1730. https://doi.org/10.1128/jvi.02639-14.

(41) Bauer, M.; Gomez-Gonzalez, A.; Suomalainen, M.; Schilling, N.; Hemmi, S.; Greber, U. F. A Viral Ubiquitination Switch Attenuates Innate Immunity and Triggers Nuclear Import of

Virion DNA and Infection. *Sci. Adv.* **2021**, *7* (51), eabl7150. https://doi.org/10.1126/sciadv.abl7150.
(42) Sarbanes, S. L.; Blomen, V. A.; Lam, E.; Heissel, S.; Luna, J. M.; Brummelkamp, T. R.; Falck-Pedersen, E.; Hoffmann, H.-H.; Rice, C. M. E3 Ubiquitin Ligase Mindbomb 1 Facilitates Nuclear Delivery of Adenovirus Genomes. *Proc. Natl. Acad. Sci. U. S. A.* **2021**, *118* (1), e2015794118. https://doi.org/10.1073/pnas.2015794118.
(43) Crawford, S. E.; Ramani, S.; Tate, J. E.; Parashar, U. D.; Svensson, L.; Hagbom, M.; Franco, M. A.; Greenberg, H. B.; O'Ryan, M.; Kang, G.; Desselberger, U.; Estes, M. K. Rotavirus Infection. *Nat. Rev. Dis. Primer* **2017**, *3* (1), 17083. https://doi.org/10.1038/nrdp.2017.83.
(44) Troeger, C.; Khalil, I. A.; Rao, P. C.; Cao, S.; Blacker, B. F.; Ahmed, T.; Armah, G.; Bines, J. E.; Brewer, T. G.; Colombara, D. V.; Kang, G.; Kirkpatrick, B. D.; Kirkwood, C. D.; Mwenda, J. M.; Parashar, U. D.; Petri, W. A., Jr; Riddle, M. S.; Steele, A. D.; Thompson, R. L.; Walson, J. L.; Sanders, J. W.; Mokdad, A. H.; Murray, C. J. L.; Hay, S. I.; Reiner, R. C., Jr. Rotavirus Vaccination and the Global Burden of Rotavirus Diarrhea Among Children Younger Than 5 Years. *JAMA Pediatr.* **2018**, *172* (10), 958–965. https://doi.org/10.1001/jamapediatrics.2018.1960.
(45) Bomidi, C.; Robertson, M.; Coarfa, C.; Estes, M. K.; Blutt, S. E. Single-Cell Sequencing of Rotavirus-Infected Intestinal Epithelium Reveals Cell-Type Specific Epithelial Repair and Tuft Cell Infection. *Proc. Natl. Acad. Sci. U. S. A.* **2021**, *118* (45), e2112814118. https://doi.org/10.1073/pnas.2112814118.
(46) Dong, Y.; Zeng, C. Q.-Y.; Ball, J. M.; Estes, M. K.; Morris, A. P. The Rotavirus Enterotoxin NSP4 Mobilizes Intracellular Calcium in Human Intestinal Cells by Stimulating Phospholipase C-Mediated Inositol 1,4,5-Trisphosphate Production. *Proc. Natl. Acad. Sci.* **1997**, *94* (8), 3960–3965. https://doi.org/10.1073/pnas.94.8.3960.
(47) Ball, J. M.; Tian, P.; Zeng, C. Q.; Morris, A. P.; Estes, M. K. Age-Dependent Diarrhea Induced by a Rotaviral Nonstructural Glycoprotein. *Science* **1996**, *272* (5258), 101–104. https://doi.org/10.1126/science.272.5258.101.
(48) Chang-Graham, A. L.; Perry, J. L.; Engevik, M. A.; Engevik, K. A.; Scribano, F. J.; Gebert, J. T.; Danhof, H. A.; Nelson, J. C.; Kellen, J. S.; Strtak, A. C.; Sastri, N. P.; Estes, M. K.; Britton, R. A.; Versalovic, J.; Hyser, J. M. Rotavirus Induces Intercellular Calcium Waves through ADP Signaling. *Science* **2020**, *370* (6519), eabc3621. https://doi.org/10.1126/science.abc3621.
(49) Costa, F. B.; Flores, P. S.; Amorim, A. R.; Mendes, G. da S.; Santos, N. Porcine Rotavirus C Strains Carrying Human-like NSP4 and NSP5. *Zoonoses Public Health* **2020**, *67* (8), 849–861. https://doi.org/10.1111/zph.12713.
(50) Dhama, K.; Chauhan, R. S.; Mahendran, M.; Malik, S. V. S. Rotavirus Diarrhea in Bovines and Other Domestic Animals. *Vet. Res. Commun.* **2009**, *33* (1), 1–23. https://doi.org/10.1007/s11259-008-9070-x.
(51) Luchs, A.; Timenetsky, M. do C. S. T. Group A Rotavirus Gastroenteritis: Post-Vaccine Era, Genotypes and Zoonotic Transmission. *Einstein* **2016**, *14* (2), 278–287. https://doi.org/10.1590/S1679-45082016RB3582.
(52) Martella, V.; Bányai, K.; Matthijnssens, J.; Buonavoglia, C.; Ciarlet, M. Zoonotic Aspects of Rotaviruses. *Vet. Microbiol.* **2010**, *140* (3), 246–255. https://doi.org/10.1016/j.vetmic.2009.08.028.

(53) Matthijnssens, J.; Ciarlet, M.; McDonald, S. M.; Attoui, H.; Bányai, K.; Brister, J. R.; Buesa, J.; Esona, M. D.; Estes, M. K.; Gentsch, J. R.; Iturriza-Gómara, M.; Johne, R.; Kirkwood, C. D.; Martella, V.; Mertens, P. P. C.; Nakagomi, O.; Parreño, V.; Rahman, M.; Ruggeri, F. M.; Saif, L. J.; Santos, N.; Steyer, A.; Taniguchi, K.; Patton, J. T.; Desselberger, U.; Van Ranst, M. Uniformity of Rotavirus Strain Nomenclature Proposed by the Rotavirus Classification Working Group (RCWG). *Arch. Virol.* **2011**, *156* (8), 1397–1413. https://doi.org/10.1007/s00705-011-1006-z.

(54) Chansaenroj, J.; Chuchaona, W.; Lestari, F. B.; Pasittungkul, S.; Klinfueng, S.; Wanlapakorn, N.; Vongpunsawad, S.; Chirathaworn, C.; Poovorawan, Y. High Prevalence of DS-1-like Rotavirus Infection in Thai Adults between 2016 and 2019. *PLOS ONE* **2020**, *15* (6), e0235280. https://doi.org/10.1371/journal.pone.0235280.

(55) Hungerford, D.; Vivancos, R.; Members, E. network. In-Season and out-of-Season Variation of Rotavirus Genotype Distribution and Age of Infection across 12 European Countries before the Introduction of Routine Vaccination, 2007/08 to 2012/13. *Eurosurveillance* **2016**, *21* (2), 30106. https://doi.org/10.2807/1560-7917.ES.2016.21.2.30106.

(56) Leshem, E.; Lopman, B.; Glass, R.; Gentsch, J.; Bányai, K.; Parashar, U.; Patel, M. Distribution of Rotavirus Strains and Strain-Specific Effectiveness of the Rotavirus Vaccine after Its Introduction: A Systematic Review and Meta-Analysis. *Lancet Infect. Dis.* **2014**, *14* (9), 847–856. https://doi.org/10.1016/S1473-3099(14)70832-1.

(57) Yeager, M.; Dryden, K. A.; Olson, N. H.; Greenberg, H. B.; Baker, T. S. Three-Dimensional Structure of Rhesus Rotavirus by Cryoelectron Microscopy and Image Reconstruction. *J. Cell Biol.* **1990**, *110* (6), 2133–2144. https://doi.org/10.1083/jcb.110.6.2133.

(58) Li, Z.; Baker, M. L.; Jiang, W.; Estes, M. K.; Prasad, B. V. V. Rotavirus Architecture at Subnanometer Resolution. *J. Virol.* **2009**, *83* (4), 1754–1766. https://doi.org/10.1128/JVI.01855-08.

(59) Aoki, S. T.; Settembre, E. C.; Trask, S. D.; Greenberg, H. B.; Harrison, S. C.; Dormitzer, P. R. Structure of Rotavirus Outer-Layer Protein VP7 Bound with a Neutralizing Fab. *Science* **2009**, *324* (5933), 1444–1447. https://doi.org/10.1126/science.1170481.

(60) Chen, J. Z.; Settembre, E. C.; Aoki, S. T.; Zhang, X.; Bellamy, A. R.; Dormitzer, P. R.; Harrison, S. C.; Grigorieff, N. Molecular Interactions in Rotavirus Assembly and Uncoating Seen by High-Resolution Cryo-EM. *Proc. Natl. Acad. Sci.* **2009**, *106* (26), 10644–10648. https://doi.org/10.1073/pnas.0904024106.

(61) Settembre, E. C.; Chen, J. Z.; Dormitzer, P. R.; Grigorieff, N.; Harrison, S. C. Atomic Model of an Infectious Rotavirus Particle. *EMBO J.* **2011**, *30* (2), 408–416. https://doi.org/10.1038/emboj.2010.322.

(62) Crawford, S. E.; Mukherjee, S. K.; Estes, M. K.; Lawton, J. A.; Shaw, A. L.; Ramig, R. F.; Prasad, B. V. V. Trypsin Cleavage Stabilizes the Rotavirus VP4 Spike. *J. Virol.* **2001**, *75* (13), 6052–6061. https://doi.org/10.1128/JVI.75.13.6052-6061.2001.

(63) Shah, P. N. M.; Gilchrist, J. B.; Forsberg, B. O.; Burt, A.; Howe, A.; Mosalaganti, S.; Wan, W.; Radecke, J.; Chaban, Y.; Sutton, G.; Stuart, D. I.; Boyce, M. Characterization of the Rotavirus Assembly Pathway in Situ Using Cryoelectron Tomography. *Cell Host Microbe* **2023**, *31* (4), 604-615.e4. https://doi.org/10.1016/j.chom.2023.03.004.

(64) Ramani, S.; Hu, L.; Venkataram Prasad, B. V.; Estes, M. K. Diversity in Rotavirus–Host Glycan Interactions: A "Sweet" Spectrum. *Cell. Mol. Gastroenterol. Hepatol.* **2016**, *2* (3), 263–273. https://doi.org/10.1016/j.jcmgh.2016.03.002.
(65) McClain, B.; Settembre, E.; Temple, B. R. S.; Bellamy, A. R.; Harrison, S. C. X-Ray Crystal Structure of the Rotavirus Inner Capsid Particle at 3.8 Å Resolution. *J. Mol. Biol.* **2010**, *397* (2), 587–599. https://doi.org/10.1016/j.jmb.2010.01.055.
(66) Long, C. P.; McDonald, S. M. Rotavirus Genome Replication: Some Assembly Required. *PLOS Pathog.* **2017**, *13* (4), e1006242. https://doi.org/10.1371/journal.ppat.1006242.
(67) Díaz-Salinas, M. A.; Romero, P.; Espinosa, R.; Hoshino, Y.; López, S.; Arias, C. F. The Spike Protein VP4 Defines the Endocytic Pathway Used by Rotavirus To Enter MA104 Cells. *J. Virol.* **2013**, *87* (3), 1658–1663. https://doi.org/10.1128/JVI.02086-12.
(68) Sun, X.; Li, D.; Duan, Z. Structural Basis of Glycan Recognition of Rotavirus. *Front. Mol. Biosci.* **2021**, *8*, 658029. https://doi.org/10.3389/fmolb.2021.658029.
(69) Zárate, S.; Cuadras, M. A.; Espinosa, R.; Romero, P.; Juárez, K. O.; Camacho-Nuez, M.; Arias, C. F.; López, S. Interaction of Rotaviruses with Hsc70 during Cell Entry Is Mediated by VP5. *J. Virol.* **2003**, *77* (13), 7254–7260. https://doi.org/10.1128/JVI.77.13.7254-7260.2003.
(70) Guerrero, C. A.; Méndez, E.; Zárate, S.; Isa, P.; López, S.; Arias, C. F. Integrin Avβ3 Mediates Rotavirus Cell Entry. *Proc. Natl. Acad. Sci. U. S. A.* **2000**, *97* (26), 14644–14649.
(71) Guerrero, C. A.; Bouyssounade, D.; Zárate, S.; Iša, P.; López, T.; Espinosa, R.; Romero, P.; Méndez, E.; López, S.; Arias, C. F. Heat Shock Cognate Protein 70 Is Involved in Rotavirus Cell Entry. *J. Virol.* **2002**, *76* (8), 4096–4102. https://doi.org/10.1128/JVI.76.8.4096-4102.2002.
(72) Zárate, S.; Espinosa, R.; Romero, P.; Guerrero, C. A.; Arias, C. F.; López, S. Integrin A2β1 Mediates the Cell Attachment of the Rotavirus Neuraminidase-Resistant Variant Nar3. *Virology* **2000**, *278* (1), 50–54. https://doi.org/10.1006/viro.2000.0660.
(73) Zárate, S.; Espinosa, R.; Romero, P.; Méndez, E.; Arias, C. F.; López, S. The VP5 Domain of VP4 Can Mediate Attachment of Rotaviruses to Cells. *J. Virol.* **2000**, *74* (2), 593–599.
(74) Herrmann, T.; Torres, R.; Salgado, E. N.; Berciu, C.; Stoddard, D.; Nicastro, D.; Jenni, S.; Harrison, S. C. Functional Refolding of the Penetration Protein on a Non-Enveloped Virus. *Nature* **2021**, 1–5. https://doi.org/10.1038/s41586-020-03124-4.
(75) Arias, C. F.; Silva-Ayala, D.; López, S. Rotavirus Entry: A Deep Journey into the Cell with Several Exits. *J. Virol.* **2015**, *89* (2), 890–893. https://doi.org/10.1128/JVI.01787-14.
(76) Gutiérrez, M.; Isa, P.; Sánchez-San Martin, C.; Pérez-Vargas, J.; Espinosa, R.; Arias, C. F.; López, S. Different Rotavirus Strains Enter MA104 Cells through Different Endocytic Pathways: The Role of Clathrin-Mediated Endocytosis. *J. Virol.* **2010**, *84* (18), 9161–9169. https://doi.org/10.1128/JVI.00731-10.
(77) Wolf, M.; Vo, P. T.; Greenberg, H. B. Rhesus Rotavirus Entry into a Polarized Epithelium Is Endocytosis Dependent and Involves Sequential VP4 Conformational Changes. *J. Virol.* **2011**, *85* (6), 2492–2503. https://doi.org/10.1128/JVI.02082-10.
(78) Delorme, C.; Brüssow, H.; Sidoti, J.; Roche, N.; Karlsson, K.-A.; Neeser, J.-R.; Teneberg, S. Glycosphingolipid Binding Specificities of Rotavirus: Identification of a Sialic Acid-Binding Epitope. *J. Virol.* **2001**, *75* (5), 2276–2287. https://doi.org/10.1128/JVI.75.5.2276-2287.2001.
(79) Chemello, M. E.; Aristimuño, O. C.; Michelangeli, F.; Ruiz, M.-C. Requirement for Vacuolar H+-ATPase Activity and Ca2+ Gradient during Entry of Rotavirus into MA104

Cells. *J. Virol.* **2002**, *76* (24), 13083–13087. https://doi.org/10.1128/jvi.76.24.13083-13087.2002.
(80) Albrecht, T.; Zhao, Y.; Nguyen, T. H.; Campbell, R. E.; Johnson, J. D. Fluorescent Biosensors Illuminate Calcium Levels within Defined Beta-Cell Endosome Subpopulations. *Cell Calcium* **2015**, *57* (4), 263–274. https://doi.org/10.1016/j.ceca.2015.01.008.
(81) Salgado, E. N.; Garcia Rodriguez, B.; Narayanaswamy, N.; Krishnan, Y.; Harrison, S. C. Visualization of Calcium Ion Loss from Rotavirus during Cell Entry. *J. Virol.* **2018**, *92* (24), e01327-18, /jvi/92/24/e01327-18.atom. https://doi.org/10.1128/JVI.01327-18.
(82) Trask, S. D.; Ogden, K. M.; Patton, J. T. Interactions among Capsid Proteins Orchestrate Rotavirus Particle Functions. *Curr. Opin. Virol.* **2012**, *2* (4), 373–379. https://doi.org/10.1016/j.coviro.2012.04.005.
(83) Méndez, E.; Arias, C. F.; López, S. Interactions between the Two Surface Proteins of Rotavirus May Alter the Receptor-Binding Specificity of the Virus. *J. Virol.* **1996**, *70* (2), 1218–1222. https://doi.org/10.1128/jvi.70.2.1218-1222.1996.
(84) Díaz-Salinas, M. A.; Silva-Ayala, D.; López, S.; Arias, C. F. Rotaviruses Reach Late Endosomes and Require the Cation-Dependent Mannose-6-Phosphate Receptor and the Activity of Cathepsin Proteases To Enter the Cell. *J. Virol.* **2014**, *88* (8), 4389–4402. https://doi.org/10.1128/JVI.03457-13.
(85) Abdelhakim, A. H.; Salgado, E. N.; Fu, X.; Pasham, M.; Nicastro, D.; Kirchhausen, T.; Harrison, S. C. Structural Correlates of Rotavirus Cell Entry. *PLOS Pathog.* **2014**, *10* (9), e1004355. https://doi.org/10.1371/journal.ppat.1004355.
(86) Arias, C. F.; López, S. Rotavirus Cell Entry: Not so Simple after All. *Curr. Opin. Virol.* **2021**, *48*, 42–48. https://doi.org/10.1016/j.coviro.2021.03.011.
(87) Borodavka, A.; Desselberger, U.; Patton, J. T. Genome Packaging in Multi-Segmented DsRNA Viruses: Distinct Mechanisms with Similar Outcomes. *Curr. Opin. Virol.* **2018**, *33*, 106–112. https://doi.org/10.1016/j.coviro.2018.08.001.
(88) McDonald, S. M.; Matthijnssens, J.; McAllen, J. K.; Hine, E.; Overton, L.; Wang, S.; Lemey, P.; Zeller, M.; Ranst, M. V.; Spiro, D. J.; Patton, J. T. Evolutionary Dynamics of Human Rotaviruses: Balancing Reassortment with Preferred Genome Constellations. *PLOS Pathog.* **2009**, *5* (10), e1000634. https://doi.org/10.1371/journal.ppat.1000634.
(89) Matthijnssens, J.; Van Ranst, M. Genotype Constellation and Evolution of Group A Rotaviruses Infecting Humans. *Curr. Opin. Virol.* **2012**, *2* (4), 426–433. https://doi.org/10.1016/j.coviro.2012.04.007.
(90) Selsted, M. E.; Ouellette, A. J. Mammalian Defensins in the Antimicrobial Immune Response. *Nat. Immunol.* **2005**, *6* (6), 551–557. https://doi.org/10.1038/ni1206.
(91) Lehrer, R. I.; Bevins, C. L.; Ganz, T. Defensins and Other Antimicrobial Peptides and Proteins. *Mucosal Immunol.* **2005**, 95–110. https://doi.org/10.1016/B978-012491543-5/50010-3.
(92) Shafee, T. M. A.; Lay, F. T.; Phan, T. K.; Anderson, M. A.; Hulett, M. D. Convergent Evolution of Defensin Sequence, Structure and Function. *Cell. Mol. Life Sci.* **2017**, *74* (4), 663–682. https://doi.org/10.1007/s00018-016-2344-5.
(93) Xu, D.; Lu, W. Defensins: A Double-Edged Sword in Host Immunity. *Front. Immunol.* **2020**, *11*, 764. https://doi.org/10.3389/fimmu.2020.00764.
(94) Cascales, L.; Craik, D. J. Naturally Occurring Circular Proteins: Distribution, Biosynthesis and Evolution. *Org. Biomol. Chem.* **2010**, *8* (22), 5035–5047. https://doi.org/10.1039/C0OB00139B.

(95) Tang, Y.-Q.; Yuan, J.; Ösapay, G.; Ösapay, K.; Tran, D.; Miller, C. J.; Ouellette, A. J.; Selsted, M. E. A Cyclic Antimicrobial Peptide Produced in Primate Leukocytes by the Ligation of Two Truncated α-Defensins. *Science* **1999**, *286* (5439), 498–502. https://doi.org/10.1126/science.286.5439.498.

(96) Shafee, T. M. A.; Lay, F. T.; Hulett, M. D.; Anderson, M. A. The Defensins Consist of Two Independent, Convergent Protein Superfamilies. *Mol. Biol. Evol.* **2016**, *33* (9), 2345–2356. https://doi.org/10.1093/molbev/msw106.

(97) Rajabi, M.; de Leeuw, E.; Pazgier, M.; Li, J.; Lubkowski, J.; Lu, W. The Conserved Salt Bridge in Human α-Defensin 5 Is Required for Its Precursor Processing and Proteolytic Stability. *J. Biol. Chem.* **2008**, *283* (31), 21509–21518. https://doi.org/10.1074/jbc.M801851200.

(98) Andersson, H. S.; Figueredo, S. M.; Haugaard-Kedström, L. M.; Bengtsson, E.; Daly, N. L.; Qu, X.; Craik, D. J.; Ouellette, A. J.; Rosengren, K. J. The α-Defensin Salt-Bridge Induces Backbone Stability to Facilitate Folding and Confer Proteolytic Resistance. *Amino Acids* **2012**, *43* (4), 1471–1483. https://doi.org/10.1007/s00726-012-1220-3.

(99) Clark, R. J.; Phan, T. H.; Song, A.; Ouellette, A. J.; Conibear, A. C.; Rosengren, K. J. A Conserved β-Bulge Glycine Residue Facilitates Folding and Increases Stability of the Mouse α-Defensin Cryptdin-4. *Pept. Sci.* **2022**, *114* (1), e24250. https://doi.org/10.1002/pep2.24250.

(100) Xie, C.; Prahl, A.; Ericksen, B.; Wu, Z.; Zeng, P.; Li, X.; Lu, W.-Y.; Lubkowski, J.; Lu, W. Reconstruction of the Conserved Beta-Bulge in Mammalian Defensins Using D-Amino Acids. *J. Biol. Chem.* **2005**, *280* (38), 32921–32929. https://doi.org/10.1074/jbc.M503084200.

(101) Pazgier, M.; Wei, G.; Ericksen, B.; Jung, G.; Wu, Z.; De Leeuw, E.; Yuan, W.; Szmacinski, H.; Lu, W.-Y.; Lubkowski, J.; Lehrer, R. I.; Lu, W. Sometimes It Takes Two to Tango. *J. Biol. Chem.* **2012**, *287* (12), 8944–8953. https://doi.org/10.1074/jbc.M111.332205.

(102) Rajabi, M.; Ericksen, B.; Wu, X.; de Leeuw, E.; Zhao, L.; Pazgier, M.; Lu, W. Functional Determinants of Human Enteric α-Defensin HD5. *J. Biol. Chem.* **2012**, *287* (26), 21615–21627. https://doi.org/10.1074/jbc.M112.367995.

(103) Gounder, A. P.; Wiens, M. E.; Wilson, S. S.; Lu, W.; Smith, J. G. Critical Determinants of Human α-Defensin 5 Activity against Non-Enveloped Viruses. *J. Biol. Chem.* **2012**, *287* (29), 24554–24562. https://doi.org/10.1074/jbc.M112.354068.

(104) Patterson-Delafield, J.; Martinez, R. J.; Lehrer, R. I. Microbicidal Cationic Proteins in Rabbit Alveolar Macrophages: A Potential Host Defense Mechanism. *Infect. Immun.* **1980**, *30* (1), 180–192. https://doi.org/10.1128/iai.30.1.180-192.1980.

(105) Patterson-Delafield, J.; Szklarek, D.; Martinez, R. J.; Lehrer, R. I. Microbicidal Cationic Proteins of Rabbit Alveolar Macrophages: Amino Acid Composition and Functional Attributes. *Infect. Immun.* **1981**, *31* (2), 723–731. https://doi.org/10.1128/iai.31.2.723-731.1981.

(106) Selsted, M. E.; Szklarek, D.; Lehrer, R. I. Purification and Antibacterial Activity of Antimicrobial Peptides of Rabbit Granulocytes. *Infect. Immun.* **1984**, *45* (1), 150–154. https://doi.org/10.1128/iai.45.1.150-154.1984.

(107) Ganz, T. Extracellular Release of Antimicrobial Defensins by Human Polymorphonuclear Leukocytes. *Infect. Immun.* **1987**, *55* (3), 568–571. https://doi.org/10.1128/iai.55.3.568-571.1987.

(108) Daher, K. A.; Selsted, M. E.; Lehrer, R. I. Direct Inactivation of Viruses by Human Granulocyte Defensins. *J. Virol.* **1986**, *60* (3), 1068–1074. https://doi.org/10.1128/JVI.60.3.1068-1074.1986.
(109) Wilson, S. S.; Wiens, M. E.; Smith, J. G. Antiviral Mechanisms of Human Defensins. *J. Mol. Biol.* **2013**, *425* (24), 4965–4980. https://doi.org/10.1016/j.jmb.2013.09.038.
(110) Ghosh, D.; Porter, E.; Shen, B.; Lee, S. K.; Wilk, D.; Drazba, J.; Yadav, S. P.; Crabb, J. W.; Ganz, T.; Bevins, C. L. Paneth Cell Trypsin Is the Processing Enzyme for Human Defensin-5. *Nat. Immunol.* **2002**, *3* (6), 583–590. https://doi.org/10.1038/ni797.
(111) Ayabe, T.; Satchell, D. P.; Wilson, C. L.; Parks, W. C.; Selsted, M. E.; Ouellette, A. J. Secretion of Microbicidal α-Defensins by Intestinal Paneth Cells in Response to Bacteria. *Nat. Immunol.* **2000**, *1* (2), 113–118. https://doi.org/10.1038/77783.
(112) Eisenhauer, P. B.; Lehrer, R. I. Mouse Neutrophils Lack Defensins. *Infect. Immun.* **1992**, *60* (8), 3446–3447. https://doi.org/10.1128/iai.60.8.3446-3447.1992.
(113) Holly, M. K.; Diaz, K.; Smith, J. G. Defensins in Viral Infection and Pathogenesis. *Annu. Rev. Virol.* **2017**, *4* (1), 369–391. https://doi.org/10.1146/annurev-virology-101416-041734.
(114) Patil, A. A.; Cai, Y.; Sang, Y.; Blecha, F.; Zhang, G. Cross-Species Analysis of the Mammalian β-Defensin Gene Family: Presence of Syntenic Gene Clusters and Preferential Expression in the Male Reproductive Tract. *Physiol. Genomics* **2005**, *23* (1), 5–17. https://doi.org/10.1152/physiolgenomics.00104.2005.
(115) Nguyen, T. X.; Cole, A. M.; Lehrer, R. I. Evolution of Primate Theta-Defensins: A Serpentine Path to a Sweet Tooth. *Peptides* **2003**, *24* (11), 1647–1654. https://doi.org/10.1016/j.peptides.2003.07.023.
(116) Cheng, D.-Q.; Li, Y.; Huang, J.-F. Molecular Evolution of the Primate α-/θ-Defensin Multigene Family. *PLOS ONE* **2014**, *9* (5), e97425. https://doi.org/10.1371/journal.pone.0097425.
(117) Penberthy, W. T.; Chari, S.; Cole, A. L.; Cole, A. M. Retrocyclins and Their Activity against HIV-1. *Cell. Mol. Life Sci. CMLS* **2011**, *68* (13), 2231–2242. https://doi.org/10.1007/s00018-011-0715-5.
(118) Münk, C.; Wei, G.; Yang, O. O.; Waring, A. J.; Wang, W.; Hong, T.; Lehrer, R. I.; Landau, N. R.; Cole, A. M. The Theta-Defensin, Retrocyclin, Inhibits HIV-1 Entry. *AIDS Res. Hum. Retroviruses* **2003**, *19* (10), 875–881. https://doi.org/10.1089/088922203322493049.
(119) Kohlgraf, K. G.; Pingel, L. C.; Dietrich, D. E.; Brogden, K. A. Defensins as Anti-Inflammatory Compounds and Mucosal Adjuvants. *Future Microbiol.* **2010**, *5*, 99. https://doi.org/10.2217/fmb.09.104.
(120) Kagan, B. L.; Selsted, M. E.; Ganz, T.; Lehrer, R. I. Antimicrobial Defensin Peptides Form Voltage-Dependent Ion-Permeable Channels in Planar Lipid Bilayer Membranes. *Proc. Natl. Acad. Sci.* **1990**, *87* (1), 210–214. https://doi.org/10.1073/pnas.87.1.210.
(121) Lehrer, R. I.; Barton, A.; Daher, K. A.; Harwig, S. S.; Ganz, T.; Selsted, M. E. Interaction of Human Defensins with Escherichia Coli. Mechanism of Bactericidal Activity. *J. Clin. Invest.* **1989**, *84* (2), 553–561. https://doi.org/10.1172/JCI114198.
(122) Ganz, T.; Selsted, M. E.; Szklarek, D.; Harwig, S. S.; Daher, K.; Bainton, D. F.; Lehrer, R. I. Defensins. Natural Peptide Antibiotics of Human Neutrophils. *J. Clin. Invest.* **1985**, *76* (4), 1427–1435. https://doi.org/10.1172/JCI112120.
(123) Kota, S.; Sabbah, A.; Chang, T. H.; Harnack, R.; Xiang, Y.; Meng, X.; Bose, S. Role of Human Beta-Defensin-2 during Tumor Necrosis Factor-Alpha/NF-KappaB-Mediated

Innate Antiviral Response against Human Respiratory Syncytial Virus. *J. Biol. Chem.* **2008**, *283* (33), 22417–22429. https://doi.org/10.1074/jbc.M710415200.

(124) Ding, J.; Chou, Y.-Y.; Chang, T. L. Defensins in Viral Infections. *J. Innate Immun.* **2009**, *1* (5), 413–420. https://doi.org/10.1159/000226256.

(125) Park, M. S.; Kim, J. I.; Lee, I.; Park, S.; Bae, J.-Y.; Park, M.-S. Towards the Application of Human Defensins as Antivirals. *Biomol. Ther.* **2018**, *26* (3), 242–254. https://doi.org/10.4062/biomolther.2017.172.

(126) Brice, D. C.; Diamond, G. Antiviral Activities of Human Host Defense Peptides. *Curr. Med. Chem.* **2020**, *27* (9), 1420–1443. https://doi.org/10.2174/0929867326666190805151654.

(127) Bastian, A.; Schafer, H. Human A-Defensin 1 (HNP-1) Inhibits Adenoviral Infection in Vitro. **2001**, 5.

(128) Smith, J. G.; Nemerow, G. R. Mechanism of Adenovirus Neutralization by Human α-Defensins. *Cell Host Microbe* **2008**, *3* (1), 11–19. https://doi.org/10.1016/j.chom.2007.12.001.

(129) Buck, C. B.; Day, P. M.; Thompson, C. D.; Lubkowski, J.; Lu, W.; Lowy, D. R.; Schiller, J. T. Human Alpha-Defensins Block Papillomavirus Infection. *Proc. Natl. Acad. Sci. U. S. A.* **2006**, *103* (5), 1516–1521. https://doi.org/10.1073/pnas.0508033103.

(130) Virella-Lowell, I.; Poirier, A.; Chesnut, K. A.; Brantly, M.; Flotte, T. R. Inhibition of Recombinant Adeno-Associated Virus (RAAV) Transduction by Bronchial Secretions from Cystic Fibrosis Patients. *Gene Ther.* **2000**, *7* (20), 1783–1789. https://doi.org/10.1038/sj.gt.3301268.

(131) Dugan, A. S.; Maginnis, M. S.; Jordan, J. A.; Gasparovic, M. L.; Manley, K.; Page, R.; Williams, G.; Porter, E.; O'Hara, B. A.; Atwood, W. J. Human Alpha-Defensins Inhibit BK Virus Infection by Aggregating Virions and Blocking Binding to Host Cells. *J. Biol. Chem.* **2008**, *283* (45), 31125–31132. https://doi.org/10.1074/jbc.M805902200.

(132) Zins, S. R.; Nelson, C. D. S.; Maginnis, M. S.; Banerjee, R.; O'Hara, B. A.; Atwood, W. J. The Human Alpha Defensin HD5 Neutralizes JC Polyomavirus Infection by Reducing Endoplasmic Reticulum Traffic and Stabilizing the Viral Capsid. *J. Virol.* **2014**, *88* (2), 948–960. https://doi.org/10.1128/JVI.02766-13.

(133) Porter, J. M.; Oswald, M. S.; Sharma, A.; Emmanuel, S.; Kansol, A.; Bennett, A.; McKenna, R.; Smith, J. G. A Single Surface-Exposed Amino Acid Determines Differential Neutralization of AAV1 and AAV6 by Human Alpha-Defensins. *J. Virol.* **2023**, *97* (3), e00060-23. https://doi.org/10.1128/jvi.00060-23.

(134) Nguyen, E. K.; Nemerow, G. R.; Smith, J. G. Direct Evidence from Single-Cell Analysis That Human {alpha}-Defensins Block Adenovirus Uncoating to Neutralize Infection. *J. Virol.* **2010**, *84* (8), 4041–4049. https://doi.org/10.1128/JVI.02471-09.

(135) Wiens, M. E.; Smith, J. G. α-Defensin HD5 Inhibits Human Papillomavirus 16 Infection via Capsid Stabilization and Redirection to the Lysosome. *mBio* **2017**, *8* (1), e02304-16, /mbio/8/1/e02304-16.atom. https://doi.org/10.1128/mBio.02304-16.

(136) Hazrati, E.; Galen, B.; Lu, W.; Wang, W.; Ouyang, Y.; Keller, M. J.; Lehrer, R. I.; Herold, B. C. Human α- and β-Defensins Block Multiple Steps in Herpes Simplex Virus Infection. *J. Immunol.* **2006**, *177* (12), 8658–8666. https://doi.org/10.4049/jimmunol.177.12.8658.

(137) Yasin, B.; Wang, W.; Pang, M.; Cheshenko, N.; Hong, T.; Waring, A. J.; Herold, B. C.; Wagar, E. A.; Lehrer, R. I. Theta Defensins Protect Cells from Infection by Herpes Simplex

Virus by Inhibiting Viral Adhesion and Entry. *J. Virol.* **2004**, *78* (10), 5147–5156. https://doi.org/10.1128/jvi.78.10.5147-5156.2004.

(138) Gallo, S. A.; Wang, W.; Rawat, S. S.; Jung, G.; Waring, A. J.; Cole, A. M.; Lu, H.; Yan, X.; Daly, N. L.; Craik, D. J.; Jiang, S.; Lehrer, R. I.; Blumenthal, R. Theta-Defensins Prevent HIV-1 Env-Mediated Fusion by Binding Gp41 and Blocking 6-Helix Bundle Formation. *J. Biol. Chem.* **2006**, *281* (27), 18787–18792. https://doi.org/10.1074/jbc.M602422200.

(139) Demirkhanyan, L. H.; Marin, M.; Padilla-Parra, S.; Zhan, C.; Miyauchi, K.; Jean-Baptiste, M.; Novitskiy, G.; Lu, W.; Melikyan, G. B. Multifaceted Mechanisms of HIV-1 Entry Inhibition by Human α-Defensin. *J. Biol. Chem.* **2012**, *287* (34), 28821–28838. https://doi.org/10.1074/jbc.M112.375949.

(140) Leikina, E.; Delanoe-Ayari, H.; Melikov, K.; Cho, M.-S.; Chen, A.; Waring, A. J.; Wang, W.; Xie, Y.; Loo, J. A.; Lehrer, R. I.; Chernomordik, L. V. Carbohydrate-Binding Molecules Inhibit Viral Fusion and Entry by Crosslinking Membrane Glycoproteins. *Nat. Immunol.* **2005**, *6* (10), 995–1001. https://doi.org/10.1038/ni1248.

(141) Smith, J. G.; Silvestry, M.; Lindert, S.; Lu, W.; Nemerow, G. R.; Stewart, P. L. Insight into the Mechanisms of Adenovirus Capsid Disassembly from Studies of Defensin Neutralization. *PLOS Pathog.* **2010**, *6* (6), e1000959. https://doi.org/10.1371/journal.ppat.1000959.

(142) Snijder, J.; Reddy, V. S.; May, E. R.; Roos, W. H.; Nemerow, G. R.; Wuite, G. J. L. Integrin and Defensin Modulate the Mechanical Properties of Adenovirus. *J. Virol.* **2013**, *87* (5), 2756–2766. https://doi.org/10.1128/JVI.02516-12.

(143) Wiens, M. E.; Smith, J. G. Alpha-Defensin HD5 Inhibits Furin Cleavage of Human Papillomavirus 16 L2 To Block Infection. *J. Virol.* **2014**, *89* (5), 2866–2874. https://doi.org/10.1128/JVI.02901-14.

(144) Chang, T. L.; Vargas, J.; DelPortillo, A.; Klotman, M. E. Dual Role of Alpha-Defensin-1 in Anti-HIV-1 Innate Immunity. *J. Clin. Invest.* **2005**, *115* (3), 765–773. https://doi.org/10.1172/JCI21948.

(145) Salvatore, M.; García-Sastre, A.; Ruchala, P.; Lehrer, R. I.; Chang, T.; Klotman, M. E. Alpha-Defensin Inhibits Influenza Virus Replication by Cell-Mediated Mechanism(s). *J. Infect. Dis.* **2007**, *196* (6), 835–843. https://doi.org/10.1086/521027.

(146) Fruitwala, S.; El-Naccache, D. W.; Chang, T. L. Multifaceted Immune Functions of Human Defensins and Underlying Mechanisms. *Semin. Cell Dev. Biol.* **2019**, *88*, 163–172. https://doi.org/10.1016/j.semcdb.2018.02.023.

(147) Dürr, M.; Peschel, A. Chemokines Meet Defensins: The Merging Concepts of Chemoattractants and Antimicrobial Peptides in Host Defense. *Infect. Immun.* **2002**, *70* (12), 6515–6517. https://doi.org/10.1128/IAI.70.12.6515-6517.2002.

(148) Rapista, A.; Ding, J.; Benito, B.; Lo, Y.-T.; Neiditch, M. B.; Lu, W.; Chang, T. L. Human Defensins 5 and 6 Enhance HIV-1 Infectivity through Promoting HIV Attachment. *Retrovirology* **2011**, *8* (1), 45. https://doi.org/10.1186/1742-4690-8-45.

(149) Pace, B. T.; Lackner, A. A.; Porter, E.; Pahar, B. The Role of Defensins in HIV Pathogenesis. *Mediators Inflamm.* **2017**, *2017*, 5186904. https://doi.org/10.1155/2017/5186904.

(150) Holly, M. K.; Smith, J. G. Adenovirus Infection of Human Enteroids Reveals Interferon Sensitivity and Preferential Infection of Goblet Cells. *J. Virol.* **2018**, *92* (9), e00250-18. https://doi.org/10.1128/JVI.00250-18.

(151) Tartaglia, L. J.; Badamchi-Zadeh, A.; Abbink, P.; Blass, E.; Aid, M.; Gebre, M. S.; Li, Z.; Pastores, K. C.; Trott, S.; Gupte, S.; Larocca, R. A.; Barouch, D. H. Alpha-Defensin 5 Differentially Modulates Adenovirus Vaccine Vectors from Different Serotypes in Vivo. *PLOS Pathog.* **2019**, *15* (12), e1008180. https://doi.org/10.1371/journal.ppat.1008180.

(152) Diaz, K.; Hu, C. T.; Sul, Y.; Bromme, B. A.; Myers, N. D.; Skorohodova, K. V.; Gounder, A. P.; Smith, J. G. Defensin-Driven Viral Evolution. *PLOS Pathog.* **2020**, *16* (11), e1009018. https://doi.org/10.1371/journal.ppat.1009018.

(153) Gounder, A. P.; Myers, N. D.; Treuting, P. M.; Bromme, B. A.; Wilson, S. S.; Wiens, M. E.; Lu, W.; Ouellette, A. J.; Spindler, K. R.; Parks, W. C.; Smith, J. G. Defensins Potentiate a Neutralizing Antibody Response to Enteric Viral Infection. *PLOS Pathog.* **2016**, *12* (3), e1005474. https://doi.org/10.1371/journal.ppat.1005474.

(154) Wilson, S. S.; Bromme, B. A.; Holly, M. K.; Wiens, M. E.; Gounder, A. P.; Sul, Y.; Smith, J. G. Alpha-Defensin-Dependent Enhancement of Enteric Viral Infection. *PLoS Pathog.* **2017**, *13* (6), e1006446. https://doi.org/10.1371/journal.ppat.1006446.

(155) Cullen, T. W.; Schofield, W. B.; Barry, N. A.; Putnam, E. E.; Rundell, E. A.; Trent, M. S.; Degnan, P. H.; Booth, C. J.; Yu, H.; Goodman, A. L. Gut Microbiota. Antimicrobial Peptide Resistance Mediates Resilience of Prominent Gut Commensals during Inflammation. *Science* **2015**, *347* (6218), 170–175. https://doi.org/10.1126/science.1260580.

(156) Masuda, K.; Sakai, N.; Nakamura, K.; Yoshioka, S.; Ayabe, T. Bactericidal Activity of Mouse α-Defensin Cryptdin-4 Predominantly Affects Noncommensal Bacteria. *J. Innate Immun.* **2011**, *3* (3), 315–326. https://doi.org/10.1159/000322037.

(157) Salzman, N. H.; Hung, K.; Haribhai, D.; Chu, H.; Karlsson-Sjöberg, J.; Amir, E.; Teggatz, P.; Barman, M.; Hayward, M.; Eastwood, D.; Stoel, M.; Zhou, Y.; Sodergren, E.; Weinstock, G. M.; Bevins, C. L.; Williams, C. B.; Bos, N. A. Enteric Defensins Are Essential Regulators of Intestinal Microbial Ecology. *Nat. Immunol.* **2010**, *11* (1), 76–83. https://doi.org/10.1038/ni.1825.

(158) Xu, D.; Liao, C.; Xiao, J.; Fang, K.; Zhang, W.; Yuan, W.; Lu, W. Human Enteric Defensin 5 Promotes Shigella Infection of Macrophages. *Infect. Immun.* **2019**, *88* (1), e00769-19. https://doi.org/10.1128/IAI.00769-19.

(159) Xu, D.; Liao, C.; Zhang, B.; Tolbert, W. D.; He, W.; Dai, Z.; Zhang, W.; Yuan, W.; Pazgier, M.; Liu, J.; Yu, J.; Sansonetti, P. J.; Bevins, C. L.; Shao, Y.; Lu, W. Human Enteric α-Defensin 5 Promotes Shigella Infection by Enhancing Bacterial Adhesion and Invasion. *Immunity* **2018**, *48* (6), 1233-1244.e7. https://doi.org/10.1016/j.immuni.2018.04.014.

(160) Myers, N. D.; Skorohodova, K. V.; Gounder, A. P.; Smith, J. G. Directed Evolution of Mutator Adenoviruses Resistant to Antibody Neutralization. *J. Virol.* **2013**, *87* (10), 6047–6050. https://doi.org/10.1128/JVI.00473-13.

(161) Wiens, M. E.; Smith, J. G. Alpha-Defensin HD5 Inhibits Furin Cleavage of Human Papillomavirus 16 L2 to Block Infection. *J. Virol.* **2015**, *89* (5), 2866–2874. https://doi.org/10.1128/JVI.02901-14.

(162) Gulati, N. M.; Miyagi, M.; Wiens, M. E.; Smith, J. G.; Stewart, P. L. α-Defensin HD5 Stabilizes Human Papillomavirus 16 Capsid/Core Interactions. *Pathog. Immun.* **2019**, *4* (2), 196–234. https://doi.org/10.20411/pai.v4i2.314.

(163) Klotman, M. E.; Rapista, A.; Teleshova, N.; Micsenyi, A.; Jarvis, G. A.; Lu, W.; Porter, E.; Chang, T. L. Neisseria Gonorrhoeae-Induced Human Defensins 5 and 6 Increase HIV

Infectivity: Role in Enhanced Transmission. *J. Immunol. Baltim. Md 1950* **2008**, *180* (9), 6176–6185. https://doi.org/10.4049/jimmunol.180.9.6176.

(164) Tenge, V. R.; Gounder, A. P.; Wiens, M. E.; Lu, W.; Smith, J. G. Delineation of Interfaces on Human Alpha-Defensins Critical for Human Adenovirus and Human Papillomavirus Inhibition. *PLoS Pathog.* **2014**, *10* (9), e1004360. https://doi.org/10.1371/journal.ppat.1004360.

(165) Arcasoy, S. M.; Latoche, J. D.; Gondor, M.; Pitt, B. R.; Pilewski, J. M. Polycations Increase the Efficiency of Adenovirus-Mediated Gene Transfer to Epithelial and Endothelial Cells in Vitro. *Gene Ther.* **1997**, *4* (1), 32–38. https://doi.org/10.1038/sj.gt.3300349.

(166) Chandra, N.; Frängsmyr, L.; Imhof, S.; Caraballo, R.; Elofsson, M.; Arnberg, N. Sialic Acid-Containing Glycans as Cellular Receptors for Ocular Human Adenoviruses: Implications for Tropism and Treatment. *Viruses* **2019**, *11* (5), 395. https://doi.org/10.3390/v11050395.

(167) Lynn, D. J.; Lloyd, A. T.; Fares, M. A.; O'Farrelly, C. Evidence of Positively Selected Sites in Mammalian Alpha-Defensins. *Mol. Biol. Evol.* **2004**, *21* (5), 819–827. https://doi.org/10.1093/molbev/msh084.

(168) Kanai, Y.; Komoto, S.; Kawagishi, T.; Nouda, R.; Nagasawa, N.; Onishi, M.; Matsuura, Y.; Taniguchi, K.; Kobayashi, T. Entirely Plasmid-Based Reverse Genetics System for Rotaviruses. *Proc. Natl. Acad. Sci.* **2017**, *114* (9), 2349–2354. https://doi.org/10.1073/pnas.1618424114.

(169) Lehrer, R. I.; Lu, W. α-Defensins in Human Innate Immunity. *Immunol. Rev.* **2012**, *245* (1), 84–112. https://doi.org/10.1111/j.1600-065X.2011.01082.x.

(170) Das, S.; Nikolaidis, N.; Goto, H.; McCallister, C.; Li, J.; Hirano, M.; Cooper, M. D. Comparative Genomics and Evolution of the Alpha-Defensin Multigene Family in Primates. *Mol. Biol. Evol.* **2010**, *27* (10), 2333–2343. https://doi.org/10.1093/molbev/msq118.

(171) Tang, Y. Q.; Yuan, J.; Miller, C. J.; Selsted, M. E. Isolation, Characterization, CDNA Cloning, and Antimicrobial Properties of Two Distinct Subfamilies of Alpha-Defensins from Rhesus Macaque Leukocytes. *Infect. Immun.* **1999**, *67* (11), 6139–6144. https://doi.org/10.1128/IAI.67.11.6139-6144.1999.

(172) Vasudevan, S.; Yuan, J.; Ösapay, G.; Tran, P.; Tai, K.; Liang, W.; Kumar, V.; Selsted, M. E.; Cocco, M. J. Synthesis, Structure, and Activities of an Oral Mucosal α-Defensin from Rhesus Macaque. *J. Biol. Chem.* **2008**, *283* (51), 35869–35877. https://doi.org/10.1074/jbc.M806915200.

(173) Tanabe, H.; Yuan, J.; Zaragoza, M. M.; Dandekar, S.; Henschen-Edman, A.; Selsted, M. E.; Ouellette, A. J. Paneth Cell α-Defensins from Rhesus Macaque Small Intestine. *Infect. Immun.* **2004**, *72* (3), 1470–1478. https://doi.org/10.1128/IAI.72.3.1470-1478.2004.

(174) Shanahan, M. T.; Tanabe, H.; Ouellette, A. J. Strain-Specific Polymorphisms in Paneth Cell α-Defensins of C57BL/6 Mice and Evidence of Vestigial Myeloid α-Defensin Pseudogenes. *Infect. Immun.* **2011**, *79* (1), 459–473. https://doi.org/10.1128/IAI.00996-10.

(175) Wu, Z.; Ericksen, B.; Tucker, K.; Lubkowski, J.; Lu, W. Synthesis and Characterization of Human Alpha-Defensins 4-6. *J. Pept. Res. Off. J. Am. Pept. Soc.* **2004**, *64* (3), 118–125. https://doi.org/10.1111/j.1399-3011.2004.00179.x.

(176) Wu, Z.; Powell, R.; Lu, W. Productive Folding of Human Neutrophil Alpha-Defensins in Vitro without the pro-Peptide. *J. Am. Chem. Soc.* **2003**, *125* (9), 2402–2403. https://doi.org/10.1021/ja0294257.
(177) Jones, D. T.; Taylor, W. R.; Thornton, J. M. The Rapid Generation of Mutation Data Matrices from Protein Sequences. *Comput. Appl. Biosci. CABIOS* **1992**, *8* (3), 275–282. https://doi.org/10.1093/bioinformatics/8.3.275.
(178) Kumar, S.; Stecher, G.; Li, M.; Knyaz, C.; Tamura, K. MEGA X: Molecular Evolutionary Genetics Analysis across Computing Platforms. *Mol. Biol. Evol.* **2018**, *35* (6), 1547–1549. https://doi.org/10.1093/molbev/msy096.
(179) Malherbe, H., * Harwin, R.* & Ulrich M.**. The Cytopathic Effects of Vervet Monkey Viruses. *S. Afr. Med. J.* **1963**, *37* (16), 407–411. https://doi.org/10.10520/AJA20785135_43205.
(180) Kumar, S.; Stecher, G.; Suleski, M.; Hedges, S. B. TimeTree: A Resource for Timelines, Timetrees, and Divergence Times. *Mol. Biol. Evol.* **2017**, *34* (7), 1812–1819. https://doi.org/10.1093/molbev/msx116.
(181) Broome, R. L.; Vo, P. T.; Ward, R. L.; Clark, H. F.; Greenberg, H. B. Murine Rotavirus Genes Encoding Outer Capsid Proteins VP4 and VP7 Are Not Major Determinants of Host Range Restriction and Virulence. *J. Virol.* **1993**, *67* (5), 2448–2455. https://doi.org/10.1128/JVI.67.5.2448-2455.1993.
(182) Feng, N.; Yasukawa, L. L.; Sen, A.; Greenberg, H. B. Permissive Replication of Homologous Murine Rotavirus in the Mouse Intestine Is Primarily Regulated by VP4 and NSP1. *J. Virol.* **2013**, *87* (15), 8307–8316. https://doi.org/10.1128/JVI.00619-13.
(183) Salzman, N. H.; Bevins, C. L. Dysbiosis--a Consequence of Paneth Cell Dysfunction. *Semin. Immunol.* **2013**, *25* (5), 334–341. https://doi.org/10.1016/j.smim.2013.09.006.
(184) Tanabe, H.; Ouellette, A. J.; Cocco, M. J.; Robinson, W. E. Differential Effects on Human Immunodeficiency Virus Type 1 Replication by α-Defensins with Comparable Bactericidal Activities. *J. Virol.* **2004**, *78* (21), 11622–11631. https://doi.org/10.1128/JVI.78.21.11622-11631.2004.
(185) Heida, F. H.; Beyduz, G.; Bulthuis, M. L. C.; Kooi, E. M. W.; Bos, A. F.; Timmer, A.; Hulscher, J. B. F. Paneth Cells in the Developing Gut: When Do They Arise and When Are They Immune Competent? *Pediatr. Res.* **2016**, *80* (2), 306–310. https://doi.org/10.1038/pr.2016.67.
(186) Dhaliwal, W.; Bajaj-Elliott, M.; Kelly, P. Intestinal Defensin Gene Expression in Human Populations. *Mol. Immunol.* **2003**, *40* (7), 469–475. https://doi.org/10.1016/S0161-5890(03)00156-1.
(187) Dhaliwal, W.; Shawa, T.; Khanam, M.; Jagatiya, P.; Simuyandi, M.; Ndulo, N.; Bevins, C. L.; Sanderson, I. R.; Kelly, P. Intestinal Antimicrobial Gene Expression: Impact of Micronutrients in Malnourished Adults during a Randomized Trial. *J. Infect. Dis.* **2010**, *202* (6), 971–978. https://doi.org/10.1086/655903.
(188) Wehkamp, J.; Salzman, N. H.; Porter, E.; Nuding, S.; Weichenthal, M.; Petras, R. E.; Shen, B.; Schaeffeler, E.; Schwab, M.; Linzmeier, R.; Feathers, R. W.; Chu, H.; Lima, H.; Fellermann, K.; Ganz, T.; Stange, E. F.; Bevins, C. L. Reduced Paneth Cell Alpha-Defensins in Ileal Crohn's Disease. *Proc. Natl. Acad. Sci. U. S. A.* **2005**, *102* (50), 18129–18134. https://doi.org/10.1073/pnas.0505256102.
(189) Velasquez, D. E.; Jiang, B. Evolution of P[8], P[4], and P[6] VP8* Genes of Human Rotaviruses Globally Reported during 1974 and 2017: Possible Implications for Rotavirus

Vaccines in Development. *Hum. Vaccines Immunother.* **2019**, *15* (12), 3003–3008. https://doi.org/10.1080/21645515.2019.1619400.

(190) Hu, C. T.; Diaz, K.; Yang, L. C.; Sharma, A.; Greenberg, H. B.; Smith, J. G. VP4 Is a Determinant of Alpha-Defensin Modulation of Rotaviral Infection. *J. Virol.* **2022**, *96* (7), e02053-21. https://doi.org/10.1128/jvi.02053-21.

(191) Blanchard, H.; Yu, X.; Coulson, B. S.; von Itzstein, M. Insight into Host Cell Carbohydrate-Recognition by Human and Porcine Rotavirus from Crystal Structures of the Virion Spike Associated Carbohydrate-Binding Domain (VP8*). *J. Mol. Biol.* **2007**, *367* (4), 1215–1226. https://doi.org/10.1016/j.jmb.2007.01.028.

(192) Yu, X.; Dang, V. T.; Fleming, F. E.; von Itzstein, M.; Coulson, B. S.; Blanchard, H. Structural Basis of Rotavirus Strain Preference toward N-Acetyl- or N-Glycolylneuraminic Acid-Containing Receptors. *J. Virol.* **2012**, *86* (24), 13456–13466. https://doi.org/10.1128/jvi.06975-11.

(193) Dormitzer, P. R. The Rhesus Rotavirus VP4 Sialic Acid Binding Domain Has a Galectin Fold with a Novel Carbohydrate Binding Site. *EMBO J.* **2002**, *21* (5), 885–897. https://doi.org/10.1093/emboj/21.5.885.

(194) Mohanty, S. K.; Donnelly, B.; Temple, H.; Mowery, S.; Poling, H. M.; Meller, J.; Malik, A.; McNeal, M.; Tiao, G. Rhesus Rotavirus Receptor-binding Site Affects High Mobility Group Box 1 Release, Altering the Pathogenesis of Experimental Biliary Atresia. *Hepatol. Commun.* **2022**, *6* (10), 2702–2714. https://doi.org/10.1002/hep4.2024.

(195) Jenni, S.; Salgado, E. N.; Herrmann, T.; Li, Z.; Grant, T.; Grigorieff, N.; Trapani, S.; Estrozi, L. F.; Harrison, S. C. In Situ Structure of Rotavirus VP1 RNA-Dependent RNA Polymerase. *J. Mol. Biol.* **2019**, *431* (17), 3124–3138. https://doi.org/10.1016/j.jmb.2019.06.016.

(196) Kumar, D.; Yu, X.; Crawford, S. E.; Moreno, R.; Jakana, J.; Sankaran, B.; Anish, R.; Kaundal, S.; Hu, L.; Estes, M. K.; Wang, Z.; Prasad, B. V. V. 2.7 Å Cryo-EM Structure of Rotavirus Core Protein VP3, a Unique Capping Machine with a Helicase Activity. *Sci. Adv.* **2020**, *6* (16), eaay6410. https://doi.org/10.1126/sciadv.aay6410.

(197) Morelli, M.; Ogden, K. M.; Patton, J. T. Silencing the Alarms: Innate Immune Antagonism by Rotavirus NSP1 and VP3. *Virology* **2015**, *479*, 75–84. https://doi.org/10.1016/j.virol.2015.01.006.

(198) Fleming, F. E.; Böhm, R.; Dang, V. T.; Holloway, G.; Haselhorst, T.; Madge, P. D.; Deveryshetty, J.; Yu, X.; Blanchard, H.; von Itzstein, M.; Coulson, B. S. Relative Roles of GM1 Ganglioside, N-Acylneuraminic Acids, and A2β1 Integrin in Mediating Rotavirus Infection. *J. Virol.* **2014**, *88* (8), 4558–4571. https://doi.org/10.1128/jvi.03431-13.

(199) Graham, K. L.; Halasz, P.; Tan, Y.; Hewish, M. J.; Takada, Y.; Mackow, E. R.; Robinson, M. K.; Coulson, B. S. Integrin-Using Rotaviruses Bind A2β1 Integrin A2 I Domain via VP4 DGE Sequence and Recognize AXβ2 and AVβ3 by Using VP7 during Cell Entry. *J. Virol.* **2003**, *77* (18), 9969–9978. https://doi.org/10.1128/jvi.77.18.9969-9978.2003.

(200) Kim, I. S.; Trask, S. D.; Babyonyshev, M.; Dormitzer, P. R.; Harrison, S. C. Effect of Mutations in VP5* Hydrophobic Loops on Rotavirus Cell Entry. *J. Virol.* **2010**, *84* (12), 6200–6207. https://doi.org/10.1128/JVI.02461-09.

(201) Aoki, S. T.; Trask, S. D.; Coulson, B. S.; Greenberg, H. B.; Dormitzer, P. R.; Harrison, S. C. Cross-Linking of Rotavirus Outer Capsid Protein VP7 by Antibodies or Disulfides

Inhibits Viral Entry. *J. Virol.* **2011**, *85* (20), 10509–10517. https://doi.org/10.1128/JVI.00234-11.

(202) Cole, A. L.; Yang, O. O.; Warren, A. D.; Waring, A. J.; Lehrer, R. I.; Cole, A. M. HIV-1 Adapts to a Retrocyclin with Cationic Amino Acid Substitutions That Reduce Fusion Efficiency of Gp41. *J. Immunol.* **2006**, *176* (11), 6900–6905. https://doi.org/10.4049/jimmunol.176.11.6900.

(203) Matthijnssens, J.; Ciarlet, M.; Heiman, E.; Arijs, I.; Delbeke, T.; McDonald, S. M.; Palombo, E. A.; Iturriza-Gómara, M.; Maes, P.; Patton, J. T.; Rahman, M.; Van Ranst, M. Full Genome-Based Classification of Rotaviruses Reveals a Common Origin between Human Wa-Like and Porcine Rotavirus Strains and Human DS-1-like and Bovine Rotavirus Strains. *J. Virol.* **2008**, *82* (7), 3204–3219. https://doi.org/10.1128/JVI.02257-07.

(204) Babji, S.; Sindhu, K. N.; Selvarajan, S.; Ramani, S.; Venugopal, S.; Khakha, S. A.; Hemavathy, P.; Ganesan, S. K.; Giri, S.; Reju, S.; Gopalakrishnan, K.; Ninan, B.; Iturriza-Gomara, M.; Srikanth, P.; Kang, G. Persistence of G10P[11] Neonatal Rotavirus Infections in Southern India. *J. Clin. Virol. Off. Publ. Pan Am. Soc. Clin. Virol.* **2021**, *144*, 104989. https://doi.org/10.1016/j.jcv.2021.104989.

(205) Lehrer, R. I.; Jung, G.; Ruchala, P.; Andre, S.; Gabius, H. J.; Lu, W. Multivalent Binding of Carbohydrates by the Human α-Defensin, HD5. *J. Immunol.* **2009**, *183* (1), 480–490. https://doi.org/10.4049/jimmunol.0900244.

(206) Liao, C.; Fang, K.; Xiao, J.; Zhang, W.; Zhang, B.; Yuan, W.; Lu, W.; Xu, D. Critical Determinants of Human Neutrophil Peptide 1 for Enhancing Host Epithelial Adhesion of Shigella Flexneri. *Cell. Microbiol.* **2019**, *21* (10), e13069. https://doi.org/10.1111/cmi.13069.

(207) Tani, K.; Murphy, W. J.; Chertov, O.; Salcedo, R.; Koh, C. Y.; Utsunomiya, I.; Funakoshi, S.; Asai, O.; Herrmann, S. H.; Wang, J. M.; Kwak, L. W.; Oppenheim, J. J. Defensins Act as Potent Adjuvants That Promote Cellular and Humoral Immune Responses in Mice to a Lymphoma Idiotype and Carrier Antigens. *Int. Immunol.* **2000**, *12* (5), 691–700. https://doi.org/10.1093/intimm/12.5.691.

(208) Trask, S. D.; Dormitzer, P. R. Assembly of Highly Infectious Rotavirus Particles Recoated with Recombinant Outer Capsid Proteins. *J. Virol.* **2006**, *80* (22), 11293–11304. https://doi.org/10.1128/JVI.01346-06.

(209) Dormitzer, P. R.; Greenberg, H. B.; Harrison, S. C. Proteolysis of Monomeric Recombinant Rotavirus VP4 Yields an Oligomeric VP5* Core. *J. Virol.* **2001**, *75* (16), 7339–7350. https://doi.org/10.1128/JVI.75.16.7339-7350.2001.

(210) Padilla-Noriega, L.; Werner-Eckert, R.; Mackow, E. R.; Gorziglia, M.; Larralde, G.; Taniguchi, K.; Greenberg, H. B. Serologic Analysis of Human Rotavirus Serotypes P1A and P2 by Using Monoclonal Antibodies. *J. Clin. Microbiol.* **1993**, *31* (3), 622–628. https://doi.org/10.1128/jcm.31.3.622-628.1993.

(211) Denisova, E.; Dowling, W.; LaMonica, R.; Shaw, R.; Scarlata, S.; Ruggeri, F.; Mackow, E. R. Rotavirus Capsid Protein VP5* Permeabilizes Membranes. *J. Virol.* **1999**, *73* (4), 3147–3153.

(212) Arias, C. F.; Romero, P.; Alvarez, V.; López, S. Trypsin Activation Pathway of Rotavirus Infectivity. *J. Virol.* **1996**, *70* (9), 5832–5839. https://doi.org/10.1128/jvi.70.9.5832-5839.1996.

(213) Warming, S.; Costantino, N.; Court, D. L.; Jenkins, N. A.; Copeland, N. G. Simple and Highly Efficient BAC Recombineering Using GalK Selection. *Nucleic Acids Res.* **2005**, *33* (4), e36. https://doi.org/10.1093/nar/gni035.

(214) Vogt, D.; Zaver, S.; Ranjan, A.; DiMaio, T.; Gounder, A. P.; Smith, J. G.; Lagunoff, M. STING Is Dispensable during KSHV Infection of Primary Endothelial Cells. *Virology* **2020**, *540*, 150–159. https://doi.org/10.1016/j.virol.2019.11.012.

(215) Cauthen, A. N.; Welton, A. R.; Spindler, K. R. Construction of Mouse Adenovirus Type 1 Mutants. *Methods Mol. Med.* **2007**, *130*, 41–59. https://doi.org/10.1385/1-59745-166-5:41.

(216) McQuin, C.; Goodman, A.; Chernyshev, V.; Kamentsky, L.; Cimini, B. A.; Karhohs, K. W.; Doan, M.; Ding, L.; Rafelski, S. M.; Thirstrup, D.; Wiegraebe, W.; Singh, S.; Becker, T.; Caicedo, J. C.; Carpenter, A. E. CellProfiler 3.0: Next-Generation Image Processing for Biology. *PLoS Biol.* **2018**, *16* (7), e2005970. https://doi.org/10.1371/journal.pbio.2005970.

(217) Pace, C. N.; Vajdos, F.; Fee, L.; Grimsley, G.; Gray, T. How to Measure and Predict the Molar Absorption Coefficient of a Protein. *Protein Sci. Publ. Protein Soc.* **1995**, *4* (11), 2411–2423. https://doi.org/10.1002/pro.5560041120.

(218) Buchholz, U. J.; Finke, S.; Conzelmann, K. K. Generation of Bovine Respiratory Syncytial Virus (BRSV) from CDNA: BRSV NS2 Is Not Essential for Virus Replication in Tissue Culture, and the Human RSV Leader Region Acts as a Functional BRSV Genome Promoter. *J. Virol.* **1999**, *73* (1), 251–259. https://doi.org/10.1128/JVI.73.1.251-259.1999.

(219) McNeal, M. M.; Broome, R. L.; Ward, R. L. Active Immunity against Rotavirus Infection in Mice Is Correlated with Viral Replication and Titers of Serum Rotavirus IgA Following Vaccination. *Virology* **1994**, *204* (2), 642–650. https://doi.org/10.1006/viro.1994.1579.

(220) Schindelin, J.; Arganda-Carreras, I.; Frise, E.; Kaynig, V.; Longair, M.; Pietzsch, T.; Preibisch, S.; Rueden, C.; Saalfeld, S.; Schmid, B.; Tinevez, J.-Y.; White, D. J.; Hartenstein, V.; Eliceiri, K.; Tomancak, P.; Cardona, A. Fiji: An Open-Source Platform for Biological-Image Analysis. *Nat. Methods* **2012**, *9* (7), 676–682. https://doi.org/10.1038/nmeth.2019.

VITA

EDUCATION

B.A. in Biological Sciences with Specialization in Microbiology, 2016
Minor in Human Rights, 2016
The University of Chicago
Chicago, IL

PUBLICATIONS

1. Banday, Zeeshan Z, Nicolás M Cecchini, DeQuantarius J Speed, Allison T Scott, Claire Parent, **Ciara T Hu**, Rachael C Filzen, Elinam Agbo, and Jean T Greenberg. "Friend or Foe: Hybrid Proline-Rich Proteins Determine How Plants Respond to Beneficial and Pathogenic Microbes." *Plant Physiology*, June 1, 2022, kiac263. https://doi.org/10.1093/plphys/kiac263.

2. **Hu, Ciara T.**, Karina Diaz, Linda C. Yang, Anjali Sharma, Harry B. Greenberg, and Jason G. Smith. "VP4 Is a Determinant of Alpha-Defensin Modulation of Rotaviral Infection." *Journal of Virology* 96, no. 7 (April 13, 2022): e02053-21. https://doi.org/10.1128/jvi.02053-21.

3. Diaz, Karina, **Ciara T. Hu**, Youngmee Sul, Beth A. Bromme, Nicolle D. Myers, Ksenia V. Skorohodova, Anshu P. Gounder, and Jason G. Smith. "Defensin-Driven Viral Evolution." *PLOS Pathogens* 16, no. 11 (November 24, 2020): e1009018. https://doi.org/10.1371/journal.ppat.1009018.

4. Jung, Hyun Min, **Ciara T Hu**, Alexandra M Fister, Andrew E Davis, Daniel Castranova, Van N Pham, Lisa M Price, and Brant M Weinstein. "MicroRNA-Mediated Control of Developmental Lymphangiogenesis." *ELife* 8 (September 3, 2019): e46007. https://doi.org/10.7554/eLife.46007.

PRESENTATIONS

1. **Hu C.**, Diaz, K., Yang, L., Sharma, A., Greenberg, H., Smith, J.G. (2022) Alpha-defensin modulation of rotaviral infection. 2022 American Society of Virology Meeting, Madison, WI, U.S.A. [Oral and poster presentation]

2. **Hu C.**, Jung H.M., Pham V.N., Weinstein B.M. (2018). MicroRNA-Mediated Control of Lymphatic Vessel Development. *NIH Postbac Poster Day*, Bethesda, MD, U.S.A. [Poster presentation]

3. **Hu C.**, Jung H.M., Pham V.N., Weinstein B.M. (2017). The role of Transient Receptor Potential Cation Channel Subfamily M Member 3 in vascular development. *2017 Mid-Atlantic Regional Zebrafish Meeting (Spring)*, Baltimore, MD, U.S.A. [Poster presentation]

4. **Hu C.**, Jung H.M., Pham V.N., Weinstein B.M. (2017). The role of Transient Receptor Potential Cation Channel Subfamily M Member 3 in vascular development. *NIH Postbac Poster Day*, Bethesda, MD, U.S.A. [Poster presentation]

GRANTS RECEIVED

National Institutes of Health/NIAID – Viral Pathogenesis and Evolution Training Program – T32-AI083203
Project Title: Characterizing Rhesus Rotavirus Neutralization by Alpha-Defensins. 2020-2022